FY2024 Ph.D. Degree Thesis

Overlapping and Non-overlapping Unfoldings in Convex Polyhedra

Takumi SHIOTA

237G0001

Supervisor : Professor Toshiki Saitoh

Division of Artificial Intelligence
Department of Creative Informatics
Graduate School of Computer Science and Systems Engineering
Kyushu Institute of Technology

December 2024

Absrtact

An unfolding of a polyhedron is a flat polygon obtained by cutting along the polyhedron's cutting lines and flattening its faces onto a plane. The origin of unfoldings can be traced back to Albrecht Dürer's work in 1525. Depending on the shape of the polyhedron and the method of unfolding, the resulting shape may overlap, where two distinct faces intersect on the plane, or their boundaries are in touch. When the cutting lines are restricted to the edges of the polyhedron, the unfolding is called an edge unfolding. Shephard proposed the conjecture that for any convex polyhedron, at least one non-overlapping edge unfolding exists; however, this conjecture remains unsolved.

To solve this conjecture, some studies are ongoing. Horiyama et al. showed that the edge unfoldings of Platonic solids and five types of Archimedean solids do not have overlaps. On the other hand, overlapping edge unfoldings have been found for five other types of Archimedean solids. There remains the problem of whether overlapping edge unfoldings exist for other convex regular-faced polyhedra, such as the snub cube, icosidodecahedron, rhombitruncated cuboctahedron, Archimedean prisms, Archimedean antiprisms, and Johnson solids.

For cuboids, when the cutting lines are aligned with the unit squares on the faces, the unfolding is called a lattice unfolding. Uno showed that the lattice unfolding of a $1 \times 1 \times z$ cuboid, where $z \geq 3$, has overlapping lattice unfoldings, and Mitani et al. showed an overlapping lattice unfolding for an $x \times y \times z$ cuboid with $x \geq 1, y \geq 2$, and $z \geq 3$. Conversely, Hearn showed that the lattice unfolding of a $1 \times 1 \times 2$ cuboid does not overlap, and Sugihara demonstrated the same for a $2 \times 2 \times 2$ cuboid. However, determining the conditions under which overlapping lattice unfoldings exist for cuboids with diagonal lattice cutting lines remains an open problem.

In this study, we address two main problems. The first problem is determining whether a given polyhedron has overlapping unfoldings. The second problem is counting the number of overlapping and non-overlapping unfoldings when a given polyhedron has overlapping unfoldings.

For the first problem, we introduce an algorithm called rotational unfolding, which efficiently determines whether overlapping unfoldings exist for a given polyhedron. The basic principle of our method is similar to the rolling and unfolding method proposed by DeSplinter et al., but it is extended to n-gons by proposing pruning techniques that use a polyhedron's distance properties and symmetry. Using this algorithm, we show the existence of overlapping unfoldings for both edge unfoldings of convex regular-faced polyhedra and lattice unfoldings of cuboids. As a result, we solve the problem of whether overlapping edge unfoldings exist for convex

regular-faced polyhedra and present the conditions for overlapping lattice unfoldings in cuboids with diagonal lattice cutting lines.

For the second problem, we propose an algorithm to count non-overlapping unfoldings in polyhedra that have overlapping unfoldings. The algorithm first enumerates the minimal overlapping partial unfoldings (MOPUs), which are the minimal units of edge unfoldings with overlaps. Then, we construct a zero-suppressed binary decision diagram (ZDD) representing non-overlapping unfoldings by subtracting the ZDDs of overlapping edge unfoldings containing the MOPUs from the ZDD representing all edge unfoldings. By applying this algorithm, we calculate the number of non-overlapping edge unfoldings for several convex regular-faced polyhedra and lattice unfoldings of cuboids. These results provide partial answers to the problems of counting overlapping and non-overlapping unfoldings for given polyhedra.

Acknowledgements

It is my pleasure to acknowledge the many individuals who have significantly contributed to the completion of this dissertation. I am especially grateful to my supervisor, Professor Toshiki Saitoh of Kyushu Institute of Technology, for his invaluable academic insight and dedicated guidance throughout my research. His support was instrumental to the success of my research, and his mentorship enabled me to complete my doctoral program in a shortened period.

I would also like to thank Professor Eiji Miyano, Associate Professor Akiko Fujimoto, and Assistant Professor Hiroshi Eto of Kyushu Institute of Technology for their valuable insights on this research and feedback on my seminar presentations. They also provided essential guidance for my JSPS Research Fellowship for Young Scientists application.

I am deeply grateful to Professor Ryuhei Uehara and Assistant Professor Tonan Kamata of the Japan Advanced Institute of Science and Technology, Professor Takashi Horiyama of Hokkaido University, as well as Mr. Yudai Enomoto and Mr. Masashi Gorobe, for the engaging discussions that contributed to the outcomes of our collaborative research. Special thanks to Professor Horiyama for his generous support in covering travel expenses, conference fees, and providing various other assistance.

I would like to express my heartfelt gratitude to Professor Shin-ichi Minato of Kyoto University, the leader of the AFSA group, and to the many faculty members affiliated with the group. Through the Short Stay Seminar Series (SSSS), I had the valuable opportunity to engage in discussions on various topics in theoretical computer science with numerous professors, which was extremely educational. Additionally, the research stay with Dr. Jason Ku in Singapore, made possible by the AFSA overseas staying program, allowed me to broaden my international perspective.

I would like to extend my heartfelt gratitude to all the members of the Kyutech Algorithms Group. Being part of this dynamic research group has significantly enriched my research experience and made it more enjoyable.

Finally, I wish to express my deepest gratitude to my family for their unwavering and constant support throughout this journey.

Contents

List of Figures

List of Tables

Chapter 1

Introduction

An unfolding of a polyhedron is a flat polygon obtained by cutting along the polyhedron's cutting lines and unfolding the polygon onto a plane. The origin of unfoldings is recognized as the illustrations found in Albrecht Dürer's "Underweysung der messung mit dem zirckel un richt scheyt" [Dür25], published in 1525 [DO07]. However, depending on the shape of the polyhedron and how it is unfolded, unfoldings can sometimes result in overlapping polygons, i.e., two distinct faces overlap, or their boundaries are in touch (see Figure 1.1). If we restrict the cutting lines to the edges of the polyhedron, the unfolding is called an *edge unfolding.* Shephard proposed the following conjecture about edge unfoldings.

Conjecture 1.1 ([She75])**.** *For any convex polyhedron, at least one non-overlapping edge unfolding exists.*

This conjecture is still unsolved, and some studies to solve it are ongoing. One such study is determining whether an overlapping edge unfolding exists for a given polyhedron. Biedl et al. in 1998 and Grünbaum in 2003 showed that there exist non-convex polyhedra whose every edge unfolding overlaps [BDD$^+$98, Grü03]. Schlickenrieder showed that n-gonal prisms have overlapping edge unfoldings, as shown in Figure 1.2. There are some results for convex regular-faced polyhedra, which are polyhedra with no concave regions and are composed entirely of regular polygons (see Table 1.1). This is because focusing on simpler structures is a natural starting point. When we deal with simpler structures, the algorithms become easier to implement, and it is simpler to check whether the approach works. Once these basic cases are well understood, they can serve as foundational ideas for developing algorithms that handle more complex structures. Horiyama and Shoji presented an algorithm for enumerating overlapping edge unfoldings of polyhedra, and they also showed that Platonic solids do not have any overlapping edge unfoldings [HS11]. Their algorithm first enumerates edge unfoldings, which are represented as spanning trees of a polyhedral graph, using binary decision diagrams (BDDs) and then checks the overlapping by numerical calculations for each unfolding. Additionally, a truncated dodecahedron, truncated icosahedron, rhombicosidodecahedron, rhombitruncated icosidodecahedron, and a snub dodecahedron (all of which are Archimedean solids, see Figure 1.3) are known to have overlapping edge unfoldings [CFG91, HS11]. Hirose showed that five shapes of Archimedean solids do not have overlapping edge

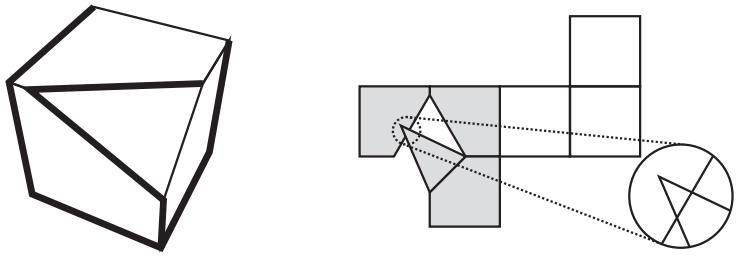

Figure 1.1: A cube with truncated corners and its overlapping unfolding [NF93].

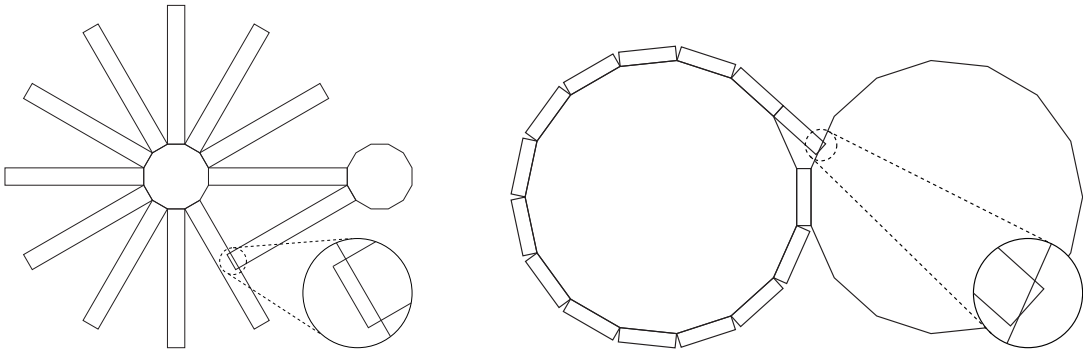

(a) 12-gonal prism **(b)** 15-gonal prism

Figure 1.2: Overlapping edge unfoldings for n-gonal prisms.

unfoldings by enumerating paths between two faces of the polyhedron and checking whether those paths have any overlaps [Hir15]. On the other hand, for edge unfoldings of convex regular-faced polyhedra, the following problem remains:

Problem 1.2 (see Table 1.1)**.** *Do three types of Archimedean solids (a snub cube, an icosidodecahedron, or a rhombitruncated cuboctahedron), n-gonal Archimedean prisms, m-gonal Archimedean antiprisms, and Johnson solids have overlapping edge unfoldings?*

There are also some results for higher-dimensional polyhedra. DeSplinter et al. recently showed that the edge unfoldings of high-dimensional cubes and demonstrated that a spanning tree of a Roberts graph can represent an edge unfolding [DDRW20]. They proposed a *rolling and unfolding method*, where the cubes are rotated along a spanning tree and the edges are cut to avoid overlap.

There are studies on general unfoldings that allow cutting the faces of the polyhedron, not just its edges. Sharir et al. in 1986 and Aronov et al. in 1992 showed a method for the general unfolding of any convex polyhedron without overlaps [SS86, AO92]. Thus, there is a gap between edge unfoldings and general unfoldings. Bridging this gap is necessary as a foothold on Conjecture 1.1. There are also general unfoldings where we can cut only along specific candidate lines drawn on the faces. One such example is the pseudo-edge unfolding, where the vertices correspond to the original vertices of the polyhedron, the edges are distance-minimizing geodesic paths between pairs of vertices, and the unfolding requires cuts along the shortest paths for each pair of vertices. Barvinok and Ghomi showed an example of a convex

Table 1.1: Overlapping edge unfoldings for convex regular-faced polyhedra.

Convex regular-faced polyhedra	Is there an overlapping edge unfolding?
Platonic solids (Total 5 types)	No [HS11]
Archimedean solids (Total 13 types)	No (5 types) [Hir15] Yes (5 types) [CFG91, HS11] **Open** (3 types)
Johnson solids (Total 92 types)	**Open**
n-gonal Archimedean prisms ($n \geq 3$)	**Open**
m-gonal Archimedean antiprisms ($m \geq 3$)	**Open**

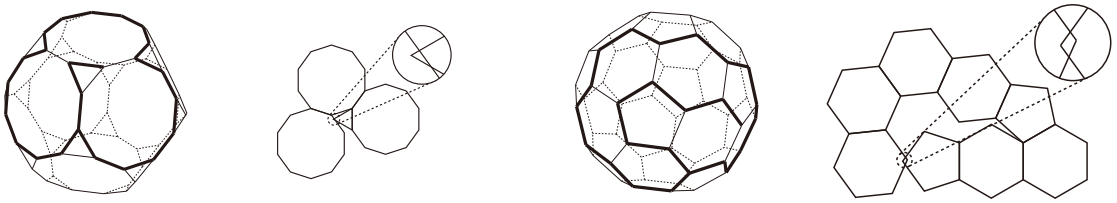

(a) Truncated dodecahedron

(b) Truncated icosahedron

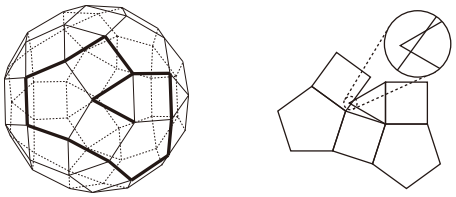

(c) Rhombicosidodecahedron

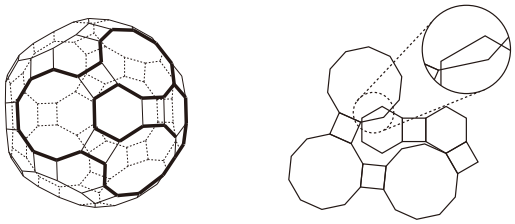

(d) Rhombitruncated icosidodecahedron

Figure 1.3: Examples of overlapping edge unfoldings in Archimedean solids [HS11]. The right edge unfolding can be obtained by cutting along the thick line of the left polyhedron.

polyhedron that does not have a non-overlapping pseudo-edge unfolding [BG20]. Another example is the lattice unfolding of a cuboid formed by connecting multiple $1 \times 1 \times 1$-cubes. In lattice unfolding, we cut along the edges of the lattice formed by unit squares. In 2008, Uno showed that a $1 \times 1 \times 3$ cuboid, and Mitani et al. showed that an $1 \times 2 \times 3$ cuboid have overlapping lattice unfoldings, as shown in Figure 1.4 [Uno08, MU08]. Additionally, each of these cutting methods can be extended to the $1 \times 1 \times z$ cuboid where $z \geq 3$ and the $x \times y \times z$ cuboid where $x \geq 1,\ y \geq 2$ and $z \geq 3$, respectively. The following theorems are obtained:

Theorem 1.3 ([Uno08]). *The $1 \times 1 \times z$ cuboid, where $z \in \mathbb{N}$ and $z \geq 3$, has an overlapping lattice unfolding.*

Theorem 1.4 ([MU08]). *The $x \times y \times z$ cuboid, where $x, y, z \in \mathbb{N}$, $x \geq 1,\ y \geq 2,\ z \geq 3$, and $x \leq y \leq z$, has an overlapping lattice unfolding.*

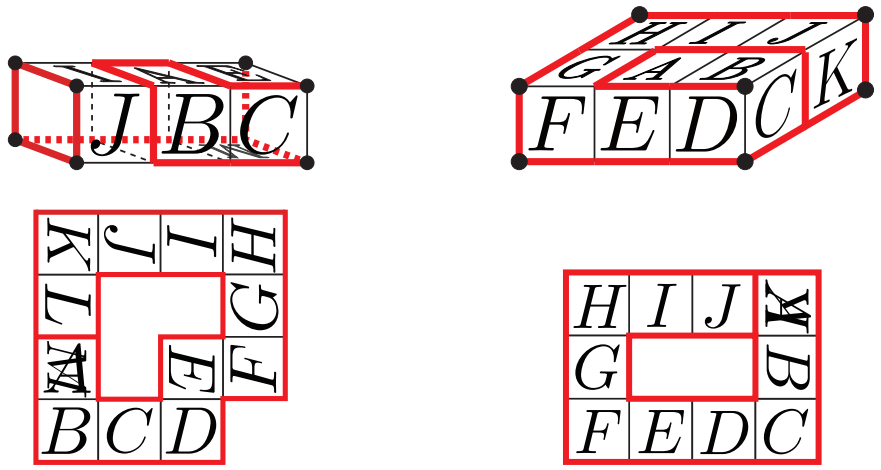

(a) $1 \times 1 \times 3$ cuboid. **(b)** $1 \times 2 \times 3$ cuboid.

Figure 1.4: Examples of overlapping lattice unfoldings for cuboids.

Figure 1.5: An example of a cuboid with diagonal lattice cutting lines. Solid lines are cutting lines, and dashed lines are non-cutting lines. Cut along the thick lines on the left cuboid to obtain the lattice unfolding on the right.

On the other hand, the following results are known for the non-existence of overlapping lattice unfolding:

Theorem 1.5 ([Hea18]). *The* $1 \times 1 \times 2$ *cuboid has no overlapping lattice unfolding.*

Theorem 1.6 ([Sug18]). *The* $2 \times 2 \times 2$ *cuboid has no overlapping lattice unfolding.*

Furthermore, cutting lines can be taken not only parallel to the edges of the cuboid but also diagonally, as shown in Figure 1.5. Thus, when considering cutting lines that can also be diagonal, we can consider the following problem:

Problem 1.7. *For cuboids with diagonal lattice cutting lines, what are the conditions for overlapping unfoldings?*

There are studies on counting the number of unfoldings. The number of edge unfoldings (including those with overlaps) is known to be equal to the number of spanning trees formed by the cutting edges of the polyhedron. Similarly, the number of lattice unfoldings (including those with overlaps) corresponds to the number of Steiner trees that satisfy specific conditions on the cutting lines of the polyhedron [MU08]. We can count the number of spanning trees using Kirchhoff's theorem [Lew82]. Additionally, both spanning trees and Steiner trees can be efficiently

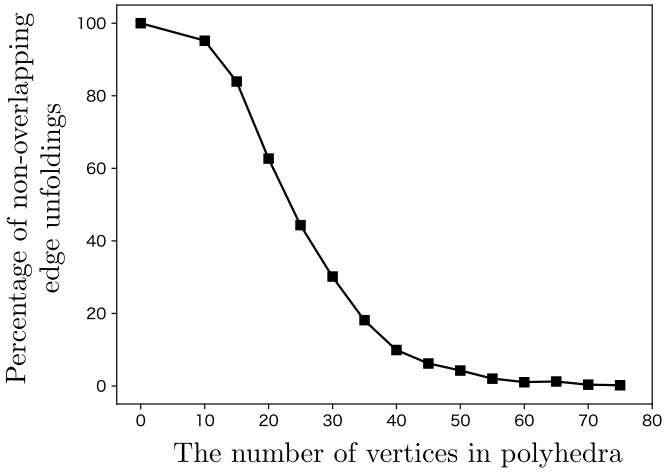

Figure 1.6: Schevon's experiment on randomly generated convex polyhedra. Each point represents the average percentage of non-overlapping edge unfoldings for five randomly generated convex polyhedra. The percentage is the proportion of overlapping unfoldings among 1000 randomly selected edge unfoldings for each polyhedron.

counted using a data structure called *binary decision diagrams (BDDs)* [Bry86] or *zero-suppressed binary decision diagrams (ZDDs)* [Min93]. BDDs/ZDDs are compact data structures for representing families of sets and support algebraic operations on these families (i.e., union, intersection, and set difference). Additionally, BDDs/ZDDs allow for counting, enumeration, and extraction of optimal families of sets. BDDs/ZDDs are used to enumerate specific structures on graphs [KIIM17]. Horiyama et al. used BDDs/ZDDs to enumerate spanning trees and count the number of edge unfoldings for convex regular-faced polyhedra [HS13, HMS18]. Horiyama and Shoji proposed a method for counting the number of non-overlapping edge unfoldings for Platonic solids by extracting each spanning tree one by one from BDDs [HS11]. However, this method only applies to the polyhedra with few edge unfoldings. For example, the truncated icosahedron (Figure 1.3 (b)) has $375,291,866,372,898,816,000$ (approximately 3.75×10^{20}) edge unfoldings [HS13], so checking each unfolding one by one would take over ten thousand years with current computers. Based on this, Schevon adopted a method of randomly selecting edge unfoldings [Sch89]. She showed that for randomly generated convex polyhedra, the percentage of non-overlapping edge unfoldings decreases as the number of vertices increases, as shown in Figure 1.6. On the other hand, when a polyhedron has overlapping unfoldings, the exact number of overlapping / non-overlapping unfoldings is not known. Therefore, we can consider the following two problems.

Problem 1.8. *Given a convex regular-faced polyhedron with overlapping edge unfoldings, how many overlapping / non-overlapping unfoldings are there?*

Problem 1.9. *Given a cuboid with overlapping lattice unfoldings, how many overlapping / non-overlapping lattice unfoldings are there?*

Our Contributions In this study, we addressed two problems. The first problem is to determine whether a given polyhedron has overlapping unfoldings. The second problem is counting the number of overlapping and non-overlapping unfoldings when a given polyhedron has overlapping unfoldings.

For the first problem, we propose a method for determining an overlapping edge unfolding called *rotational unfolding* for a polyhedron. The basic principle of our method is similar to that of the rolling and unfolding method. First, a polyhedron is placed on a plane, and the following three steps are performed repeatedly: cutting the bottom edges, rotating the polyhedron in the plane, and searching for overlapping edge unfoldings. The rolling and unfolding method is suitable for determining edge unfoldings for high-dimensional cubes but is not applicable to general shapes. Therefore, we extend the method to n-gons by proposing pruning techniques in the rotational unfolding that use a polyhedron's distance property and symmetry to determine overlapping unfoldings efficiently. As a result, we solve Problem 1.2, proving the existence of overlapping edge unfoldings for convex regular-faced polyhedra. Additionally, by extending the rotational unfolding to the lattice unfolding of cuboids, we also present the conditions for Problem 1.7.

For the second problem, we propose an enumeration algorithm for counting non-overlapping unfoldings in a given polyhedron using ZDDs and their operations. The algorithm first enumerates the minimal overlapping partial unfoldings (MOPUs), which are the minimal units of edge unfoldings with overlaps (the gray faces in Figure 1.1 correspond to this). Next, we construct a ZDD representing non-overlapping unfoldings by subtracting the ZDDs of overlapping edge unfoldings containing the MOPUs from the ZDD representing all edge unfoldings. We apply this algorithm to the edge unfoldings of convex regular-faced polyhedra and the lattice unfoldings of cuboids, counting the number of non-overlapping unfoldings for various convex polyhedra. These results provide partial answers to Problems 1.8 and 1.9.

Chapter 2

Preliminaries

2.1 Graph

Let $G = (V, E)$ be a simple graph where V is a set of vertices and $E \subseteq V \times V$ is a set of edges. A sequence of vertices $\langle v_1, \ldots, v_k \rangle$ is a *path* if $v_i \neq v_j$ $(v_i,\ v_j \in V,\ 1 \leq i \neq j \leq k)$ and every consecutive two vertices are adjacent. A graph is *connected* if a path exists between any two vertices of the graph. If a graph $T = (V_T, E_T)$ is connected and $|E_T| = |V_T| - 1$, the graph is called a *tree*. A tree $T = (V_T, E_T)$ is a *spanning tree* of G if $V_T = V$ and $E_T \subseteq E$. For a subset of vertices $V' \subseteq V$ in graph G, the graph $G[V'] = (V', \{(p, q) \mid p, q \in V' \text{ and } (p, q) \in E\})$ is called the *subgraph induced by* V'.

2.2 Convex regular-faced polyhedron

A *polyhedron* is a three-dimensional object consisting of at least four polygons, called *faces*, joined at their edges. A *convex polyhedron* is a polyhedron with the interior angles of all two faces less than π. A *convex regular-faced polyhedron* is a convex polyhedron with all faces being regular polygon. A *Platonic solid* is a convex regular-faced polyhedron with faces composed of congruent regular polygons. An n *prism* is a polyhedron composed of two identical n-sided polygons, called *bases*, facing each other, and n parallelograms, called *side faces*, connecting the corresponding edges of the two bases. An n *antiprism* is a polyhedron composed of two bases of congruent n-sided polygons and $2n$-sided alternating triangles. An n-*gonal (anti)prism* is an n (anti)prism if the bases are n-sided regular polygons and an n-*gonal Archimedean (anti)prism* is an n-gonal (anti)prism if it is a convex regular-faced polyhedron (i.e., the side faces are also regular). An *Archimedean solid* is a convex regular-faced polyhedron composed of regular polygons with the same type and order of regular polygons gathered at the vertices, except for Platonic solids, and Archimedean (anti)prisms. A *Johnson solid* is a convex regular-faced polyhedron, except Platonic solids, Archimedean solids, and Archimedean (anti)prisms. It is known that there are 92 Johnson solids [Joh66].

2.3 Edge unfolding

Let Q be a polyhedron. An *unfolding* (also called a net, a development, or a general unfolding) of the polyhedron Q is a flat polygon formed by cutting Q's edges or faces and unfolding it into a plane. An *edge unfolding* of Q is an unfolding formed by cutting only edges. Q can be viewed as a graph $G_Q = (V_Q, E_Q)$, where V_Q is a set of vertices and E_Q is a set of edges. We have the following lemma for an edge unfolding of Q.

Lemma 2.1 (see e.g., [DO07] Lemma 22.1.1)**.** *The cut edges of an edge unfolding for Q form a spanning tree of G_Q.*

This lemma implies that counting the spanning trees of Q is equal to counting the edge unfoldings of Q. Two faces in Q are *neighbors* if they contain a common edge. The *dual graph* of a polyhedron Q is a graph $G_D = (V_D, E_D)$, where each vertex in V_D corresponds to a face of Q, and two vertices are connected by an edge in E_D if and only if the corresponding faces are adjacent. A spanning tree of the dual graph of Q can also be considered an edge unfolding [Sch97]. A *partial edge unfolding* is a flat polygon consisting of a set of faces that correspond to a connected induced subgraph of G_D.

We say that two distinct polygons *overlap* if there exists a point p contained in both of the two polygons. Note that any point on a boundary is included in the polygons in this paper. That is, the polygons overlap if they are in contact on the boundaries. An unfolding is *overlapping* if there exists a pair of distinct faces such that the faces overlap. The following proposition is used to determine whether an edge unfolding of a polyhedron Q is overlapping.

Proposition 2.2 ([HS11])**.** *If the circumscribed circles of the two faces do not overlap for any two faces in an edge unfolding, then the edge unfolding is not overlapping.*

This proposition is useful for efficiently checking the overlapping of an edge unfolding, and it is a necessary condition for overlapping edge unfoldings. If the circumscribed circles of two faces of Q intersect, we use numerical calculations to check the overlapping.

A *minimal partial overlapping edge unfolding (MOPE)* is a path-like partial edge unfolding that consists of faces along any path between two vertices in an induced subgraph of G_D, with overlapping faces at the two end vertices. Note that "minimal" means that removing any additional faces would make the unfolding lose its path-like structure; it does not imply that the unfolding has the smallest possible number of faces. Figure 2.1 shows examples of MOPEs and non-MOPE partial edge unfoldings.

One method for counting spanning trees in a graph is using a *Zero-suppressed Decision Diagram (ZDD)*. A ZDD is a data structure that represent families of sets compactly as a directed acyclic graph. In a ZDD, there are two types of nodes: *terminal nodes* with the out-degree zero $\top$, $\bot$, and *branching nodes*. Branching nodes are labeled by elements of the set, and each has two outgoing edges: a 1-*edge* and a 0-*edge*. The 1-edge means the inclusion of the labeled element, while

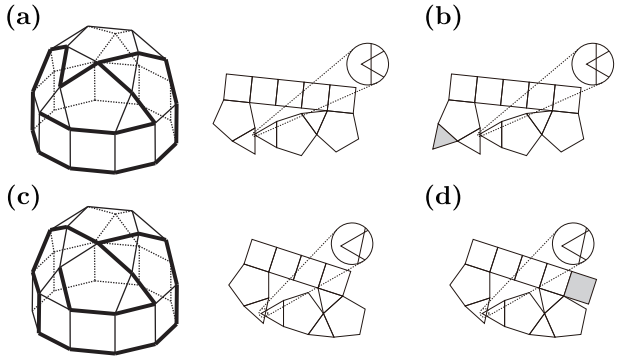

Figure 2.1: Examples of MOPEs and non-MOPEs in Johnson solid J21. In (a) and (c), they are MOPEs because removing any additional faces would make them disconnected. In (b) and (d), removing the gray faces results in MOPEs.

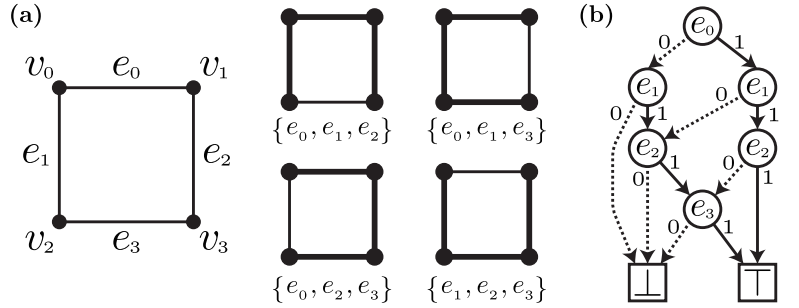

Figure 2.2: (a) An example of the graph C_4 and its spanning trees. (b) A ZDD representing the spanning trees of C_4. Circles represent branching nodes, labels are inside the circles, solid lines represent 1-edges, and dashed lines represent 0-edges. A path from the root node (labeled e_0) following a 1-edge, a 1-edge, a 0-edge, and a 1-edge leading to $\top$ means that the set $\{e_0, e_1, e_3\}$ forms a spanning tree.

the 0-edge means the exclusion of the element. In a ZDD, there is a *root node* with no incoming edges. Figure 2.2 shows an example of the ZDD representing a spanning tree. ZDDs have some operations, such as union, intersection, and set difference. Additionally, ZDDs allow for counting, enumeration, and extraction of optimal families of sets [Min93].

2.4 Lattice cuboid

Let's consider a square lattice where each square has an area of 1×1. Suppose $A = (a, 0)$ and $B = (0, b)$ are a pair of lattice points, where $a \in \mathbb{N}^+,\ b \in \mathbb{N},\ a \geq b$, as shown in Figure 2.3. Consider a square with side AB, whose length is $L = \sqrt{a^2 + b^2}$. A *cube with a side length of* L is constructed by assembling squares as its faces (an example is shown in Figure 2.4).

An (xL, yL, zL)-*cuboid* is defined as a box with edge lengths xL, yL, and zL along the x-axis, the y-axis, and the z-axis, respectively, where $x, y, z \in \mathbb{Z}^+$ (an example is shown in Figure 2.5). Here, $x \leq y \leq z$ is assumed without

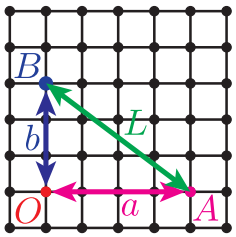

Figure 2.3: Definition of the edge length L of a cube.

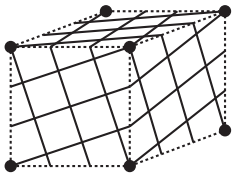

Figure 2.4: A cube with a side of length $\sqrt{10}$ ($a = 3,\ b = 1$).

loss of generality. We only consider the cuboids that satisfy $\gcd(a, b) = 1$ because the $(c(xL), c(yL), c(zL))$-cuboid (multiplied (xL, yL, zL)-cuboid by c) and the $(x(cL), y(cL), z(cL))$-cuboid (multiplied (cL, cL, cL)-cuboid by x, y, z) can be regarded as the same shape (see Figure 2.6).

2.5 Lattice unfolding

A *lattice unfolding* of a cuboid C is a planar shape obtained by cutting along the edges of unit squares on the faces of the cuboid. C can be viewed as a graph $G_C = (V_C, E_C)$, where V_C is a set of vertices and E_C is a set of edges of C. We have the following lemma for a lattice unfolding of C.

Lemma 2.3 ([MU08] Theorem 1, Theorem 3, and Figure 2.8)**.** *Let $S(V_C) \subseteq V_C$ be the set of lattice points located at the vertices of C. Then, the following are equivalent for a subgraph $G_L \subseteq G_C$:*

(1) *A lattice unfolding can be obtained by cutting along G_L.*

(2) *G_L is a tree that satisfies $S(V_C) \subseteq G_L$, and for any vertex v in G_L, if the degree of vertex v is 1, then $v \in S(V_C)$.*

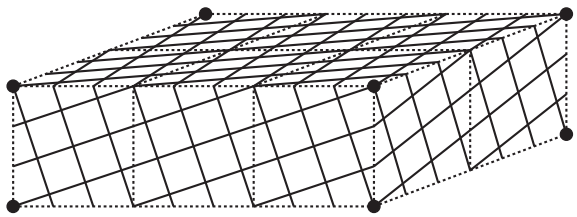

Figure 2.5: A $(3\sqrt{10}, 2\sqrt{10}, \sqrt{10})$-cuboid obtained by assembling six units of the cube shown in Figure 2.4 ($x = 3,\ y = 2,\ z = 1$).

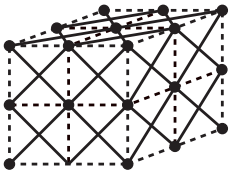

(a) $a = b = 1$, $\gcd(a, b) = 1$, $L = \sqrt{2}$, $x = y = z = 2$

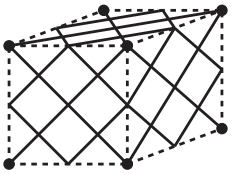

(b) $a = b = 2$, $\gcd(a, b) = 2$, $L = 2\sqrt{2}$, $x = y = z = 1$

Figure 2.6: Two $(2\sqrt{2}, 2\sqrt{2}, 2\sqrt{2})$-cuboids that can be regarded as the same shape. This paper focuses only on (a).

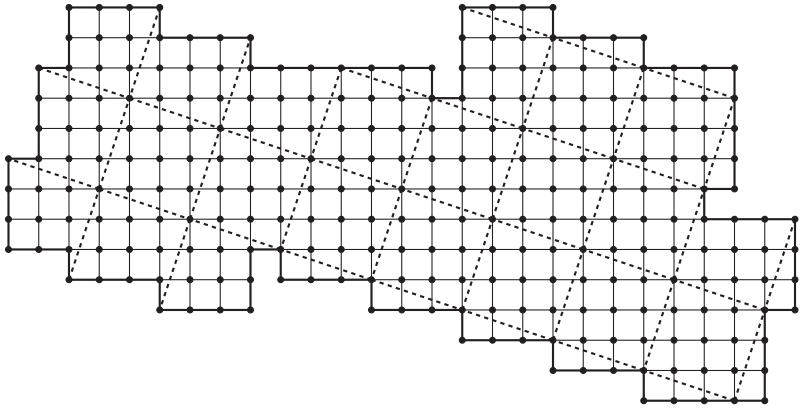

Figure 2.7: An example of a lattice unfolding of a $(\sqrt{10}, 2\sqrt{10}, 3\sqrt{10})$-cuboid (Figure 2.5). Note that dotted lines are fold lines and not cutting lines.

The dual graph of a cuboid C can be viewed as a graph $G_{DC} = (V_{DC}, E_{DC})$, where each vertex in V_{DC} corresponds to a unit square of C and two vertices are connected by an edge in E_{DC} if and only if the corresponding unit squares are adjacent. A *partial lattice unfolding* is a flat polygon consisting of a set of faces that correspond to a connected induced subgraph of G_{DC}.

In a lattice unfolding, the original cuboid's unit squares are arranged on a plane, with their edges connected. The relationship between any pair of unit squares that are not adjacent on the original cuboid is classified as follows:

(1) Overlap in the same position (Figure 2.9 (a)).

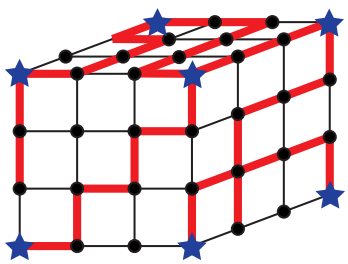

Figure 2.8: An example of a cutting line in a $(3, 3, 3)$-cuboid. The cutting line forms a tree that includes all eight lattice cuboid vertices (the starred ones).

(2) Share one edge (Figure 2.9 (b)).

(3) Share one vertex (Figure 2.9 (c)).

(4) Do not share any edges or vertices.

Herein, we say that a lattice unfolding is *faces-in-touch* if it has a pair of unit squares satisfying (1). Similarly, we define *edges-in-touch* and *vertices-in-touch* for conditions (2) and (3), respectively. When all pairs of unit squares that are not adjacent on the original cuboid satisfy condition (4), we say the *lattice unfolding is non-overlapping*. Conversely, if any of the conditions (1), (2), or (3) is satisfied, we say the *lattice unfolding is overlapping*. Note that for any cuboid, the following inclusion relationship holds: {faces-in-touch unfoldings} $\subset$ {edges-in-touch unfoldings} $\subset$ {vertices-in-touch unfoldings}.

A *minimal partial overlapping lattice unfolding (MOPL)* is a path-like partial lattice unfolding that consists of faces along any path between two vertices in an induced subgraph of G_{DC}, with overlapping faces at the two end vertices. Figure 2.10 shows examples of MOPLs and non-MOPL partial lattice unfoldings.

(a) Faces-in-touch unfolding

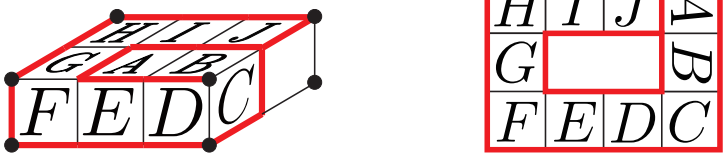

(b) Edges-in-touch unfolding

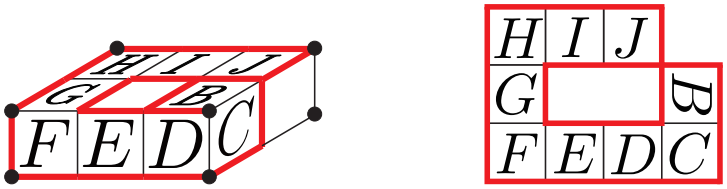

(c) Vertices-in-touch unfolding

Figure 2.9: Overlapping lattice unfolding in the $(1, 2, 3)$-cuboid [MU08].

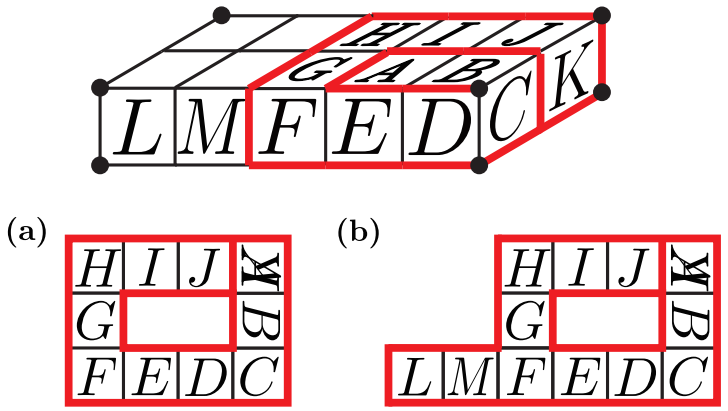

Figure 2.10: Example of an MOPL and a non-MOPL in a $(1, 2, 5)$-cuboid. In (a), it is an MOPL because removing any additional faces would make them disconnected. In (b), removing faces L and M results in a MOPL.

Chapter 3

Overlapping unfolding for convex polyhedra

3.1 Rotational unfolding

In this section, we first propose an algorithm for detecting overlapping edge unfoldings for a polyhedron Q. A spanning tree $T(U)$ of the dual graph G_D of Q represents an edge unfolding U. We can determine all overlapping edge unfoldings by enumerating all spanning trees of G_D and then checking the overlapping of the corresponding unfoldings. However, a polyhedron generally contains a large number of spanning trees. Our algorithm employs Lemma 3.1 to enumerate the paths rather than the spanning trees to efficiently search for overlapping edge unfoldings.

Lemma 3.1 ([DDRW20, Hir15]). *Let U be an overlapping edge unfolding of a polyhedron Q, and $T(U)$ be a spanning tree corresponding to U in the dual graph G_D. If two nodes $n, n' \in T(U)$ correspond to overlapping faces in U, then the path from n to n' in $T(U)$ represents a consecutive sequence of overlapping faces in U.*

For a polyhedron Q, we present a simple and recursive procedure called *rotational unfolding* to find paths and check their overlap. In this procedure, we first place Q in the plane. The *start face* f_s of Q is the bottom face. We rotate Q and unfold the current bottom in the rotational unfolding. Let f_ℓ be the current bottom face, called the *last face*. In the first step of the procedure, f_ℓ is the start face f_s. The rotational unfolding first checks whether there exists a neighbor face of f_ℓ in Q. Then, for each neighbor face f, we run the following three steps: we cut the edges of f_ℓ except for the edge sharing f, roll the polyhedron Q to be the bottom f, and check the overlap between f_s and f. To check the overlapping of edge unfoldings, we compute the coordinate of the circumscribed circle's center of f from that of f_ℓ and the angle of the shared edge. Then, we check the overlap between f_s and f using Proposition 2.2 or numerical calculations. Let v_{f_s} and v_f be the vertices corresponding to the face f_s and f of the dual graph G_D of Q, respectively. If f_s and f overlap, we output a part of the edge unfolding corresponding to a path from v_{f_s} to v_f. Otherwise, we run the procedure recursively. Figure 3.1 illustrates the rotational unfolding procedure.

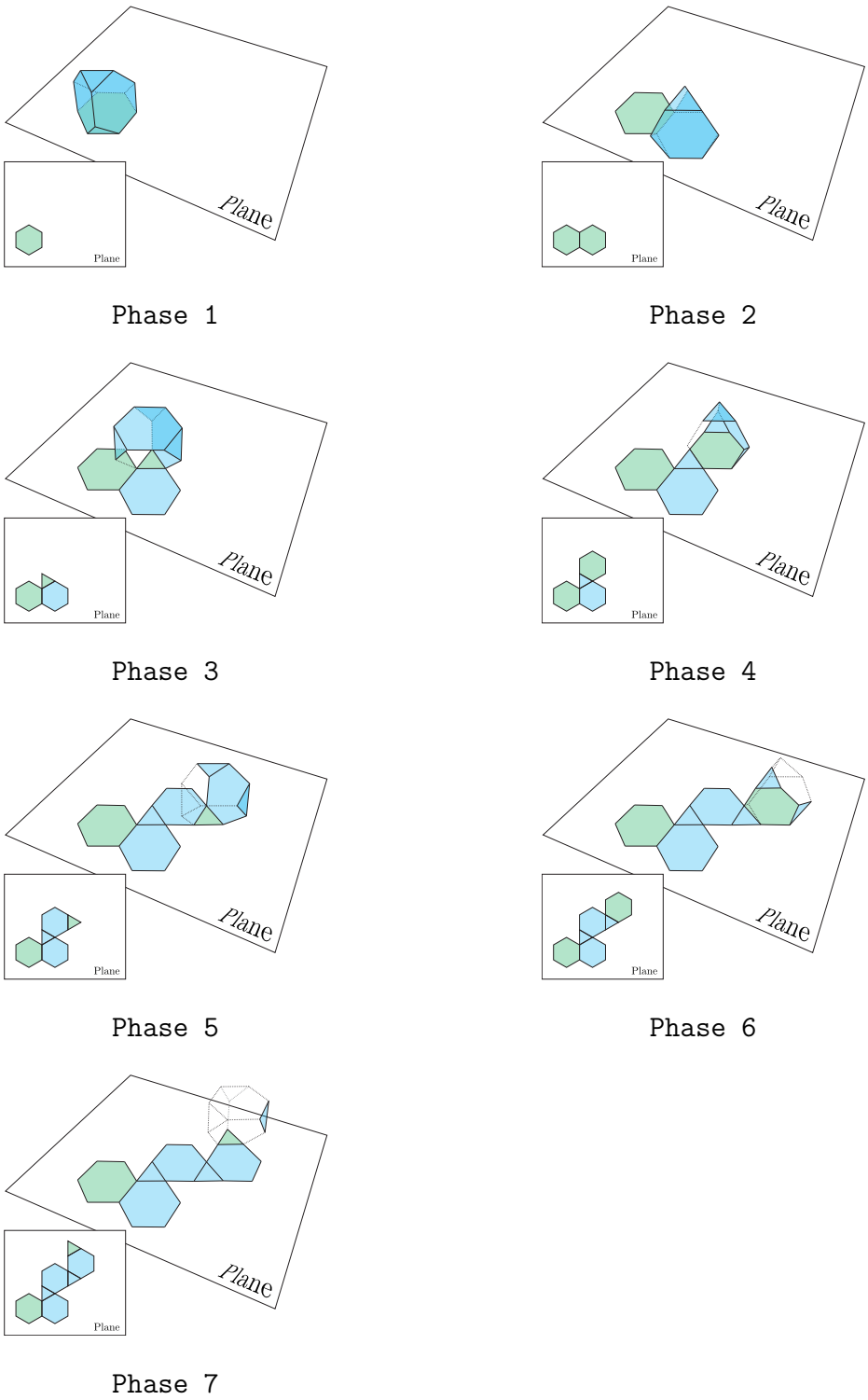

Figure 3.1: Illustration of rotational unfolding.

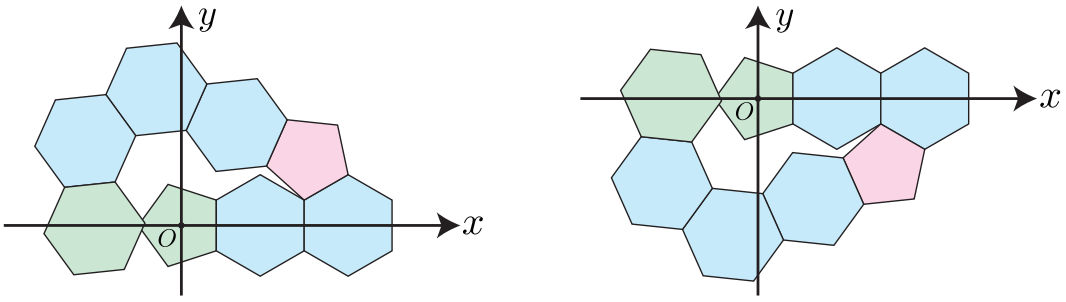

(a) (b)

Figure 3.2: An example of a symmetric partial edge unfolding with respect to the x-axis. If (a) is reflected along the x-axis, (b) is obtained.

Although the number of paths is smaller than the number of spanning trees, it is still large. To reduce the search space, we implement three methods for speeding up the search. The first method uses the simple distance property. Let D be the Euclidean distance between the circumscribed circle's center of f_s and that of f, r_s and r be the circumscribed circle radii of f_s and f, respectively, and W be the sum of circumscribed circle diameters of the remaining faces in Q. For f_s and a face in Q to overlap, the distance between f_s and f has to be smaller than W; that is, if $W + r_s + r < D$, f_s does not overlap any other faces in Q for any unfolding because f_s is too far from the other faces in Q. Thus, if $W + r_s + r < D$, we prune the search.

The second method uses the symmetry of the polyhedron. Figure 3.2 shows a symmetric edge unfolding. If a polyhedron has such symmetric unfoldings, we only compute one of them to check if a self-overlapping edge unfolding exists. To implement this pruning, we maintain the y-coordinate of the circumscribed circle's center of the last face before it becomes non-zero. We prune the search if the y-coordinate becomes negative for the first time. Note that this pruning does not work for a snub cube, a snub dodecahedron, and Johnson solids because they do not have mirror symmetry.

In the third method, we run the rotational unfolding by fixing a few steps of the search. In the rotational unfolding, we first select the start face f_s and then roll the polyhedron Q in every possible direction. However, when Q has symmetry, it allows us to fix both the start face f_s and the rolling direction. For example, in the case of a truncated tetrahedron, which consists of regular triangles and regular hexagons, as shown in Figure 3.3, we only consider three patterns of the start and next face pairs: (a) a triangle and a hexagon, (b) a hexagon and a triangle, and (c) a hexagon and a hexagon.

The partial edge unfolding obtained through rotational unfolding has overlapping faces at both ends, and removing any additional faces would make it disconnected. Thus, based on the definition in Section 2.3, this partial edge unfolding is a MOPE. In other words, the rotational unfolding can be seen as an algorithm for enumerating MOPEs in a polyhedron Q.

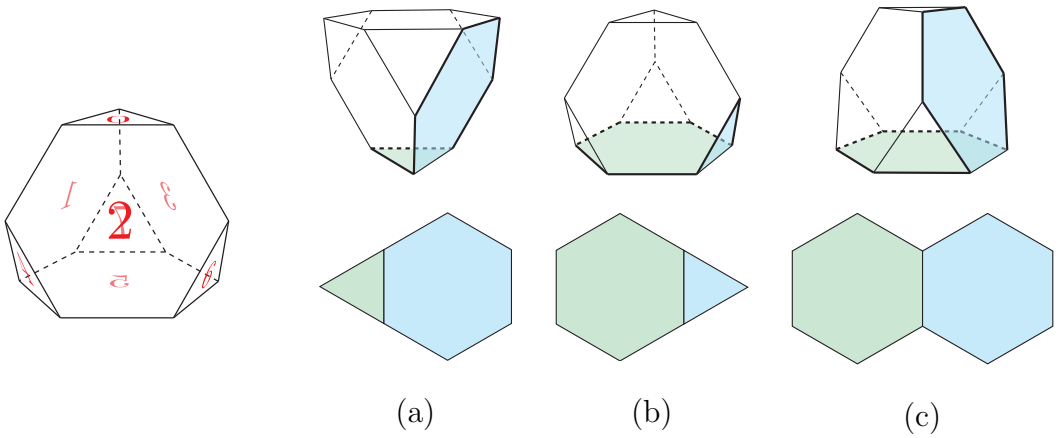

Figure 3.3: Cases of the first two faces in the rotational unfolding. Starting with face 0, 4, 6, or 7 results in pattern (a). Starting with face 2 and rolling to face 0 results in pattern (b), while rolling to face 1 leads to the pattern (c).

3.2 Overlapping unfolding for convex regular-faced polyhedra

We implemented rotational unfolding in C++ and adapted it for convex regular-faced polyhedra to find their overlapping edge unfoldings[1]. In the following sections, we present results concerning four types of convex regular-faced polyhedra for which the existence of overlaps remained open. All computational experiments were conducted on an Intel(R) Xeon(R) CPU E5-2643 v4 at 3.40 GHz with 512 GB of memory, running CentOS 7.9. The numerical calculations were performed using WolframScript 1.11.0 with a precision of 100 decimal places.

3.2.1 Archimedean and Johnson solids

We obtained the following theorems for Archimedean solids and Johnson solids:

Theorem 3.2 (Archimedean solids, see Table 3.1)**.**

(a) *An icosidodecahedron and a rhombitruncated cuboctahedron have no overlapping edge unfoldings.*

(b) *A snub cube has overlapping edge unfoldings.*

Theorem 3.3 (Johnson solids, see Table 3.2)**.**

(a) *48 Johnson solids have no overlapping edge unfoldings.*

(b) *44 Johnson solids have overlapping edge unfoldings.*

[1]Image files and adjacency list data were sourced from `https://mitani.cs.tsukuba.ac.jp/polyhedron/data/polyhedron.zip`.

Table 3.1: Existence of overlapping edge unfoldings for Archimedean solids. The timeout was set to 28,800 minutes (20 days).

Name	Number of edge unfoldings [HS13]	Is there an overlapping edge unfolding?	Number of nonisomorphic MOPEs
Truncated tetrahedron	6,000	No [Hir15]	-
Cuboctahedron	331,776	No [Hir15]	-
Truncated hexahedron	32,400,000	No [Hir15]	-
Truncated octahedron	101,154,816	No [Hir15]	-
Rhombicuboctahedron	301,056,000,000	No [Hir15]	-
Snub cube	89,904,012,853,248	**Yes**	**3**
Icosidodecahedron	208,971,104,256,000	**No**	-
Rhombitruncated cuboctahedron	12,418,325,780,889,600	**No**	-
Truncated dodecahedron	4,982,259,375,000,000,000	Yes [HS11]	**1**
Truncated icosahedron	375,291,866,372,898,816,000	Yes [HS11]	**2**
Rhombicosidodecahedron	201,550,864,919,150,779,950,956,544,000	Yes [HS11]	Timeout
Snub dodecahedron	438,201,295,386,966,498,858,139,607,040,000,000	Yes [CFG91]	Timeout
Rhombitruncated icosidodecahedron	21,789,262,703,685,125,511,464,767,107,171,876,864,000	Yes [HS11]	Timeout

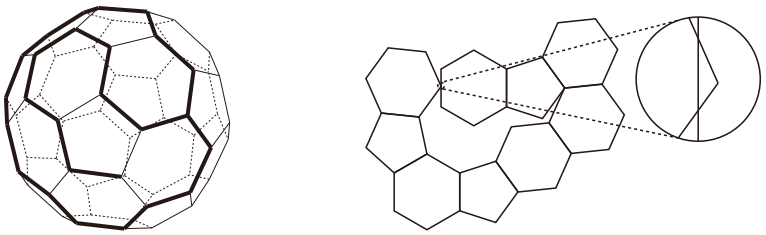

Figure 3.4: Another type of MOPE we found in a truncated icosahedron. The right edge unfolding is obtained by cutting along the thick line of the left convex polyhedron.

Our algorithm enumerates the number of nonisomorphic MOPEs for three types of Archimedean solids. For the truncated dodecahedron, it was known that a type of MOPE shown in Figure 1.3 (a) exists, but we found that no other types of MOPEs exist. For the truncated icosahedron, it was known that a type of MOPE shown in Figure 1.3 (b) exists, and we found that another type of MOPE, shown in Figure 3.4. For the snub cube, we found three types of MOPEs, as shown in Figure 3.5. In the snub cube, all types of MOPEs have two vertices of faces in touch. We compared the running times of two methods in rotational unfolding to examine the effect of pruning: one that simply enumerates all paths between two faces and another that applies pruning methods. The results are shown in Table 3.3.

For the Johnson solids we enumerated the nonisomorphic MOPEs for 29 types as shown in Appendix A.1. We also found edge unfoldings with two vertices of faces in touch, two edges of faces in touch, or a vertex of one face and an edge of another face in touch in Johnson solids. For example, in J66 (Figure A.27), (5), (8), and (12) have two vertices of faces in touch, (10) has two edges of faces in touch, and (2) and (3) have a vertex of one face and an edge of another face in touch. For an analytical verification of cases with exactly two vertices of faces in touch and other types of boundary-boundary in touch, refer to Appendix B. Furthermore, for Johnson solids J68 to J82, MOPEs confirm that these Johnson solids have overlapping edge unfoldings, as illustrated in Figure A.30 and Figure A.31 in Appendix A.1.

Table 3.2: Existence of overlapping edge unfoldings for Johnson solids. The timeout was set to 28,800 minutes (20 days).

Name	Number of edge unfoldings [HS13]	Is there an overlapping edge unfolding?	Number of nonisomorphic MOPEs	Name	Number of edge unfoldings [HS13]	Is there an overlapping edge unfolding?	Number of nonisomorphic MOPEs
J1	45	No	-	J47	9,324,488,558,669,593,960	Yes	**217**
J2	121	No	-	J48	2,670,159,599,304,760,178,000	Yes	**715**
J3	1,815	No	-	J49	672	No	-
J4	24,000	No	-	J50	5,544	No	-
J5	297,025	No	-	J51	42,336	No	-
J6	78,250,050	No	-	J52	16,744	No	-
J7	361	No	-	J53	153,816	No	-
J8	3,509	No	-	J54	75,973	Yes	**1**
J9	30,976	No	-	J55	709,632	Yes	**1**
J10	27,216	No	-	J56	707,232	Yes	**1**
J11	403,202	No	-	J57	6,531,840	Yes	**1**
J12	75	No	-	J58	92,724,962	Yes	**1**
J13	1,805	No	-	J59	1,651,482,010	Yes	**1**
J14	1,728	No	-	J60	1,641,317,568	Yes	**1**
J15	31,500	No	-	J61	28,745,798,400	Yes	**1**
J16	508,805	No	-	J62	28,080	No	-
J17	207,368	No	-	J63	1,734	No	-
J18	1,609,152	No	-	J64	8,450	No	-
J19	227,402,340	No	-	J65	1,245,456	No	-
J20	29,821,320,745	Yes	**4**	J66	54,921,311,280	Yes	**13**
J21	8,223,103,375,490	Yes	**9**	J67	90,974,647,120,896	Yes	**13**
J22	37,158,912	No	-	J68	68,495,843,558,495,480,625,000	Yes	Timeout
J23	15,482,880,000	No	-	J69	936,988,158,859,771,579,003,317,600	Yes	Timeout
J24	5,996,600,870,820	Yes	**6**	J70	930,303,529,996,712,062,599,302,400	Yes	Timeout
J25	1,702,422,879,696,000	Yes	**24**	J71	12,479,653,904,364,665,921,377,091,740,032	Yes	Timeout
J26	1,176	No	-	J72	206,686,735,580,507,426,149,463,308,960	Yes	Timeout
J27	324,900	No	-	J73	211,950,222,127,067,401,293,093,928,960	Yes	Timeout
J28	29,859,840	No	-	J74	211,595,653,377,414,999,219,839,524,608	Yes	Timeout
J29	30,950,832	No	-	J75	216,255,817,875,464,148,759,178,607,616	Yes	Timeout
J30	2,518,646,460	No	-	J76	21,081,520,904,394,872,104,529,280	Yes	Timeout
J31	2,652,552,060	No	-	J77	21,635,458,027,234,604,842,992,000	Yes	Timeout
J32	699,537,024,120	Yes	**2**	J78	21,638,184,348,166,814,636,938,752	Yes	Timeout
J33	745,208,449,920	Yes	**2**	J79	22,171,247,351,297,062,278,807,776	Yes	Timeout
J34	193,003,269,869,040	Yes	**1**	J80	2,163,645,669,729,922,583,040	Yes	Timeout
J35	301,896,210	No	-	J81	2,094,253,294,125,015,611,392	Yes	Timeout
J36	302,400,000	No	-	J82	2,151,245,812,763,713,106,752	Yes	Timeout
J37	301,988,758,680	No	-	J83	197,148,908,795,401,104	Yes	**188**
J38	270,745,016,304,350	Yes	**4**	J84	8,640	No	-
J39	272,026,496,000,000	Yes	**4**	J85	1,291,795,320	No	-
J40	75,378,202,163,880,700	Yes	**32**	J86	84,480	No	-
J41	75,804,411,381,317,500	Yes	**32**	J87	652,846	No	-
J42	20,969,865,292,417,385,400	Yes	**74**	J88	2,002,440	No	-
J43	21,115,350,368,078,435,000	Yes	**70**	J89	32,373,600	No	-
J44	5,295,528,588	Yes	**4**	J90	519,556,800	No	-
J45	13,769,880,349,680	Yes	**6**	J91	870,912	No	-
J46	32,543,644,773,848,180	Yes	**13**	J92	235,726,848	No	-

3.2.2 Archimedean prisms

We obtained the following theorem for Archimedean prisms:

Theorem 3.4 (Archimedean prisms)**.** *Let n be a natural number and $P_R(n)$ be an n-gonal Archimedean prism.*

(a) *If $3 \leq n \leq 23$, $P_R(n)$ has no overlapping edge unfoldings.*

(b) *For $n \geq 24$, there exists an overlapping edge unfolding in $P_R(n)$.*

We demonstrate the case of no overlapping edge unfolding of Theorem 3.4 (a) for every $n \in \{3, \ldots, 23\}$ of $P_R(n)$ using rotational unfolding.

Theorem 3.4 (b) can be proven by constructing an overlapping edge unfolding for $P_R(n)$. Let F_T and F_B be the top and bottom faces of $P_R(n)$, respectively, and $f_0, \ldots, f_{n-1}$ be the sides, which are numbered counterclockwise viewing from the top face F_T. For $i \in \{0, \ldots, n-1\}$, let t_i and b_i be vertices on F_T and F_B such that they share two faces f_i and f_{i+1}, where $f_n = f_0$. For $n = 24$, $P_R(n)$ has an overlapping edge unfolding, as shown in Figure 3.6 (right), consisting of faces

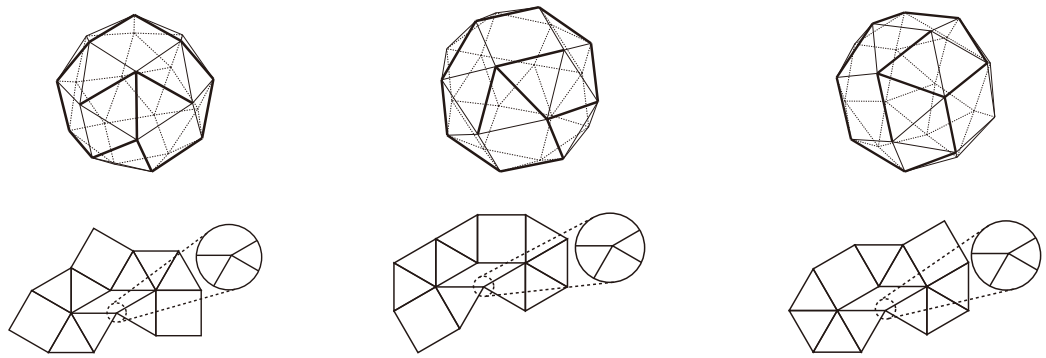

Figure 3.5: Three types of MOPEs in the snub cube. The edge unfolding can be obtained by cutting each snub cube along the thick line.

Table 3.3: Comparison of the running time for rotational unfolding: simply enumerating all paths between two faces (naive) and applying pruning methods (pruning). The timeout was set to 3,000 minutes.

Name	Number of edge unfoldings [HS13]	Naive	Pruning
Truncated tetrahedron	6,000	0m0.135s	0m0.021s
Cuboctahedron	331,776	0m0.225s	0m0.012s
Truncated hexahedron	32,400,000	0m0.652s	0m0.025s
Truncated octahedron	101,154,816	0m1.765s	0m0.049s
Rhombicuboctahedron	301,056,000,000	1m8.449s	0m1.026s
Snub cube	89,904,012,853,248	10m37.172	0m25.016s
Icosidodecahedron	208,971,104,256,000	15m56.042s	0m5.312s
Rhombitruncated cuboctahedron	12,418,325,780,889,600	1103m0.526s	6m8.364s
Truncated dodecahedron	4,982,259,375,000,000,000	2805m33.762s	10m47.283s
Truncated icosahedron	375,291,866,372,898,816,000	Timeout	2381m20.515s
Rhombicosidodecahedron	201,550,864,919,150,779,950,956,544,000	Timeout	Timeout
Snub dodecahedron	438,201,295,386,966,498,858,139,607,040,000,000	Timeout	Timeout
Rhombitruncated icosidodecahedron	21,789,262,703,685,125,511,464,767,107,171,876,864,000	Timeout	Timeout

$\{F_B, f_0, F_T, f_3, f_2, f_1\}$ obtained by cutting along the thick line of $P_R(n)$, as shown in Figure 3.6 (left). For $25 \leq n \leq 28$, $P_R(n)$ has an overlapping edge unfolding similar to $P_R(24)$, as shown in Figure A.32 of Appendix A.2.

It remains to be shown that an overlapping edge unfolding of $P_R(n)$ exists for $n \geq 29$. To prove this, we focus on the edge unfolding that consists of faces $\{F_B, f_0, F_T, f_2, f_1\}$, which overlaps as shown in Figure 3.7 (right), when cut along the thick line of $P_R(n)$ in Figure 3.7 (left). Therefore, we can obtain the following lemma.

Lemma 3.5. *For $n \geq 29$, if we cut the edges (t_0, t_1), (t_0, b_0), (b_0, b_1), and (b_1, b_2) and do not cut (t_{n-1}, t_0), (b_{n-1}, b_0), (t_1, b_1), and (t_1, t_2) of $P_R(n)$, any edge unfolding is overlapping.*

Figure 3.8 shows a part of the edge unfolding consisting of $\{F_B, f_0, F_T, f_2, f_1\}$, and an enlarged and simplified version shown in Figure A.33 of Appendix A.2. We define t_i^T and b_i^B for $i \in \{0, \ldots, n-1\}$ as vertices on F_T and F_B in the edge unfolding such that they are t_i and b_i in $P_R(n)$, respectively. Let S be a subset of faces $\{f_0, \ldots, f_{n-1}\}$. The vertices t_i and b_i in $P_R(n)$ that are shared by S in the edge unfolding are denoted as t_i^S and b_i^S, respectively. Here, we set $b_0^{f_1}$ and $b_1^{f_1,f_2}$ as $(0,0)$ and $(0,1)$ in the plane, respectively. We can obtain the following lemma.

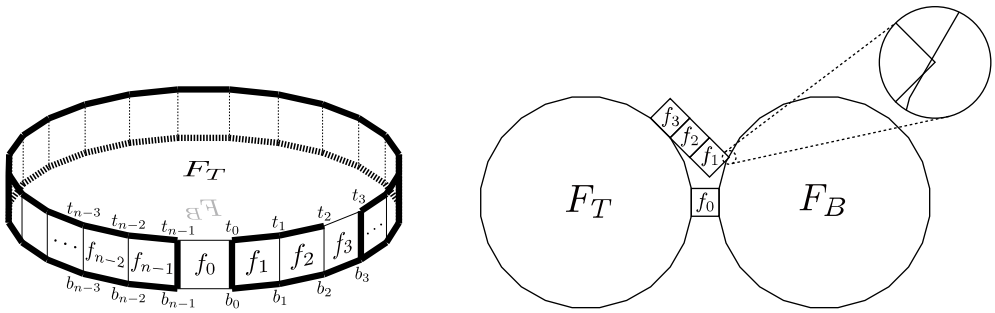

Figure 3.6: An overlapping edge unfolding in the 24-gonal Archimedean prism. The right edge unfolding is obtained by cutting along the thick line of the left convex polyhedron.

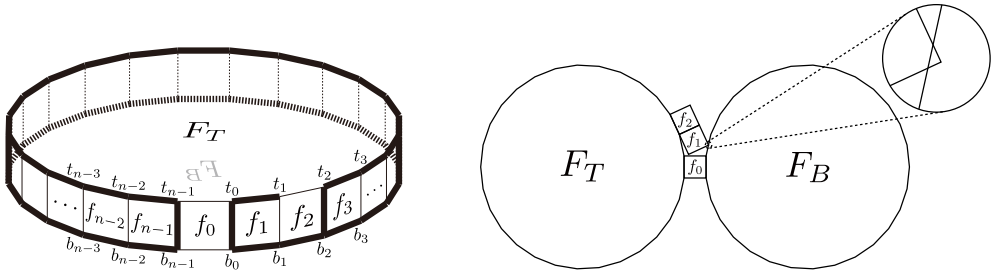

Figure 3.7: An overlapping edge unfolding in the 29-gonal Archimedean prism. The right edge unfolding is obtained by cutting along the thick line of the left convex polyhedron.

Lemma 3.6.

(i) *Point b_0^B exists in the third quadrant.*

(ii) *Point b_1^B exists in the first quadrant.*

(iii) *Let p_1 be an intersection point of the segment $b_0^B b_1^B$ and the y-axis. The y-coordinate of p_1 is positive.*

The y-coordinate of p_1 is within $(0, -1)$ to $(0, 1)$ because the length of the line segment $b_0^B b_1^B$ is one if Lemma 3.6 (i) and (ii) are satisfied. And if the y-coordinate of p_1 is positive, the line segment $b_0^{f_1} b_1^{f_1,f_2}$ intersects the line segment $b_0^B b_1^B$. Therefore, the faces f_1 and F_B overlap if Lemma 3.6 are satisfied.

We show that Lemma 3.6 is satisfied. We define the angle $\theta = 2\pi/n$ as the exterior angle of the regular n-sided polygon. The range of θ is $0 < \theta \leq 2\pi/29$ because $n \geq 29$. We make the following claim. See the details of the proofs in Appendix C.1.

Claim 3.7. *The coordinates of b_0^B and b_1^B are $(-1 - \sin\theta + \cos 2\theta, 1 - \cos\theta - \sin 2\theta)$ and $(-1 - \sin\theta + \cos 2\theta + \sin 3\theta, 1 - \cos\theta - \sin 2\theta + \cos 3\theta)$, respectively.*

From Claim 3.7 and differential analysis, we can show Lemma 3.6 (i) - (iii). See the details of the proofs in Appendix C.2.

With these established, Lemma 3.6 (i) - (iii) hold; that is, an overlapping edge unfolding exists for $P_R(n)$, where $n \geq 29$.

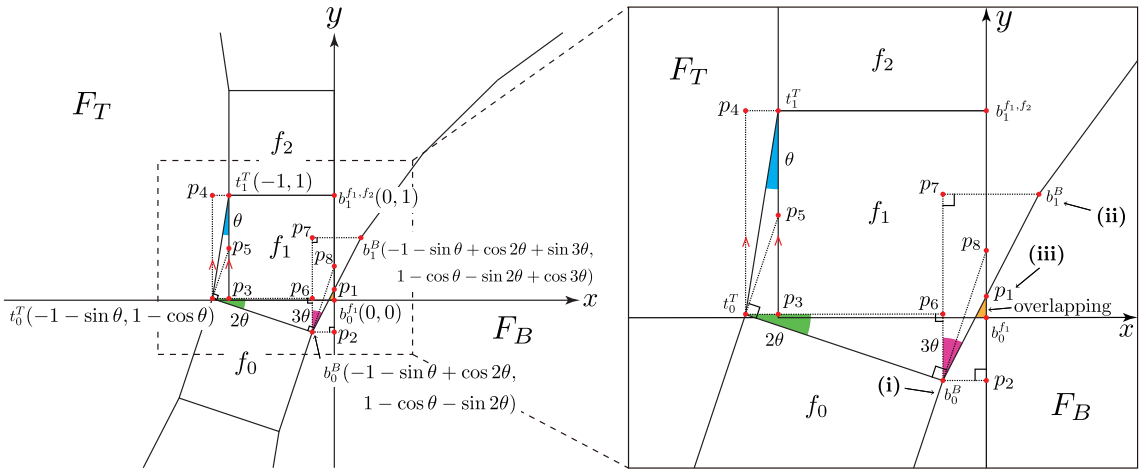

Figure 3.8: Magnified image of overlapping areas in the edge unfolding of $P_R(n)$.

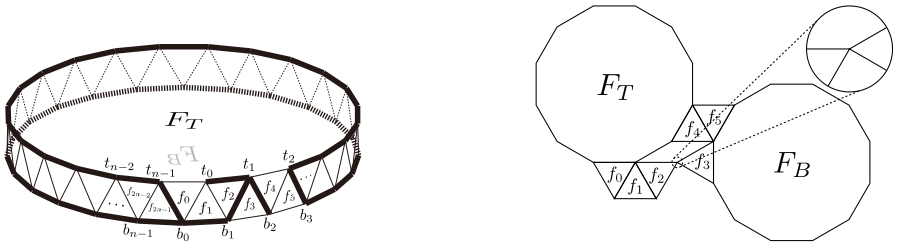

Figure 3.9: An overlapping edge unfolding in the 12-gonal Archimedean antiprism. The right edge unfolding is obtained by cutting along the thick line of the left convex polyhedron.

3.2.3 Archimedean antiprisms

We obtained the following theorem for Archimedean antiprisms:

Theorem 3.8 (Archimedean antiprisms)**.** *Let n be a natural number and $P_A(n)$ be an n-gonal Archimedean antiprism.*

(a) *If $3 \leq n \leq 11$, $P_A(n)$ has no overlapping edge unfoldings.*

(b) *For $n \geq 12$, there exists an overlapping edge unfolding in $P_A(n)$.*

We demonstrate the no overlapping edge unfolding of Theorem 3.8 (a) for every $n \in \{3, \ldots, 11\}$ of $P_A(n)$ using rotational unfolding.

Theorem 3.8 (b) can be proven by constructing an overlapping edge unfolding for $P_A(n)$. Let F_T and F_B be the top and bottom faces of $P_A(n)$, respectively, and $f_0, \ldots, f_{2n-1}$ be the sides, which are numbered counterclockwise viewing from the top face F_T. For $i \in \{0, \ldots, n-1\}$, let t_i and b_i be vertices on F_T and F_B such that they share three faces f_{2i}, f_{2i+1}, and f_{2i+2} and f_{2i-1}, f_{2i}, and f_{2i+1}, where $f_{-1} = f_{2n-1}$ and $f_{2n} = f_0$. For $n = 12$, $P_A(n)$ has an overlapping edge unfolding, as shown in Figure 3.9 (right), consisting of faces $\{f_3, F_B, f_5, f_4, F_T, f_0, f_1, f_2\}$ obtained by cutting along the thick line of $P_A(n)$, as shown in Figure 3.9 (left). For $13 \leq n \leq 16$, $P_A(n)$ has an overlapping edge unfolding similar to $P_A(12)$, as shown in Figure A.34

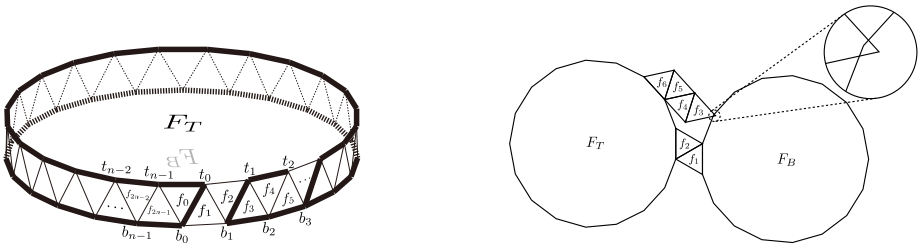

Figure 3.10: An overlapping edge unfolding in the 17-gonal Archimedean antiprism. The right edge unfolding is obtained by cutting along the thick line of the left convex polyhedron.

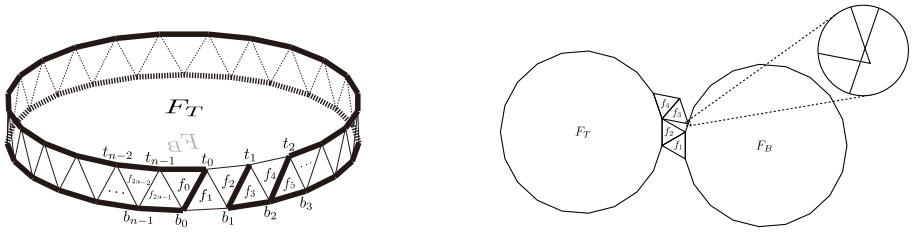

Figure 3.11: An overlapping edge unfolding in the 19-gonal Archimedean antiprism. The right edge unfolding is obtained by cutting along the thick line of the left convex polyhedron.

of Appendix A.3. For $n \in \{17, 18\}$, $P_A(n)$ has overlapping edge unfoldings consisting of faces $\{F_T, f_0, f_1, F_B, f_5, f_4, f_3, f_2\}$, as shown in Figure 3.10 (left), obtained by cutting along the thick line $P_A(n)$, as shown in Figure 3.10 (right).

It remains to be shown that an overlapping edge unfolding of $P_A(n)$ exists for $n \geq 19$. To prove this, we focus on the edge unfolding that consists of faces $\{F_B, f_1, f_2, F_T, f_4, f_3\}$ which overlaps as shown in Figure 3.11 (right), when cut along the thick line of $P_A(n)$ in Figure 3.11 (left). herefore, we can obtain the following lemma.

Lemma 3.9. *For $n \geq 19$, if we cut the edges (t_1, b_1) and (b_1, b_2) and do not cut the edges (t_0, t_1), (b_0, b_1), (t_0, b_1), (t_1, t_2), and (t_1, b_2) of $P_A(n)$, any edge unfolding is overlapping.*

Figure 3.12 shows a part of edge unfolding consisting of $\{F_B, f_1, f_2, F_T, f_4, f_3\}$, and an enlarged and simplified version shown in Figure A.35 of Appendix A.3. We define t_i^T and b_i^B for $i \in \{0 \ldots n-1\}$ as vertices on F_T and F_B in the edge unfolding such that they are t_i and b_i in $P_A(n)$, respectively. Let S be a subset of faces $\{f_0, \ldots, f_{2n-1}\}$. The vertices t_i and b_i are vertices in $P_A(n)$ that are shared by S in the edge unfolding are denoted as t_i^S and b_i^S, respectively. Here, we set $b_1^{f_3}$ and t_1^T as $(0, 0)$ and $(-1, 0)$ in the plane, respectively. We can obtain the following lemma.

Lemma 3.10.

(i) *Point b_1^B exists in the third quadrant.*

(ii) *The y-coordinate of point b_2^B is positive.*

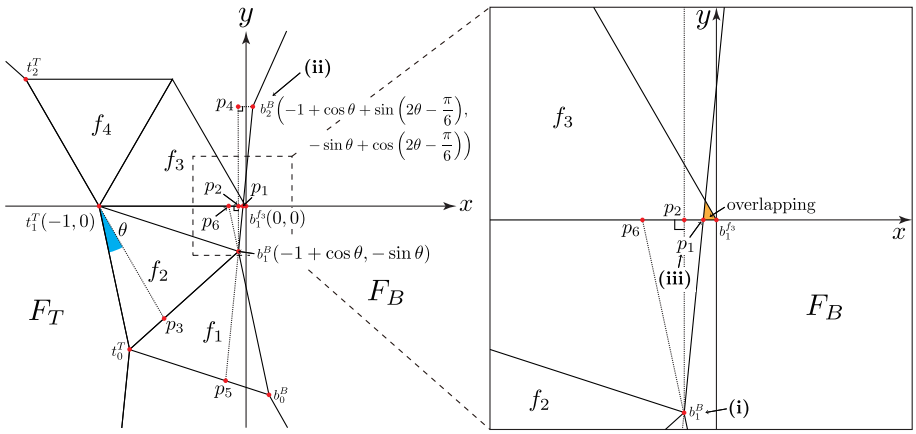

(a) The case for $19 \leq n \leq 24$

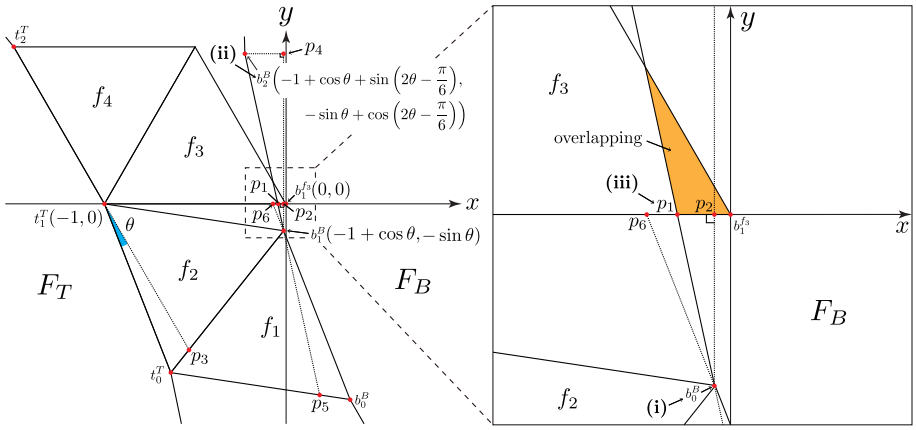

(b) The case for $n \geq 25$

Figure 3.12: Magnified image of overlapping areas in the edge unfolding of $P_A(n)$.

(iii) *Let p_1 be an intersection point of the segment $b_1^B b_2^B$ and the x-axis. The x-coordinate of point p_1 is greater than -1 and less than 0.*

Face f_3 is a triangle such that the bottom is $(-1, 0)$ to $(0, 0)$. From Lemma 3.10 (i) and (ii), there exists an intersection point p_1 of the segment $b_1^B b_2^B$ and the x-axis. Moreover, if p_1 is within $(-1, 0)$ to $(0, 0)$, the line segment $b_1^B b_2^B$ intersects f_3; that is, f_3 and F_B overlap.

We define the angle $\theta = 2\pi/n$ as the exterior angle of the regular n-sided polygon. The range of θ is $0 < \theta \leq 2\pi/19$ because $n \geq 19$. We obtain the following claim. See the details of the proofs in Appendix C.3.

Claim 3.11. *The coordinates of b_1^B and b_2^B are $(-1 + \cos\theta, -\sin\theta)$, $(-1 + \cos\theta + \sin(2\theta - \pi/6), -\sin\theta + \cos(2\theta - \pi/6))$, respectively. The x-coordinate of p_1 is $(\cos(\pi/6 - \theta)/\cos(2\theta - \pi/6)) - 1$.*

From Claim 3.11 and differential analysis, we can show Lemma 3.10 (i) - (iii). See the details of the proofs in Appendix C.4.

With these established, Lemma 3.10 (i) - (iii) hold; that is, an overlapping edge unfolding exists for $P_A(n)$, where $n \geq 19$.

3.3 Overlapping lattice unfolding for cuboid

Here, we present the following theorem for cuboids:

Theorem 3.12.

- *Both the* $(1, 1, 1)$*-cuboid and* $(\sqrt{2}, \sqrt{2}, \sqrt{2})$*-cuboid have no overlapping lattice unfolding.*
- *The* $(1, 1, 2)$*-cuboid has neither faces-in-touch lattice unfolding nor edges-in-touch lattice unfolding, but it has a vertices-in-touch lattice unfolding.*
- *Both the* $(1, 2, 2)$*-cuboid and* $(2, 2, 2)$*-cuboid have no faces-in-touch lattice unfolding, but they have edges-in-touch lattice unfoldings and vertices-in-touch lattice unfoldings.*
- *Any other type of cuboids have faces-in-touch lattice unfoldings, edges-in-touch lattice unfoldings, and vertices-in-touch lattice unfoldings.*

Hereafter, we explain the non-existence side of Theorem 3.12 in Section 3.3.1 and the existence side in Section 3.3.2.

3.3.1 Method to check for the non-existence of overlapping lattice unfoldings

First, we show a method to check the non-existence of overlapping lattice unfoldings through a computational experiment using rotational unfolding. However, using rotational unfolding directly for lattice unfolding is inefficient for the search. In this section, we present the method of extending rotational unfolding to lattice unfolding and the results of computational experiments.

In the rotational unfolding for polyhedron Q, we use the dual graph G_D. Therefore, since we are considering the lattice unfolding of a cuboid C, we consider the dual graph G_{DC} of G_C, where cuboid C is viewed as a graph. In rotational unfolding, we efficiently search for overlaps by enumerating MOPEs in the polyhedron Q. Similarly, by applying rotational unfolding to cuboids, we can enumerate overlapping partial lattice unfoldings. However, among these overlapping partial lattice unfoldings, there are non-minimal overlapping partial lattice unfoldings (non-MOPLs), as shown in Figure 3.13. Including partial lattice unfoldings that are non-MOPLs reduces the efficiency of checking for the existence of overlapping lattice unfoldings. To address this, we introduce the following characteristics to provide information about the "direction of rolling when viewed from one step before":

R: Roll to the right from one step before.

C: Roll straight from one step before.

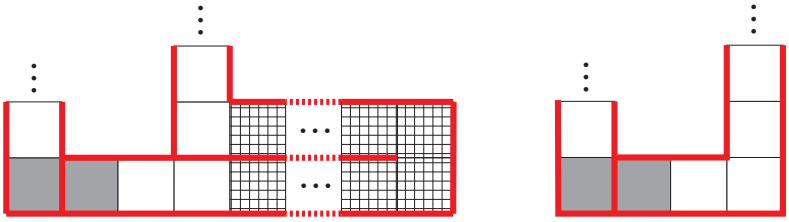

(a) Non-MOPL **(b)** MOPL

Figure 3.13: Examples of partial lattice unfoldings obtained using rotational unfolding directly. Removing the plaid faces in (a) results in (b)'s MOPL.

(a) "CCRCL" **(b)** "CLRRCRLLC"

Figure 3.14: Examples of strings corresponding to partial lattice unfoldings.

L: Roll to the left from one step before.

Therefore, the partial lattice unfolding obtained directly using the rotational unfolding can be represented as a string (see example in Figure 3.14). In the rotational unfolding, the first step is to roll straight ahead without loss of generality, so the string corresponding to the partial lattice unfolding obtained in the first step is "C." Here, we can show the following lemma:

Lemma 3.13. *When the strings corresponding to the partial lattice unfoldings include "RR" or "LL", they are non-MOPLs.*

Proof. In the second step of the rotational unfolding, we have three cases: (1) rolling to the right ("CR"; Figure 3.15 (a)), (2) rolling straight ("CC"; Figure 3.15 (b)), and (3) rolling to the left ("CL"; Figure 3.15 (c)). If we repeat the action of rolling right, or "RR", twice after the second step, we get (1) "CRRR" (Figure 3.15 (d)), (2) "CCRR" (Figure 3.15 (e)), and (3) "CLRR" (Figure 3.15 (f)). For case (1), this situation cannot occur because we have already used the face as part of the constructed partial edge unfolding. For cases (2) and (3) (Figure 3.15 (e) and Figure 3.15 (f)), these partial lattice unfoldings are non-MOPLs, and removing the plaid faces results in MOPLs Figure 3.15 (a) and Figure 3.15 (b). The same statement applies even if "RR" appears not only in the first four steps but also at any point during the rolling process. Similarly, the same can be said for "LL." □

Therefore, if "RR" or "LL" appears during rolling, it is a non-MOPL; there is no need to continue rolling, thereby pruning the search.

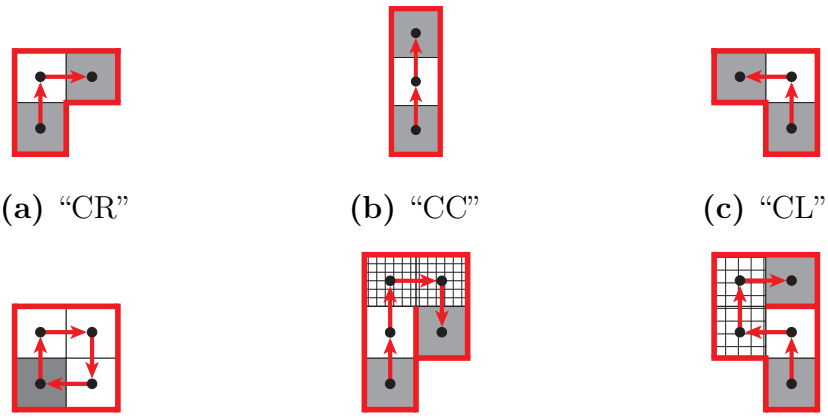

(a) "CR" **(b)** "CC" **(c)** "CL"

(d) "CRRR" **(e)** "CCRR" **(f)** "CLRR"

Figure 3.15: Examples of partial lattice unfoldings obtained through two rotations and a double right rotation. (a)-(c): Lattice unfoldings from two rotations. (d)-(f): Lattice unfoldings with an additional double right roll after two rotations.

When a cuboid has an overlapping lattice unfolding, we can determine how they overlap using the following claim:

Claim 3.14. *In rotational unfolding, compute the center coordinates of the face at one endpoint, assuming its center coordinates are* $(0, 0)$ *(see Figure 3.16 (a)). Then, while rolling the cuboid sequentially, compute the center coordinates of the face at the other endpoint in the partial lattice unfolding. We can determine the type of unfolding based on the coordinates of the center of the face at the other endpoint:*

- *If the coordinates are* $(0, 0)$*, it is a faces-in-touch unfolding (a plaid face in Figure 3.16 (b)).*
- *If the coordinates are* $(0, 1)$*,* $(-1, 0)$*, or* $(0, -1)$*, it is an edges-in-touching unfolding (polka dot faces in Figure 3.16 (b)).*
- *If the coordinates are* $(1, 1)$*,* $(1, -1)$*,* $(-1, -1)$*, or* $(-1, 1)$*, it is a vertices-in-touch unfolding (striped faces in Figure 3.16 (b)).*

We implemented the method of extending rotational unfolding to lattice unfolding and obtained the non-existence results shown in Theorem 3.12. Table 3.4 to 3.6 show the running times of computational experiments for each type of lattice cuboid. These experiment results include verifying the previous results [Hea18] and [Sug18].

3.3.2 Proving the existence of overlapping lattice unfoldings

Hereafter, we prove the existence side of the statements of Theorem 3.12 by showing specific overlapping unfoldings.

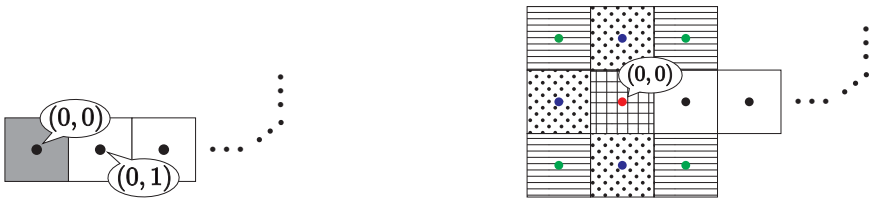

(a) The coordinates of the center of each face

(b) The coordinates of the center of the face at the other endpoint

Figure 3.16: A method for checking overlap in rotational unfoldings and identifying their types.

Table 3.4: The running time to check the non-existence of faces-in-touch unfoldings.

Lattice cuboid	$\|F\|$	$\|E\|$	$\|V\|$	Time
$(1, 1, 1)$-cuboid	6	12	8	0m0.056s
$(1, 1, 2)$-cuboid	10	20	12	0m0.106s
$(1, 2, 2)$-cuboid	16	32	18	0m1.187s
$(2, 2, 2)$-cuboid	24	48	26	0m50.757s
$(\sqrt{2}, \sqrt{2}, \sqrt{2})$-cuboid	12	24	14	0m1.009s

Table 3.5: The running time to check the non-existence of edges-in-touch unfoldings.

Lattice cuboid	$\|F\|$	$\|E\|$	$\|V\|$	Time
$(1, 1, 1)$-cuboid	6	12	8	0m0.051s
$(1, 1, 2)$-cuboid	10	20	12	0m0.132s
$(\sqrt{2}, \sqrt{2}, \sqrt{2})$-cuboid	12	24	14	0m1.021s

Table 3.6: The running time to check the non-existence of vertices-in-touch unfoldings.

Lattice cuboid	$\|F\|$	$\|E\|$	$\|V\|$	Time
$(1, 1, 1)$-cuboid	6	12	8	0m0.053s
$(\sqrt{2}, \sqrt{2}, \sqrt{2})$-cuboid	12	24	14	0m1.098s

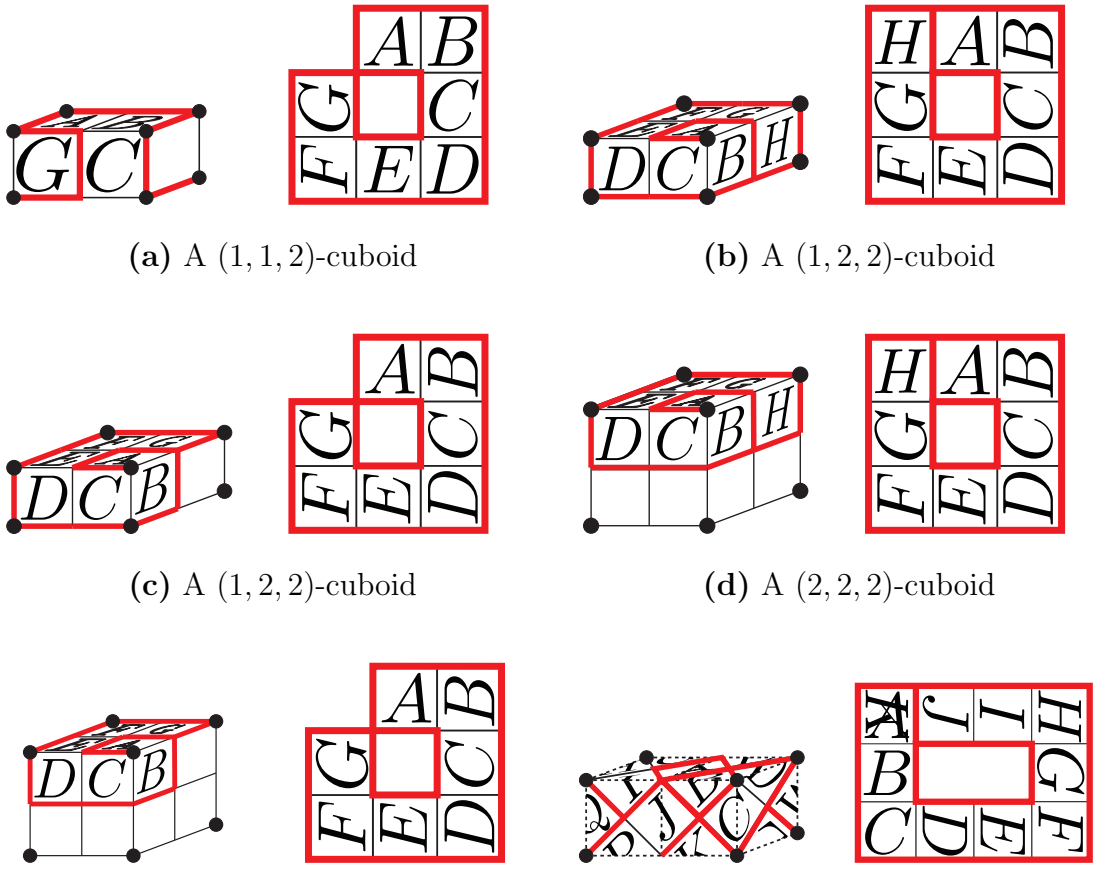

(a) A $(1, 1, 2)$-cuboid **(b)** A $(1, 2, 2)$-cuboid

(c) A $(1, 2, 2)$-cuboid **(d)** A $(2, 2, 2)$-cuboid

(e) A $(2, 2, 2)$-cuboid **(f)** A $(\sqrt{2}, \sqrt{2}, 2\sqrt{2})$-cuboid

Figure 3.17: Overlapping partial lattice unfoldings for $L = 1$ and $\sqrt{2}$. Cut along the red lines on the left cuboid to obtain the right unfoldings.

Case of $L = 1$

From Theorems 1.3 and 1.4, faces-in-touch, edges-in-touch, and vertices-in-touch unfoldings exist for the (x, y, z)-cuboid, where $z \geq 3$. For the remaining cases for the case of $L = 1$, we provide specific examples of unfoldings as follows:

Lemma 3.15.

- *The $(1, 1, 2)$-cuboid has a vertices-in-touch unfolding (Figure 3.17 (a)).*
- *The $(1, 2, 2)$-cuboid has both an edges-in-touch unfolding (Figure 3.17 (b)) and a vertices-in-touch unfolding (Figure 3.17 (c)).*
- *The $(2, 2, 2)$-cuboid has both an edges-in-touch unfolding (Figure 3.17 (d)) and a vertices-in-touch unfolding (Figure 3.17 (e)).*

Case of $L = \sqrt{2}$, $L = \sqrt{5}$, and $L = \sqrt{10}$

From the inclusion relationship between the edges-in-touch and vertices-in-touch unfolding, we have only to show the existence of the faces-in-touch unfolding.

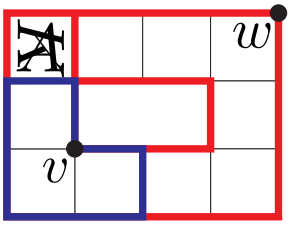

Figure 3.18: Overlapping partial lattice unfolding Q_L.

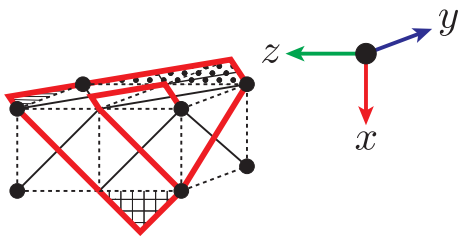

Figure 3.19: Embedding of Q_L in the three front-facing faces of the $(\sqrt{2}, \sqrt{2}, 2\sqrt{2})$-cuboid.

A faces-in-touch unfolding exist for the $(\sqrt{2}, \sqrt{2}, 2\sqrt{2})$-cuboid (Figure 3.17 (f)). From now on, we call this partial lattice unfolding as Q_L (Figure 3.18). Moreover, the $(\sqrt{2}, \sqrt{2}, 2\sqrt{2})$-cuboid can be unfolded to include the partial lattice unfolding Q_L because Q_L can be embedded in the three faces in front of the $(\sqrt{2}, \sqrt{2}, 2\sqrt{2})$-cuboid (see Figure 3.19). Note that we have to fold the three triangular faces: a plaid face in the positive y-axis direction, a polka dot face in the positive direction of the x-axis direction, and a striped face in the positive direction of the x-axis direction. This embedding method can also be applied to the $(x\sqrt{2}, y\sqrt{2}, z\sqrt{2})$-cuboid, where $x, y, z \geq 2$, as shown in Figure 3.20.

The same embedding can be performed for cases where $L = \sqrt{5}$ and $L = \sqrt{10}$ (see Figure 3.21 (a) and (b)).

Case of $L \geq \sqrt{13}$

The partial lattice unfolding Q_L can be embedded in the $(\sqrt{13}, \sqrt{13}, \sqrt{13})$-

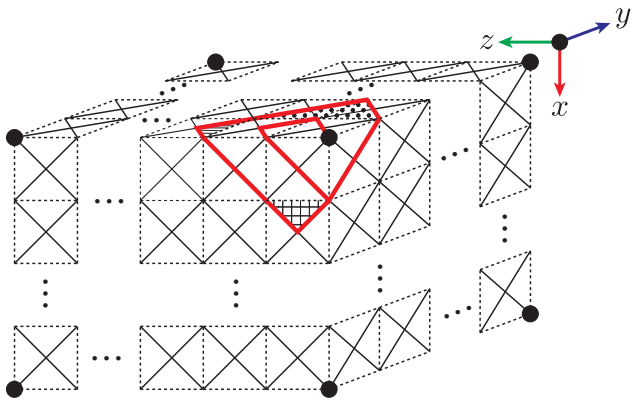

Figure 3.20: Embedding of Q_L in the $(x\sqrt{2}, y\sqrt{2}, z\sqrt{2})$-cuboid, with $z \geq 2$.

cuboid, as shown in Figure 3.21 (c). Here, we present the following lemma:

Lemma 3.16. *The partial lattice unfolding Q_L can be embedded in the (L, L, L)-cuboid, where $L \geq \sqrt{13}$.*

Proof. Consider the three unit squares with vertex v in common (Figure 3.21 (d)). The three-unit squares enclosed in blue in Figure 3.18 can be embedded in this point. Let S be the side face of a cone with the length of axis $\sqrt{13}$ and a central angle of 270° (Figure 3.22). Hereafter, S is called the *cone*. Since the central angle of the cone S is 270°, the three unit squares enclosed in blue in Figure 3.18 can be embedded with vertex v coinciding. Additionally, due to the Euclidean distance between the point v and the furthest point w in Figure 3.18 being $\sqrt{2^2 + 3^2} = \sqrt{13}$, the remaining faces, except for the three faces enclosed in blue, can be embedded as shown in Figure 3.22 (right). The cone S can be embedded in the three front faces of a (L, L, L)-cuboid where $L \geq \sqrt{13}$, as shown in Figure 3.23. From the fact that the cone S can be embedded in a (L, L, L)-cuboid and that Q_L can be embedded on top of the cone S, we can concluded that Q_L can be embedded in the three front faces of a (L, L, L)-cuboid. □

From this lemma, a faces-in-touch unfolding exists for the (xL, yL, zL)-cuboid in any of the x, y, z, where $L \geq \sqrt{13}$. The same can be said for edges-in-touch and vertices-in-touch unfolding due to the inclusion relationship.

3.4 Summary and discussion on overlapping unfoldings

In this chapter, we showed results on the existence of overlapping unfoldings in edge unfoldings of convex regular-faced polyhedra, as well as in lattice unfoldings of cuboids.

First, we proposed a rotational unfolding algorithm to determine whether a given polyhedron has overlapping edge unfoldings. The key idea of this algorithm is to focus on paths instead of spanning trees of edge unfoldings. Additionally, by using pruning methods according to the symmetry and distances, the search becomes more efficient. Applying this algorithm allowed us to confirm the existence of overlapping edge unfoldings for all Archimedean solids and Johnson solids. In addition, by combining this algorithm with analytical techniques, we clarified the conditions under which Archimedean prisms and antiprisms admit overlapping edge unfoldings.

Next, we applied a similar idea to the lattice unfoldings of cuboids. By extending the rotational unfolding, we confirmed that certain cuboids of specific sizes do not have particular types of overlapping lattice unfoldings. Furthermore, by using an embedding technique for specific lattice unfoldings, we showed that cuboids exceeding certain sizes have faces-in-touch, edges-in-touch, and vertices-in-touch unfoldings.

On the other hand, this study only considered polyhedra where all edges have the same length. As a future direction, it would be interesting to explore cases where some edges have different lengths.

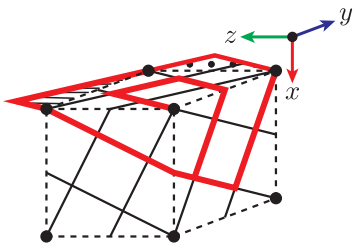

(a) The $(\sqrt{5}, \sqrt{5}, \sqrt{5})$-cuboid

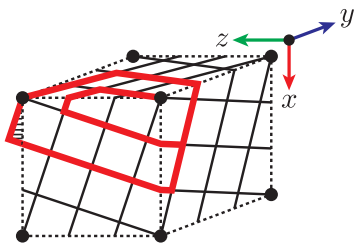

(b) The $(\sqrt{10}, \sqrt{10}, \sqrt{10})$-cuboid

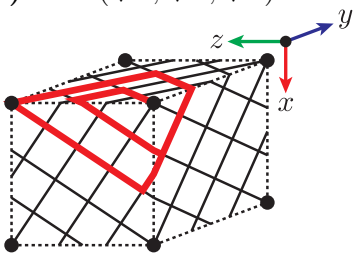

(c) The $(\sqrt{13}, \sqrt{13}, \sqrt{13})$-cuboid

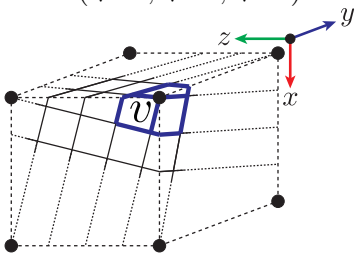

(d) The (L, L, L)-cuboid $(L \geq \sqrt{13})$

Figure 3.21: Embedding of Q_L in each cuboid.

Figure 3.22: The side face of a cone with an axis length of $\sqrt{13}$ and a central angle of 270°. Rounding the left fan shape yields the solid on the right, where Q_L can be embedded.

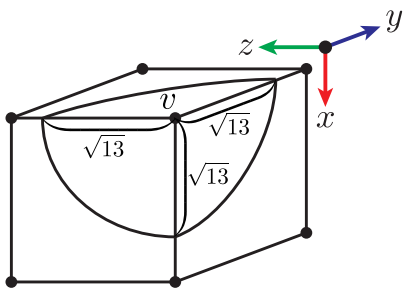

Figure 3.23: Embedding of the cone S in the three front-facing faces of the (L, L, L)-cuboid, where $L \geq \sqrt{13}$.

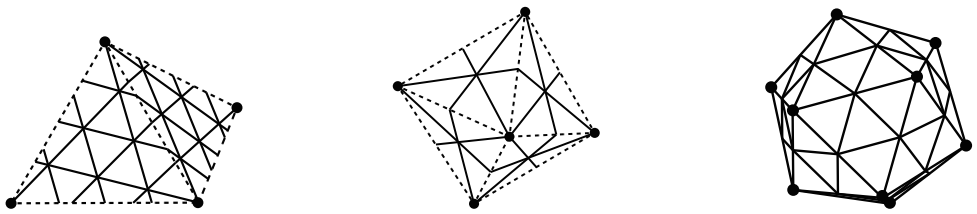

(a) Lattice tehrahedron

(b) Lattice octahedron

(c) Lattice icosahedron

Figure 3.24: Examples of Platonic solids formed from a triangular lattice.

For example, as shown in Figure 1.2, if the height of a regular n-gonal prism is increased or decreased from one, overlapping unfoldings may exist even when $n \leq 24$. From this observation, the following open problem can be considered:

Open problem 3.17. *Consider a regular n-gonal prism with height h, where the top and bottom faces are regular n-gons. Determine the values of n and h for which the prism has an overlapping edge unfolding.*

Similarly, the following open problem can be posed for antiprisms:

Open problem 3.18. *Consider a regular m-gonal antiprism with height h, where the top and bottom faces are regular m-gons. Determine the values of m and h for which the antiprism has an overlapping edge unfolding.*

In this study, we focused on cutting cuboids along a square lattice. However, as shown in Figure 3.24, we can also consider unfoldings of lattice tetrahedra, lattice octahedra, and lattice icosahedra along a triangular lattice. According to [KSU24], a tetrahedron never has a faces-in-touch unfolding, regardless of how it is unfolded. Thus, the contrast between unfoldings of tetrahedra on a triangular lattice and cuboids on a square lattice is interesting.

Chapter 4

The number of non-overlapping unfoldings in convex polyhedra

4.1 Counting algorithm for the number of non-overlapping unfoldings

In this section, we describe an algorithm for counting the number of non-overlapping unfoldings of a given polyhedron. From Lemmas 2.1 and 2.3, the number of unfoldings can be obtained by counting the number of cutting lines. The number of cutting trees can be counted by constructing a ZDD $\mathcal{Z}_{\mathcal{T}}$ [KIIM17]. However, for polyhedra where unfolding along specific cutting lines results in overlapping unfoldings, $\mathcal{Z}_{\mathcal{T}}$ includes these overlapping unfoldings. To efficiently remove the overlapping unfoldings, we use the *subsetting method*, an operation over ZDDs [IM13]. The subsetting method constructs a new ZDD $\mathcal{Z}_{\mathcal{N}}$ by extracting the family of sets that satisfy the constraint $\mathcal{C}$ from ZDD $\mathcal{Z}$.

We now present a method for removing overlapping unfoldings using the subsetting method. Hereafter, we call both MOPEs and MOPLs collectively as *minimal overlapping partial unfoldings (MOPUs)*. As described in Section 3.1, MOPUs can be enumerated using rotational unfolding. For a (partial) unfolding U, let $NC[U]$ be the set of edges that are not cut when unfolding the polyhedron. The following lemma holds for any MOPU M_i $(0 \leq i \leq k)$, where k is the number of MOPUs.

Lemma 4.1. *If an unfolding U satisfies $NC[M_i] \subseteq NC[U]$, then U is an overlapping unfolding.*

Proof. Let the sequence of faces in MOPU M_i be $f_1, f_2, \ldots, f_\ell$, and let e_j be the edge shared between each pair of adjacent faces f_j and f_{j+1} (where the faces f_1 and f_ℓ overlap). Since $NC[M_i]$ represents the set of uncut edges in the partial unfolding M_i, we can write $NC[M_i] = \{e_1, e_2, \ldots, e_{\ell-1}\}$. On the other hand, from the condition $NC[M_i] \subseteq NC[U]$, it follows that the set $e_1, e_2, \ldots, e_{\ell-1}$ must be included in the unfolding U. Therefore, the sequence of faces $f_1, f_2, \ldots, f_\ell$ appears in U, indicating that U has overlaps. □

From Lemma 4.1, removing the family of sets $\mathcal{U}_i$ (which represents unfoldings containing the MOPU M_i) from the ZDD $\mathcal{Z}_{\mathcal{T}}$ yields a ZDD that represents only

non-overlapping unfoldings that do not include the structure of M_i. On the other hand, to construct the family of sets $\mathcal{U}_i$ representing unfoldings that include MOPU M_i, we need a ZDD representing the family of spanning trees that contain $NC[M_i]$. However, by applying the following lemma, we can create a simpler ZDD.

Lemma 4.2. *Given the family of sets $\mathcal{Z}_\mathcal{T}$ representing all unfoldings, the following conditions are equivalent:*

(1) *The family of sets obtained by removing the unfoldings that include MOPU M_i from $\mathcal{Z}_\mathcal{T}$.*

(2) *The family of sets obtained by removing the family $\mathcal{F}_i = NC[M_i] \cup E' \mid E' \subseteq E \setminus NC[M_i]$, which contains all subsets that include $NC[M_i]$, from $\mathcal{Z}_\mathcal{T}$.*

Proof. From the condition, we know that $\mathcal{U}_i \subseteq \mathcal{F}_i$. Now, if we define $\mathcal{N}_i = \mathcal{F}_i \setminus \mathcal{U}_i$, then $\mathcal{N}_i$ contains no sets that represent unfoldings, meaning $\mathcal{N}_i \not\subseteq \mathcal{Z}_\mathcal{T}$. Therefore, we have the following equivalence:

$$\mathcal{Z}_\mathcal{T} \setminus \mathcal{F}_i = \mathcal{Z}_\mathcal{T} \setminus (\mathcal{N}_i \cup \mathcal{U}_i) = \mathcal{Z}_\mathcal{T} \setminus \mathcal{U}_i,$$

which completes the proof. □

Therefore, we can construct a ZDD that represents non-overlapping unfoldings by following these steps:

Step 1. Construct the ZDD $\mathcal{Z}_\mathcal{T}$ that represents all possible unfoldings.

Step 2. For each i $(0 \leq i \leq k)$, construct a ZDD $\mathcal{F}_i$ representing the family of all sets containing every element of $NC[M_i]$.

Step 3. Apply the subsetting method on $\mathcal{Z}_\mathcal{T}$ using the constraints from each $\mathcal{F}_i$, to construct a ZDD $\mathcal{Z}_\mathcal{N}$ that excludes MOPUs M_1 through M_k.

4.2 Computational experiments on counting nonoverlapping unfoldings

Here, we present the results of applying the algorithm for counting non-overlapping unfoldings to the edge unfoldings of convex regular-faced polyhedra and the lattice unfoldings of cuboids. We used the TdZdd library[1] to construct the ZDD $\mathcal{Z}_\mathcal{T}$, which represents all unfoldings, the ZDD $\mathcal{F}_i$, which represents the family of sets containing all elements of $NC[M_i]$, and applied the subsetting method. The experiments were conducted under the same conditions as described in Section 3.2. The rotational unfolding method was used to enumerate MOPUs for the convex regular-faced polyhedra, Johnson solids, Archimedean (anti)prisms, and lattice cuboids.

[1] `https://github.com/kunisura/TdZdd`

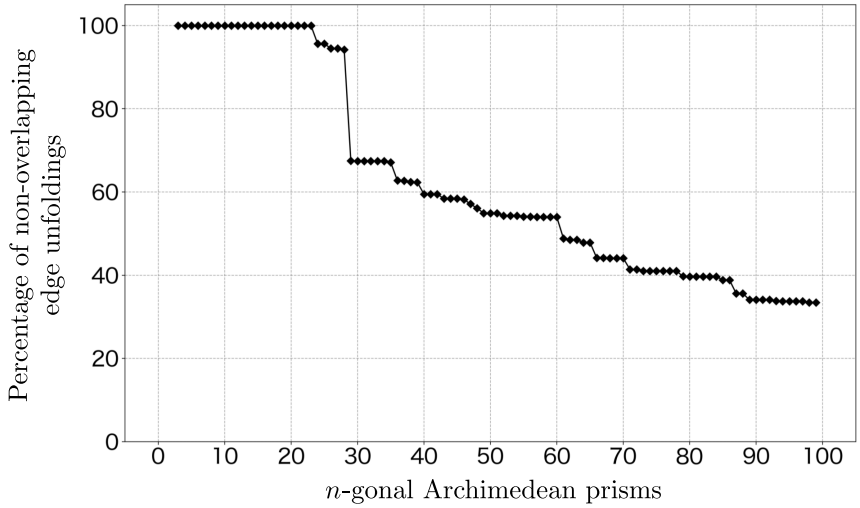

Figure 4.1: The percentage of non-overlapping edge unfoldings in Archimedean prisms.

4.2.1 The number of non-overlapping edge unfoldings for convex regular-faced polyhedra

Tables 4.1 to 4.4 show the results of counting the number of non-overlapping edge unfoldings and the percentage of non-overlapping unfoldings among all edge unfoldings, for Archimedean solids, Johnson solids, Archimedean prisms, and Archimedean antiprisms, respectively. Figures 4.1 and 4.2 show line graphs with the values of n for Archimedean n-gonal prisms and the values of m for Archimedean m-gonal antiprisms on the horizontal axis, and the percentage of non-overlapping edge unfoldings on the vertical axis.

From the results of these experiments, we can find the following. First, let's compare the truncated icosahedron and the truncated dodecahedron in Archimedean solids (Table 4.1). Both polyhedra have the same number of vertices, edges, and faces, the truncated icosahedron has more MOPUs. However, the truncated dodecahedron has a lower percentage of non-overlapping edge unfoldings. The MOPUs in the truncated icosahedron consist of eight or nine faces (Figure 1.3 (b) and Figure 3.4). On the other hand, the MOPU in the truncated dodecahedron includes only 4 faces (Figure 1.3 (a)).

Next, for Archimedean n-gonal prisms, there is an approximate 26% decrease in the percentage of non-overlapping edge unfoldings when n increases from 28 to 29. For $n = 28$, there are three types of MOPUs, consisting of six, seven, or eight faces (Figure 4.3). For $n = 29$, there are five types of MOPUs, three of which are the same as for $n = 28$, and the other two consist of four faces (Figure 4.4).

Similarly, for Archimedean m-gonal antiprisms, there is an approximate 70% decrease in the percentage of non-overlapping edge unfoldings when m increases from 17 to 18. For $m = 17$, there are two types of MOPUs, both consisting of eight faces (Figure 4.5). For $m = 18$, there are five types of MOPUs, two of which are the same as for $m = 17$, and the other three consist of six faces (Figure 4.6).

Table 4.1: The number and percentage of non-overlapping edge unfoldings for Archimedean solids.

Archimedean solids	$\|V\|$	$\|E\|$	$\|F\|$	#(MOPU)	#(Edge unfolding)	$\#\begin{pmatrix}\text{Non-overlapping}\\ \text{edge unfolding}\end{pmatrix}$	Pct.(%)
Snub cube	24	60	38	72	89,904,012,853,248	85,967,688,920,076	95.62
Truncated dodecahedron	60	90	32	120	4,982,259,375,000,000,000	1,173,681,002,295,455,040	23.56
Truncated icosahedron	60	90	32	240	375,291,866,372,898,816,000	371,723,160,733,469,233,260	99.05
Rhombicosidodecahedron	60	120	62	-	201,550,864,919,150,779,950,956,544,000	-	-
Snub dodecahedron	60	150	92	-	438,201,295,386,966,498,858,139,607,040,000,000	-	-
Rhombitruncated icosidodecahedron	120	180	62	-	21,789,262,703,685,125,511,464,767,107,171,876,864,000	-	-

Table 4.2: The number and percentage of non-overlapping edge unfoldings for Johnson solids. The timeout was set to 28,800 minutes (20 days).

Johnson solids	$\|V\|$	$\|E\|$	$\|F\|$	#(MOPU)	#(Edge unfolding)	$\#\begin{pmatrix}\text{Non-overlapping}\\ \text{edge unfolding}\end{pmatrix}$	Pct.(%)
J20	25	45	22	40	29,821,320,745	27,158,087,415	91.07
J21	30	55	27	90	8,223,103,375,490	6,297,186,667,720	76.58
J24	25	55	6	60	5,996,600,870,820	5,492,624,228,190	91.60
J25	30	65	24	240	1,702,422,879,696,000	947,565,833,513,130	55.66
J32	25	50	27	20	699,537,024,120	699,433,603,320	99.99
J33	25	50	27	20	745,208,449,920	745,105,029,120	99.99
J34	30	60	32	20	193,003,269,869,040	190,653,702,525,040	98.78
J38	30	60	32	80	270,745,016,304,350	214,085,775,357,270	79.07
J39	30	60	32	80	272,026,496,000,000	215,087,798,524,180	79.07
J40	35	70	37	320	75,378,202,163,880,700	45,541,858,035,543,690	60.42
J41	35	70	37	320	75,804,411,381,317,500	45,774,968,967,924,850	60.39
J42	40	80	42	1,480	20,969,865,292,417,385,400	8,873,953,322,249,583,330	42.32
J43	40	80	42	1,400	21,115,350,368,078,435,000	8,884,490,741,507,534,860	42.08
J44	18	42	26	24	5,295,528,588	5,231,781,954	98.80
J45	24	56	34	48	13,769,880,349,680	13,386,219,088,644	97.21
J46	30	70	42	170	32,543,644,773,848,180	25,553,553,814,333,235	78.52
J47	35	80	47	1,175	9,324,488,558,669,593,960	4,135,578,144,180,583,965	44.35
J48	40	90	52	7,290	2,670,159,599,304,760,178,000	-	-
J54	13	22	11	4	75,973	75,749	99.71
J55	14	26	14	8	709,632	705,144	99.37
J56	14	26	14	8	707,232	702,520	99.33
J57	15	30	17	12	6,531,840	6,457,860	98.87
J58	21	35	16	10	92,724,962	92,219,782	99.46
J59	22	40	20	20	1,651,482,010	1,632,941,030	98.88
J60	22	40	20	20	1,641,317,568	1,621,738,522	98.81
J61	23	45	24	30	28,745,798,400	28,183,512,978	98.04
J66	28	48	22	104	54,921,311,280	39,055,563,000	71.11
J67	32	60	30	208	90,974,647,120,896	43,437,626,181,464	47.75
J68	65	105	42	-	68,495,843,558,495,480,625,000	-	-
J69	70	120	52	-	936,988,158,859,771,579,003,317,600	-	-
J70	70	120	52	-	930,303,529,996,712,062,599,302,400	-	-
J71	75	135	62	-	12,479,653,904,364,665,921,377,091,740,032	-	-
J72	60	120	62	-	206,686,735,580,507,426,149,463,308,960	-	-
J73	60	120	62	-	211,950,222,127,067,401,293,093,928,960	-	-
J74	60	120	62	-	211,595,653,377,414,999,219,839,524,608	-	-
J75	60	120	62	-	216,255,817,875,464,148,759,178,607,616	-	-
J76	55	105	52	-	21,081,520,904,394,872,104,529,280	-	-
J77	55	105	52	-	21,635,458,027,234,604,842,992,000	-	-
J78	55	105	52	-	21,638,184,348,166,814,636,938,752	-	-
J79	55	105	52	-	22,171,247,351,297,062,278,807,776	-	-
J80	50	90	42	-	2,163,645,669,729,922,583,040	-	-
J81	50	90	42	-	2,094,253,294,125,015,611,392	-	-
J82	50	90	42	-	2,151,245,812,763,713,106,752	-	-
J83	45	75	32	1,260	197,148,908,795,401,104	143,844,293,105,396,598	72,96

Table 4.3: The number and percentage of non-overlapping edge unfoldings for Archimedean prisms.

n-prisms	$\|V\|$	$\|E\|$	$\|F\|$	#(MOPU)	#(Edge unfolding)	#(Non-overlapping edge unfolding)	Pct.(%)
24-prism	48	72	26	96	639,620,518,118,400	611,750,144,604,960	95.64
25-prism	50	75	27	100	2,486,558,615,814,025	2,378,211,063,753,525	95.64
26-prism	52	78	28	208	9,651,161,613,824,796	9,120,749,762,911,540	94.50
27-prism	54	81	29	216	37,403,957,244,654,675	35,348,297,730,550,335	94.50
28-prism	56	84	30	336	144,763,597,316,784,768	136,369,030,045,792,768	94.20
29-prism	58	87	31	580	559,560,282,425,278,229	377,763,966,359,384,333	67.51
30-prism	60	90	32	720	2,160,318,004,043,512,500	1,457,228,998,699,944,660	67.45
31-prism	62	93	33	744	8,331,163,769,982,715,231	5,619,734,416,791,278,823	67.45
32-prism	64	96	34	768	32,095,304,749,163,937,792	21,649,687,090,073,296,384	67.45
33-prism	66	99	35	792	123,524,473,883,545,449,825	83,322,661,319,000,341,161	67.45
34-prism	68	102	36	952	474,969,297,739,230,927,564	320,315,730,957,505,974,740	67.43
35-prism	70	105	37	1,120	1,824,745,126,233,358,110,635	1,224,788,877,353,311,603,655	67.12
36-prism	72	108	38	1,440	7,004,614,136,879,907,849,600	4,397,626,384,555,854,813,048	62.78
37-prism	74	111	39	1,776	26,867,730,730,869,118,775,917	16,841,247,868,506,593,664,113	62.68
38-prism	76	114	40	2,128	102,981,783,095,242,242,871,908	64,245,596,838,412,691,619,868	62.39
39-prism	78	117	41	2,496	394,447,279,575,099,709,694,775	245,972,761,433,859,004,882,155	62.36
40-prism	80	120	42	2,880	1,509,843,372,596,510,348,221,440	898,435,929,860,914,751,335,120	59.51
41-prism	82	123	43	3,116	5,775,682,482,451,356,835,464,761	3,436,774,701,162,733,316,551,373	59.50
42-prism	84	126	44	3,360	22,080,875,606,379,223,850,418,300	13,138,720,470,258,404,605,154,004	59.50
43-prism	86	129	45	3,784	84,369,019,868,106,350,841,057,283	49,292,119,107,345,418,821,464,335	58.42
44-prism	88	132	46	3,872	322,192,014,517,039,121,756,425,344	188,238,848,570,683,472,535,311,712	58.42
45-prism	90	135	47	3,960	1,229,765,080,878,981,092,880,253,125	718,483,241,070,056,103,676,962,705	58.42
46-prism	92	138	48	4,600	4,691,535,669,063,616,134,304,408,596	2,731,490,668,982,448,941,464,299,772	58.22
47-prism	94	141	49	5,076	17,889,680,992,955,476,025,801,057,807	10,224,003,439,425,442,252,695,897,017	57.15
48-prism	96	144	50	5,760	68,185,734,533,013,527,410,214,707,200	38,248,653,878,322,746,431,035,217,728	56.09
49-prism	98	147	51	6,664	259,774,138,662,539,598,798,853,632,529	142,720,047,356,681,793,679,714,971,049	54.94
50-prism	100	150	52	7,400	989,275,799,980,653,489,079,068,384,300	543,491,856,931,615,421,592,902,162,300	54.94
51-prism	102	153	53	7,752	3,765,868,099,190,667,877,509,098,288,475	2,068,859,848,320,328,618,349,489,286,879	54.94
52-prism	104	156	54	8,320	14,329,987,768,640,883,479,630,169,743,232	7,785,152,064,553,875,176,792,718,269,152	54.33
53-prism	106	159	55	8,904	54,508,708,624,877,734,355,711,282,194,973	29,613,250,778,119,135,586,129,657,023,707	54.33
54-prism	108	162	56	9,504	207,267,558,157,030,661,743,340,920,104,900	112,603,308,544,085,153,945,426,983,878,660	54.33
55-prism	110	165	57	10,120	787,857,744,058,382,475,503,456,540,986,855	425,875,823,447,530,794,507,732,415,080,195	54.05
56-prism	112	168	58	10,528	2,993,785,586,870,888,884,013,575,853,822,976	1,618,161,634,602,851,785,742,807,896,140,064	54.05
57-prism	114	171	59	10,944	11,372,477,058,547,594,072,637,405,171,464,425	6,144,514,101,474,823,054,337,696,869,965,123	54.03
58-prism	116	174	60	11,832	43,187,270,299,014,781,811,139,187,410,691,548	23,326,536,057,764,626,358,265,044,412,279,868	54.01
59-prism	118	177	61	12,744	163,956,002,289,170,289,778,245,356,488,769,459	88,555,357,584,032,953,873,552,819,154,790,741	54.01
60-prism	120	180	62	13,200	622,263,183,812,606,109,322,543,144,035,600,000	336,093,972,645,843,991,118,728,788,427,726,200	54.01
61-prism	122	183	63	14,396	2,361,023,114,629,354,318,988,404,829,601,017,461	1,153,365,956,554,130,834,065,584,588,770,576,537	48.85
62-prism	124	186	64	16,368	8,955,908,356,422,272,120,516,285,708,666,803,572	4,348,799,175,168,145,604,642,783,894,710,257,972	48.56
63-prism	126	189	65	17,136	33,963,000,256,261,477,807,141,098,532,312,144,575	16,471,862,499,365,318,605,626,349,567,981,855,893	48.50
64-prism	128	192	66	18,176	128,763,573,367,713,152,730,420,340,995,267,231,744	61,639,673,042,788,410,952,524,482,230,015,782,656	47.87
65-prism	130	195	67	18,720	488,060,826,065,747,443,959,964,835,220,252,662,465	233,636,801,403,179,720,910,996,973,994,228,508,855	47.87
66-prism	132	198	68	20,592	1,849,490,381,600,812,352,868,765,046,397,041,481,100	817,502,763,787,586,935,738,546,005,495,007,277,736	44.20
67-prism	134	201	69	21,172	7,006,973,770,308,488,575,706,974,966,641,609,633,547	3,096,713,246,303,000,494,444,990,880,370,568,593,743	44.19
68-prism	136	204	70	22,032	26,540,686,328,811,552,652,967,327,238,752,884,476,288	11,708,731,916,039,177,215,090,282,288,662,448,445,864	44.12
69-prism	138	207	71	23,184	100,507,824,991,680,378,240,003,224,046,430,181,592,525	44,338,599,512,338,312,952,849,566,215,445,778,264,511	44.11
70-prism	140	210	72	24,920	380,536,545,795,702,174,419,400,936,760,625,367,754,020	167,871,805,778,112,195,880,603,660,146,778,531,028,040	44.11
71-prism	142	213	73	26,128	1,440,470,033,375,554,519,683,181,104,192,641,139,543,191	596,980,870,760,277,516,010,511,111,996,499,418,929,177	41.44
72-prism	144	216	74	27,072	5,451,624,356,286,428,491,183,290,436,982,561,065,036,800	2,259,342,205,174,960,128,925,954,191,858,205,229,812,848	41.44
73-prism	146	219	75	28,616	20,628,318,790,905,383,592,284,267,890,431,520,768,956,313	8,469,990,610,622,325,272,650,976,154,778,586,597,435,431	41.06
74-prism	148	222	76	30,784	78,040,535,635,296,089,880,020,963,154,546,570,729,579,324	32,025,918,206,891,338,090,282,229,066,878,434,112,166,032	41.04
75-prism	150	225	77	32,100	295,187,071,662,987,687,788,834,025,600,273,039,376,171,875	121,137,505,659,975,371,817,128,867,759,297,593,082,123,025	41.04
76-prism	152	228	78	32,832	1,116,341,857,839,528,524,717,385,720,706,815,646,963,560,576	458,116,563,229,230,551,652,298,491,316,191,672,953,377,976	41.04
77-prism	154	231	79	34,496	4,221,063,539,073,913,152,987,956,742,195,551,512,005,068,837	1,732,009,405,771,917,690,525,457,067,579,534,620,683,321,047	41.03
78-prism	156	234	80	36,504	15,957,810,909,148,397,191,421,362,206,489,368,194,976,255,700	6,547,759,140,478,958,708,285,931,868,337,379,111,699,013,260	41.03
79-prism	158	237	81	38,236	60,318,891,360,909,981,287,537,928,032,449,270,480,051,118,959	23,966,231,512,837,756,482,429,326,605,666,856,951,504,314,983	39.73
80-prism	160	240	82	39,680	227,962,700,977,360,477,553,905,172,759,643,132,779,913,338,880	90,516,297,016,221,842,120,588,697,662,660,340,385,338,212,160	39.71
81-prism	162	243	83	40,500	861,402,987,056,617,421,633,941,618,402,777,587,646,191,546,225	341,995,341,132,294,891,175,058,139,558,428,542,441,464,210,039	39.70
82-prism	164	246	84	43,296	3,254,488,598,838,582,230,210,121,899,601,749,106,776,524,965,612	1,292,101,188,372,407,798,075,371,911,903,984,534,028,933,754,436	39.70
83-prism	166	249	85	45,152	12,294,037,740,147,518,091,413,729,519,608,692,068,340,007,484,603	4,880,994,415,535,251,356,999,865,904,928,194,228,585,240,087,219	39.70
84-prism	168	252	86	46,368	46,434,768,337,561,243,483,045,269,738,500,630,193,132,229,526,400	18,435,535,468,052,500,560,475,959,629,177,515,836,675,305,835,264	39.70
85-prism	170	255	87	48,620	175,359,973,181,486,662,638,962,060,133,459,799,581,503,709,666,685	68,136,242,011,705,283,282,291,593,247,449,255,410,135,074,971,535	38.86
86-prism	172	258	88	50,912	662,151,768,698,132,480,917,981,340,031,934,840,615,593,080,769,156	257,261,176,564,360,166,567,970,609,875,291,471,141,053,287,325,288	38.85
87-prism	174	261	89	53,940	2,499,918,741,278,642,349,615,482,066,241,598,681,934,395,700,879,175	890,564,328,098,014,416,825,940,792,706,208,682,651,794,408,576,921	35.62
88-prism	176	264	90	55,264	9,437,063,110,777,086,198,028,843,620,687,140,090,853,387,600,995,328	3,361,807,045,468,520,205,795,018,776,129,264,881,669,261,524,635,520	35.62
89-prism	178	267	91	58,384	35,619,821,719,604,700,475,856,960,433,270,363,377,351,219,128,623,689	12,147,147,750,557,166,009,277,266,446,164,341,729,697,940,171,357,263	34.10
90-prism	180	270	92	61,200	134,428,635,924,381,058,558,342,373,483,695,239,998,308,348,737,337,500	45,835,667,167,756,167,327,808,684,200,497,934,083,305,406,003,263,080	34.10
91-prism	182	273	93	62,680	507,268,882,587,101,907,135,928,966,969,950,901,239,037,550,690,556,691	172,961,693,284,074,318,802,898,801,630,921,272,808,376,171,618,605,053	34.10
92-prism	184	276	94	64,400	1,913,957,124,704,016,720,646,095,852,898,568,656,870,706,493,680,372,352	652,587,801,648,072,657,385,242,064,252,120,087,145,845,127,550,204,344	34.10
93-prism	186	279	95	66,588	7,220,626,376,739,743,204,712,927,445,165,724,589,272,091,607,783,034,325	2,440,735,263,004,787,039,318,901,058,435,443,959,679,578,395,810,067,499	33.80
94-prism	188	282	96	69,936	27,237,505,194,018,078,864,602,783,571,427,472,860,418,008,032,804,687,924	9,200,983,829,108,871,720,824,454,037,812,685,220,751,863,003,740,596,660	33.78
95-prism	190	285	97	72,960	102,733,154,885,874,285,090,022,412,414,655,338,630,173,029,721,095,307,295	34,703,835,672,760,725,659,254,115,573,775,525,383,657,603,505,506,462,795	33.78
96-prism	192	288	98	74,112	387,441,199,483,882,790,074,386,518,739,975,425,611,166,119,546,861,977,600	130,879,809,160,332,709,730,909,060,139,747,285,756,827,067,222,934,653,120	33.78
97-prism	194	291	99	76,084	1,461,012,223,100,730,076,686,798,067,582,261,367,840,286,394,049,834,758,177	493,533,958,003,824,346,986,768,858,213,124,355,417,772,366,581,533,141,923	33.78
98-prism	196	294	100	79,968	5,508,783,927,988,926,594,011,003,719,084,348,517,902,267,230,291,120,238,668	1,842,484,668,472,842,688,235,271,932,872,735,062,103,648,776,666,005,382,528	33.45
99-prism	198	297	101	83,556	20,768,847,849,083,459,407,230,734,273,699,231,588,352,138,676,085,736,775,275	6,946,403,315,106,848,273,582,090,103,916,680,058,367,861,,235,272,392,879,353	33.45

Table 4.4: The number and percentage of non-overlapping edge unfoldings for Archimedean antiprisms.

m-antiprisms	$\|V\|$	$\|E\|$	$\|F\|$	#(MOPU)	#(Edge unfolding)	#(Non-overlapping edge unfolding)	Pct.(%)
12-antiprism	24	48	26	48	51,599,794,176	49,743,531,024	96.40
13-antiprism	26	52	28	52	383,142,771,674	369,359,503,344	96.40
14-antiprism	28	56	30	56	2,828,107,288,188	2,726,368,290,352	96.40
15-antiprism	30	60	32	60	20,768,716,848,000	20,021,578,135,380	96.40
16-antiprism	32	64	34	64	151,840,963,183,392	146,378,600,602,880	96.40
17-antiprism	34	68	36	204	1,105,779,284,582,146	989,008,190,008,480	89.44
18-antiprism	36	72	38	432	8,024,954,790,380,544	1,517,682,139,108,200	18.91
19-antiprism	38	76	40	456	58,059,628,319,357,318	10,550,126,657,845,736	18.17
20-antiprism	40	80	42	560	418,891,171,182,561,000	72,542,787,706,846,320	17.31
21-antiprism	42	84	44	672	3,014,678,940,049,375,872	500,034,989,831,068,818	16.59
22-antiprism	44	88	46	704	21,646,865,272,061,272,716	3,449,844,625,120,946,448	15.94
23-antiprism	46	92	48	736	155,113,904,634,576,144,814	23,752,014,262,731,255,118	15.31
24-antiprism	48	96	50	960	1,109,391,149,998,449,819,648	162,941,846,136,285,049,392	14.69
25-antiprism	50	100	52	1,000	7,920,708,398,483,722,531,250	1,117,782,108,867,439,830,950	14.11
26-antiprism	52	104	54	1,040	56,460,916,728,463,179,389,652	7,655,723,643,342,875,568,936	13.56
27-antiprism	54	108	56	1,404	401,873,068,071,158,383,691,136	40,561,091,359,603,932,081,708	10.09
28-antiprism	56	112	58	1,792	2,856,496,726,273,368,888,420,984	264,478,642,931,290,919,674,648	9.26
29-antiprism	58	116	60	2,204	20,277,959,821,998,087,658,569,178	1,739,241,575,214,473,110,359,470	8.58
30-antiprism	60	120	62	2,520	143,779,866,504,299,168,102,784,000	11,718,403,001,480,040,992,138,460	8.15
31-antiprism	62	124	64	2,852	1,018,331,261,238,041,888,906,149,982	79,227,778,390,260,949,681,648,022	7.78
32-antiprism	64	128	66	2,944	7,204,899,406,395,028,729,775,662,656	535,088,808,567,353,165,252,109,504	7.42
33-antiprism	66	132	68	3,168	50,926,337,537,628,456,148,426,034,304	3,609,765,503,967,786,066,361,340,190	7.08
34-antiprism	68	136	70	3,808	359,631,713,591,480,208,135,988,999,908	23,021,698,690,971,475,731,990,378,832	6.40
35-antiprism	70	140	72	4,200	2,537,451,036,289,964,010,662,071,375,750	155,062,662,340,102,785,066,461,404,560	6.11
36-antiprism	72	144	74	4,464	17,888,860,941,014,408,891,681,749,082,112	1,043,552,488,055,809,272,918,087,425,832	5.83
37-antiprism	74	148	76	4,884	126,017,967,976,156,654,397,534,266,950,026	6,992,936,456,851,489,392,078,163,320,978	5.55
38-antiprism	76	152	78	5,168	887,084,326,468,926,324,030,843,544,372,524	44,438,923,337,128,563,356,651,187,920,012	5.01
39-antiprism	78	156	80	5,772	6,240,170,805,918,890,922,630,444,422,537,088	297,478,382,005,821,691,364,579,412,449,706	4.77
40-antiprism	80	160	82	6,400	43,867,453,323,674,409,143,926,999,140,738,000	1,983,085,398,586,205,226,911,001,715,311,520	4.52
41-antiprism	82	164	84	6,888	308,188,798,032,167,102,842,859,597,775,205,042	13,033,685,199,501,916,122,251,960,215,169,912	4.23
42-antiprism	84	168	86	7,392	2,163,878,359,899,340,120,052,552,791,046,378,496	83,997,191,224,353,764,482,646,914,913,598,624	3.88
43-antiprism	86	172	88	8,084	15,184,572,514,675,762,272,842,247,131,661,635,894	557,611,275,066,805,327,907,702,044,873,987,094	3.67
44-antiprism	88	176	90	8,624	106,496,994,569,720,990,727,767,374,869,609,730,968	3,729,635,546,799,294,784,771,659,021,890,472,664	3.50
45-antiprism	90	180	92	9,360	746,530,833,968,188,588,851,681,523,936,666,896,000	24,431,729,185,673,950,396,752,450,635,669,388,990	3.27
46-antiprism	92	184	94	10,304	5,230,505,089,344,431,048,507,144,123,815,456,787,772	158,880,058,222,038,902,280,026,924,999,326,487,380	3.04
47-antiprism	94	188	96	11,656	36,629,772,069,905,834,755,580,161,013,689,257,929,566	1,060,539,783,181,405,072,337,781,040,938,759,619,342	2.89
48-antiprism	96	192	98	12,096	256,405,984,103,100,622,357,453,677,837,305,041,649,664	7,079,805,121,439,383,694,342,635,647,608,115,253,632	2.76
49-antiprism	98	196	100	12,740	1,794,045,942,295,064,986,560,011,614,233,598,156,819,298	47,081,894,856,079,882,568,065,465,270,204,379,835,426	2.62
50-antiprism	100	200	102	13,200	12,547,524,306,762,115,327,139,640,139,635,651,225,562,500	313,979,052,982,335,359,074,797,901,078,961,675,923,700	2.50
51-antiprism	102	204	104	14,280	87,722,051,242,994,803,143,643,140,957,694,192,485,255,552	2,093,220,753,862,771,345,181,080,442,901,094,417,625,334	2.38
52-antiprism	104	208	106	15,600	613,045,214,965,087,171,516,365,035,207,733,551,443,709,736	13,847,372,368,702,386,134,230,159,841,426,631,160,249,520	2.26
53-antiprism	106	212	108	16,324	4,282,679,690,470,859,990,496,705,254,406,531,422,464,957,834	92,254,873,128,059,280,848,212,456,691,530,042,110,511,660	2.15
54-antiprism	108	216	110	17,064	29,907,770,896,467,759,248,303,121,099,365,111,834,448,227,328	612,564,147,448,713,555,111,946,603,958,121,691,610,818,284	2.04
55-antiprism	110	220	112	18,480	208,787,039,294,802,995,558,997,194,768,329,038,664,289,012,750	4,066,189,399,259,848,921,000,213,749,369,244,891,377,708,200	1.95
56-antiprism	112	224	114	20,160	1,457,066,704,859,013,168,857,939,059,215,469,544,106,252,283,632	26,882,734,603,660,531,639,929,002,113,295,431,420,663,838,960	1.84
57-antiprism	114	228	116	20,748	10,165,220,976,851,309,359,988,036,885,968,497,679,868,602,544,256	177,996,738,793,784,313,663,675,391,748,841,946,567,960,370,322	1.75
58-antiprism	116	232	118	22,272	70,895,802,507,339,433,606,655,281,989,227,262,198,207,167,104,404	1,180,051,219,817,443,505,617,832,090,129,322,320,242,838,961,804	1.66
59-antiprism	118	236	120	23,364	494,305,112,112,066,674,502,236,216,299,036,533,680,424,852,661,558	7,834,254,664,590,050,866,382,827,703,061,557,850,624,078,276,054	1.58
60-antiprism	120	240	122	25,440	3,445,441,668,665,681,646,962,862,224,080,264,597,391,436,598,272,000	50,403,377,478,963,170,902,563,467,427,787,499,348,682,069,083,400	1.46
61-antiprism	122	244	124	26,352	24,008,998,657,730,043,418,999,210,016,836,054,318,873,476,626,984,762	326,358,125,570,791,131,913,614,291,766,990,868,139,803,779,993,658	1.36
62-antiprism	124	248	126	27,528	167,257,831,873,332,437,880,307,618,553,808,550,206,593,147,036,070,876	1,854,939,808,105,063,172,332,156,437,560,469,843,454,970,270,135,872	1.11
63-antiprism	126	252	128	29,232	1,164,892,592,931,629,392,338,324,783,815,505,600,459,556,438,051,914,624	12,307,784,791,893,071,962,543,568,932,644,431,739,514,519,035,956,010	1.06
64-antiprism	128	256	130	30,720	8,111,027,415,042,412,087,059,884,505,184,466,841,764,376,870,066,703,488	81,711,622,221,644,705,528,593,850,868,389,602,010,305,415,118,773,632	1.01
65-antiprism	130	260	132	31,720	56,462,462,218,649,594,296,489,126,547,728,233,809,837,328,422,164,209,250	542,324,566,561,175,718,389,472,139,379,279,869,381,405,090,020,827,940	0.96
66-antiprism	132	264	134	33,264	392,953,311,363,100,782,765,649,901,258,650,734,263,966,574,522,587,784,192	3,596,222,163,944,667,874,762,237,572,824,582,243,007,524,492,920,016,364	0.92
67-antiprism	134	268	136	35,108	2,734,150,277,149,943,789,424,653,221,975,737,385,578,070,013,528,736,239,846	23,843,879,380,617,148,795,466,186,545,241,390,034,312,194,471,190,721,410	0.87
68-antiprism	136	272	138	37,536	19,019,848,444,227,125,038,960,788,030,632,146,757,126,643,109,790,562,588,744	158,047,277,673,032,158,023,557,741,664,008,526,923,236,605,161,466,417,144	0.83
69-antiprism	138	276	140	38,640	132,281,097,981,397,378,649,216,327,599,160,829,981,177,127,561,996,392,778,368	1,047,172,473,392,558,836,251,756,065,865,616,682,360,236,358,525,772,236,994	0.79
70-antiprism	140	280	142	40,040	919,808,251,652,716,036,371,207,892,032,413,807,786,850,000,883,510,526,443,500	6,.940,458,038,739,497,932,445,601,709,547,911,589,835,564,772,106,776,166,220	0.75
71-antiprism	142	284	144	42,600	6,394,523,254,028,788,004,842,904,160,103,465,297,190,061,440,230,870,478,513,422	45,780,684,032,708,802,155,441,190,837,474,021,683,024,682,589,684,818,605,684	0.72
72-antiprism	144	288	146	45,504	44,446,020,245,409,850,388,919,123,546,153,029,436,510,863,260,931,308,786,876,416	303,133,167,415,275,991,480,997,730,729,891,095,322,066,594,918,858,437,619,312	0.68
73-antiprism	146	292	148	47,596	308,868,631,905,426,344,328,427,311,641,720,314,433,493,675,086,071,079,589,514,514	1,993,862,494,867,116,801,892,228,563,979,771,114,995,027,333,450,860,247,871,268	0.65
74-antiprism	148	296	150	48,840	2,146,017,331,464,816,766,794,536,512,479,696,001,159,731,435,059,847,042,295,248,948	13,209,556,361,833,768,036,797,427,669,629,105,268,373,114,777,374,196,971,004,696	0.62
75-antiprism	150	300	152	51,000	14,907,792,173,512,400,291,813,743,106,474,046,926,942,024,685,661,040,985,606,000,000	87,479,366,310,664,176,876,248,551,641,616,300,775,155,031,501,800,307,738,254,650	0.59
76-antiprism	152	304	154	54,112	103,541,921,350,898,507,949,080,104,593,610,092,290,674,442,999,146,438,446,892,628,952	575,728,071,259,409,983,216,254,627,908,333,000,969,928,942,023,795,016,355,188,312	0.56
77-antiprism	154	308	156	56,056	719,024,872,072,048,704,795,415,649,743,438,922,497,201,689,435,088,835,503,134,774,586	3,803,094,888,814,534,194,244,711,198,507,594,930,371,276,487,989,070,769,505,333,618	0.53
78-antiprism	156	312	158	57,096	4,992,273,293,210,566,749,051,331,629,112,187,169,112,455,673,298,970,063,008,551,517,184	25,178,232,163,989,764,173,902,561,452,762,553,210,080,327,618,722,145,846,907,592,560	0.50
79-antiprism	158	316	160	59,724	34,656,236,736,012,517,253,147,752,391,859,302,565,359,593,442,298,439,368,730,738,540,478	166,652,766,549,703,045,550,278,222,766,074,887,734,370,837,666,827,789,428,184,155,666	0.48

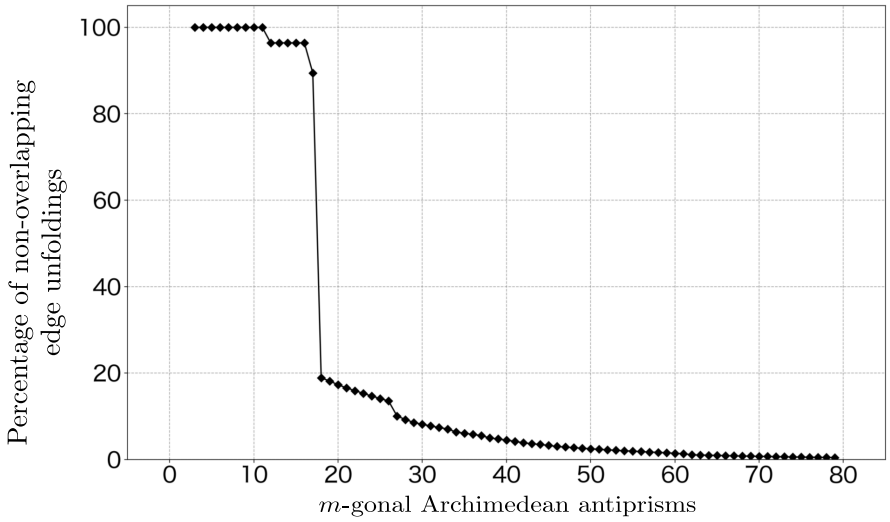

Figure 4.2: The percentage of non-overlapping edge unfoldings in Archimedean antiprisms.

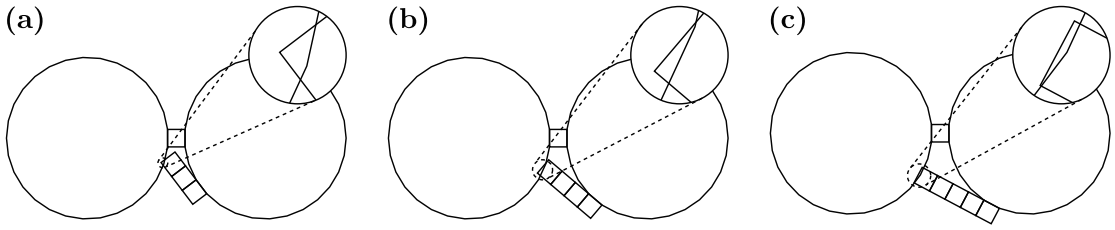

Figure 4.3: MOPUs in Archimedean 28-gonal prisms (excluding those with rotational and mirror symmetry).

From these results, we can conclude that the percentage of non-overlapping edge unfoldings depends not on the number of MOPUs in each polyhedron, but rather on the number of faces in each MOPU.

4.2.2 The number of non-overlapping lattice unfoldings for cuboids

Table 4.5 shows the results of counting the number of lattice unfoldings in (xL, yL, zL)-cuboids that do not have face contact, edge contact, or vertex contact, respectively.

Figure 4.7 shows a line graph with the values of z for $(1, 1, z)$-cuboids ($1 \leq z \leq 10$) on the horizontal axis, and the percentage of lattice unfoldings without each type of contact on the vertical axis. From these results, we can observe that in an (xL, yL, zL) cuboid, as the values of z increase while keeping x and y fixed, the percentage of non-overlapping unfoldings decreases.

There are cuboids with different side lengths that have the same surface area. The percentages of non-overlapping lattice unfoldings for cuboids with the same

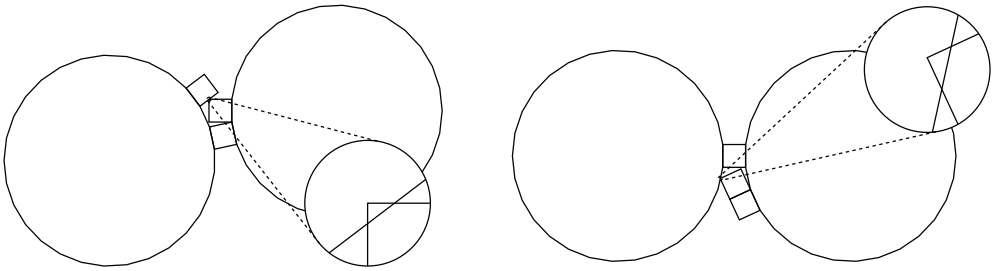

Figure 4.4: MOPUs in Archimedean 29-gonal prisms (excluding those with rotational and mirror symmetry, and the three types from $n = 28$).

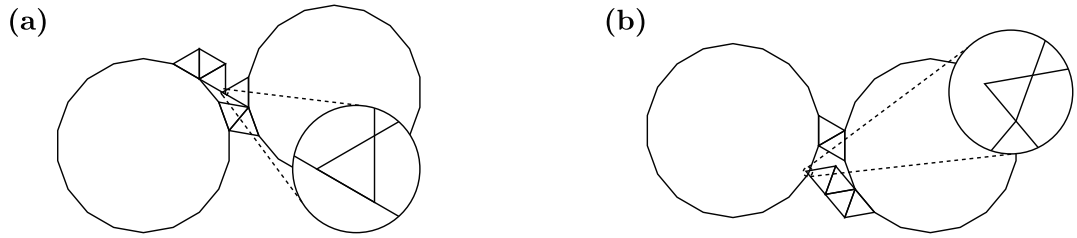

Figure 4.5: MOPUs in Archimedean 17-gonal antiprisms (excluding those with rotational and mirror symmetry).

surface area are shown in Table 4.6 to 4.10.

For cuboids with surface areas of 22 and 34, those with larger volumes tend to have a lower percentage of non-overlapping edge unfoldings. However, this tendency does not appear for cuboids with surface areas of 28, 30, and 32. These results indicate that, even for cuboids with the same surface area, a larger volume does not necessarily lead to a lower percentage of non-overlapping lattice unfoldings.

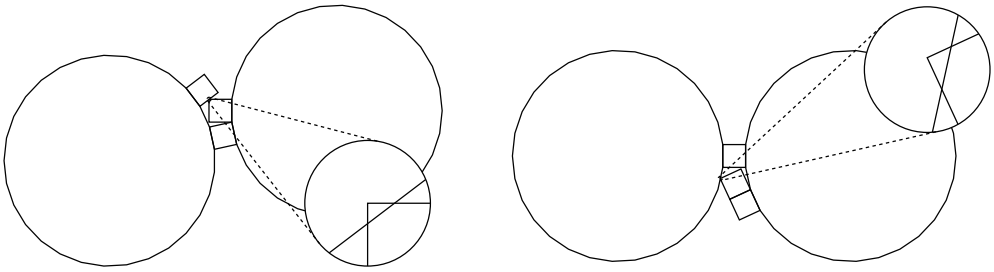

Figure 4.6: MOPUs in Archimedean 18-gonal antiprisms (excluding those with rotational and mirror symmetry, and the three types from $m = 17$).

Table 4.5: The number and percentage of non-overlapping lattice unfoldings for cuboids.

Cuboids	$\|V\|$	$\|E\|$	$\|F\|$	# (Lattice unfolding (including overlaps))	No faces-in-touch			No edges-in-touch			No vertices-in-touch		
					#(MOPU)	# (Lattice unfolding)	Pct.(%)	#(MOPU)	# (Lattice unfolding)	Pct.(%)	#(MOPU)	# (Lattice unfolding)	Pct.(%)
$(1,1,1)$	8	12	6	384	0	384	100.00	0	384	100.00	0	384	100.00
$(1,1,2)$	12	20	10	12,124	0	12,124	100.00	0	12,124	100.00	32	11,484	94.72
$(1,1,3)$	16	28	14	240,304	16	240,240	99.97	80	238,432	99.22	304	212,920	88.60
$(1,1,4)$	20	36	18	3,708,380	80	3,705,820	99.93	512	3,644,600	98.28	1,232	3,075,400	82.93
$(1,1,5)$	24	44	22	49,206,176	208	49,156,592	99.90	1,504	47,970,720	97.49	3,408	38,043,936	77.32
$(1,1,6)$	28	52	26	592,188,796	464	591,487,340	99.88	3,808	573,122,568	96.78	8,448	424,509,028	71.68
$(1,1,7)$	32	60	30	6,671,469,328	1,104	6,663,017,440	99.87	9,360	6,409,933,496	96.08	20,432	4,407,661,888	66.07
$(1,1,8)$	36	68	34	71,772,242,780	2,704	71,679,140,716	99.87	22,912	68,429,543,676	95.34	49,456	43,445,829,708	60.53
$(1,1,9)$	40	76	38	747,116,459,968	6,544	746,143,953,328	99.87	55,584	706,395,487,984	94.55	119,504	412,096,369,696	55.16
$(1,1,10)$	44	74	42	7,593,452,118,844	15,760	7,583,621,450,924	99.87	134,368	7,114,772,651,372	93.70	288,416	3,797,487,539,408	50.01
$(1,2,2)$	18	32	16	1,675,184	0	1,675,184	100.00	32	1,553,536	92.74	128	1,228,824	73.35
$(1,2,3)$	24	44	22	131,478,632	544	130,212,292	99.04	1,648	111,177,796	84.56	3,312	75,653,292	57.54
$(1,2,4)$	30	56	28	7,692,072,382	14,920	7,528,985,598	97.88	32,048	5,970,306,978	77.62	52,960	3,535,269,930	45.96
$(1,2,5)$	36	68	34	375,631,947,892	141,816	364,028,460,124	96.91	291,736	270,654,176,916	72.05	449,552	140,837,624,986	37.49
$(2,2,2)$	26	48	24	761,804,472	0	761,804,472	100.00	240	522,735,564	68.62	432	304,891,548	40.02
$(2,2,3)$	34	64	32	203,758,066,112	5,824	196,470,177,268	96.42	19,392	109,840,848,592	53.91	34,704	48,990,450,676	24.04
$(1,3,3)$	32	60	30	37,054,664,336	18,656	35,759,106,992	96.50	53,824	26,138,414,976	70.54	87,057	14,279,985,328	38.54
$(\sqrt{2},\sqrt{2},\sqrt{2})$	14	24	12	80,352	0	80,352	100.00	0	80,352	100.00	0	80,352	100.00
$(\sqrt{2},\sqrt{2},2\sqrt{2})$	22	40	20	36,045,144	64	35,810,728	99.35	416	32,634,384	90.54	832	26,150,088	72.55
$(\sqrt{2},\sqrt{2},3\sqrt{2})$	30	56	28	8,178,632,284	9,744	8,051,279,652	98.44	21,824	6,849,636,840	83.75	35,440	4,579,514,256	55.99
$(\sqrt{2},\sqrt{2},4\sqrt{2})$	38	72	36	1,332,665,934,528	189,696	1,304,508,754,808	97.89	360,912	1,043,581,316,640	78.31	580,353	594,311,017,928	44.60
$(\sqrt{2},2\sqrt{2},2\sqrt{2})$	34	64	32	207,761,826,744	13,296	198,307,283,288	95.45	45,776	135,619,116,108	65.28	76,432	67,737,527,156	32.60
$(\sqrt{5},\sqrt{5},\sqrt{5})$	32	60	30	59,902,047,024	336	58,033,038,468	96.88	2,520	35,216,407,908	58.79	3,600	14,389,530,720	24.02

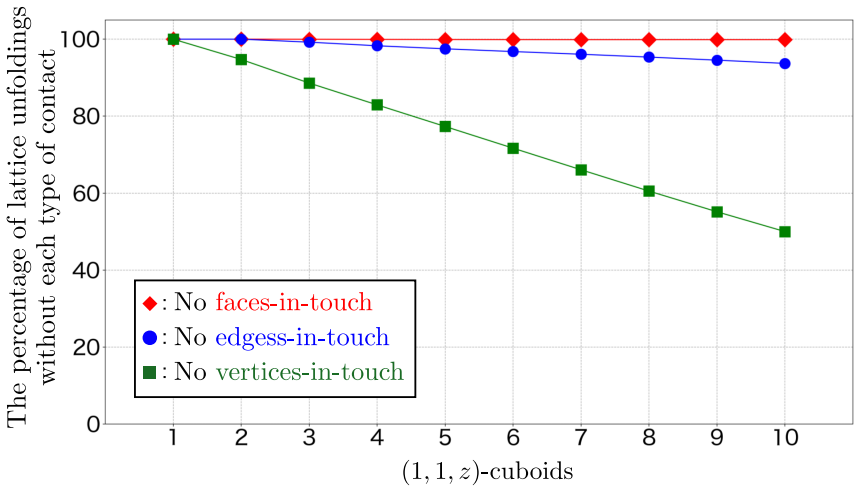

Figure 4.7: The percentage of lattice unfoldings without each type of contact for $(1,1,z)$-cuboids.

4.3 Summary and discussion on the number of non-overlapping unfoldings

In this chapter, we presented results on counting the number of non-overlapping unfoldings in edge unfoldings of convex regular-faced polyhedra and lattice unfoldings of cuboids.

First, we proposed an algorithm for counting non-overlapping unfoldings using Zero-suppressed Decision Diagrams (ZDDs) and the subsetting method. In this process, we focused on the minimal overlapping partial unfoldings (MOPUs), which were enumerated by rotational unfolding. We then conducted computational experiments on the edge unfoldings of several Archimedean solids, Johnson solids, Archimedean prisms, and Archimedean antiprisms, counting the number of non-overlapping edge unfoldings.

Table 4.6: The percentage of non-overlapping lattice unfoldings for a cuboid with a surface area of 22.

Cuboids	Volume	No faces-in-touch	No edges-in-touch	No vertices-in-touch
$(1, 1, 5)$	5	99.90	97.49	77.32
$(1, 2, 3)$	6	99.04	84.56	57.54

Table 4.7: The percentage of non-overlapping lattice unfoldings for a cuboid with a surface area of 28.

Cuboids	Volume	No faces-in-touch	No edges-in-touch	No vertices-in-touch
$(1, 2, 4)$	8	97.88	77.62	45.96
$(\sqrt{2}, \sqrt{2}, 3\sqrt{2})$	$6\sqrt{2}$	98.44	83.75	55.99

As a result, we showed that the percentage of non-overlapping edge unfoldings is influenced not by the number of MOPUs, but by the number of faces constituting each MOPU. Additionally, for n-gonal Archimedean prisms and m-gonal Archimedean antiprisms, we observed that increasing the values of n and m decreases the percentage of non-overlapping edge unfoldings.

Next, we extended the same approach to counting non-overlapping lattice unfoldings of cuboids, we counted unfoldings without faces-in-touch, edges-in-touch, or vertices-in-touch. As a result, we found that cuboids with increasing side lengths tend to have a lower percentage of non-overlapping lattice unfoldings. However, for cuboids with the same surface area but different volumes, there was no clear relationship between volume and the percentage of non-overlapping unfoldings. Contrary to expectations, increasing the volume did not necessarily lead to a higher percentage of non-overlapping unfoldings.

On the other hand, for the Rhombicosidodecahedron, Snub dodecahedron, and Rhombitruncated icosidodecahedron in Table 4.1, as well as J68 to J82 in Table 4.2, the enumeration of MOPUs resulted in a timeout, making it impossible to count the number of non-overlapping edge unfoldings. Furthermore, even if the MOPU enumeration succeeds, as seen in the case of J48 in Table 4.2, counting the number of non-overlapping unfoldings can still result in a timeout. This suggests that when MOPU enumeration results in a timeout, counting the number of non-overlapping unfoldings is also likely to result in a timeout. Therefore, improving the efficiency of both the rotational unfolding and the algorithm for counting non-overlapping unfoldings becomes essential. One possible improvement lies in refining the pruning

Table 4.8: The percentage of non-overlapping lattice unfoldings for a cuboid with a surface area of 30.

Cuboids	Volume	No faces-in-touch	No edges-in-touch	No vertices-in-touch
$(1, 1, 7)$	7	99.87	96.08	66.07
$(1, 3, 3)$	9	96.50	70.54	38.54
$(\sqrt{5}, \sqrt{5}, \sqrt{5})$	$5\sqrt{5}$	96.88	58.79	24.02

Table 4.9: The percentage of non-overlapping lattice unfoldings for a cuboid with a surface area of 32.

Cuboids	Volume	No faces-in-touch	No edges-in-touch	No vertices-in-touch
$(\sqrt{2}, 2\sqrt{2}, 2\sqrt{2})$	$8\sqrt{2}$	95.45	65.28	32.60
$2, 2, 3$	12	96.42	53.91	24.04

Table 4.10: The percentage of non-overlapping lattice unfoldings for a cuboid with a surface area of 34.

Cuboids	Volume	No faces-in-touch	No edges-in-touch	No vertices-in-touch
$(1, 1, 8)$	8	99.87	95.34	60.53
$(1, 2, 5)$	10	96.91	72.05	37.49

process. In the current rotational unfolding, pruning based on distances is implemented, yet the estimation of the sum of the circumradii of the remaining faces remains insufficient. To address this limitation, by calculating the reachable distances for the remaining faces using techniques such as dynamic programming, it becomes feasible to perform pruning at an earlier stage.

Additionally, this study only considered polyhedra where all edge lengths are equal. As a future direction, extending this method to more general convex polyhedra would be interesting, especially to examine how the results of Schevon, as shown in Figure 1.6, would change.

Chapter 5

Conclusion

In this study, we showed the existence of overlapping unfoldings for polyhedra and, in cases where overlapping unfoldings exist, computed the number of overlapping and non-overlapping unfoldings. We achieve this by using the rotational unfolding algorithm, which efficiently determines whether overlaps exist, along with an enumeration algorithm based on MOPUs obtained through rotational unfolding.

The ultimate goal of this research is to solve the problem mentioned in Conjecture 1.1: "For any convex polyhedron, there exists at least one non-overlapping edge unfolding." This problem is known as Dürer's problem. To solve this problem, either of the following approaches must be taken [DO07]:

Approach 1 Discover a convex polyhedron that has only overlapping edge unfoldings.

Approach 2 Develop an edge unfolding algorithm that can be applied to all convex polyhedra.

As an idea for addressing Approach 1, determining the existence of overlaps in various convex polyhedra can be considered. In this method, the following two challenges are proposed as future works to bridge the gap between the current state and the intended solution.

The first challenge, as mentioned in Section 4.3, is "extending the proposed method to polyhedra that do not have equal-length edges." As shown in Proposition 2.2, the current rotational unfolding method determines overlaps in partial unfoldings by checking the overlaps of the circumcircles of the faces. However, this approach cannot be applied to faces with more general shapes. Therefore, it is necessary to precisely compute edge intersections between faces located at the ends of partial unfoldings.

The second challenge is "generating random convex polyhedra." When generating random convex polyhedra, edge lengths and face angles may become irrational numbers. Developing a method to retain and compute with these irrational values remains an important task.

As an idea for addressing Approach 2, classifying convex polyhedra and devising unfolding algorithms for each classification can be considered. The following discusses future works in pursuing this approach.

First, there are uncountably infinite convex polyhedra. However, according to Steinitz's theorem [Ste22], all convex polyhedra can be represented as polyhedral graphs (or 3-vertex-connected planar graphs). This allows us to organize convex polyhedra into a countably infinite set by considering them as polyhedral graphs. Moreover, by limiting the number of vertices to at most k, we can classify them into a finite set of polyhedral graphs, enabling enumeration.

Thus, the first task is the classification of polyhedral graphs. Classification should be performed based on various features such as vertex degrees, face shapes, and symmetries.

Next, for each classified polyhedral graph, existing edge unfolding algorithms should be applied if available. If no suitable algorithm exists, a new algorithm for generating non-overlapping edge unfoldings must be developed. This approach is expected to lead to a comprehensive edge unfolding algorithm for convex polyhedra.

The findings of this study represent a significant step toward deepening our understanding of the edge unfolding problem for polyhedra. However, substantial challenges remain in solving Dürer's problem. We hope that addressing the tasks outlined in the proposed approaches will help bridge this gap in future research.

Appendix A

Additional drawings

A.1 Additional drawings for the Johnson Solids

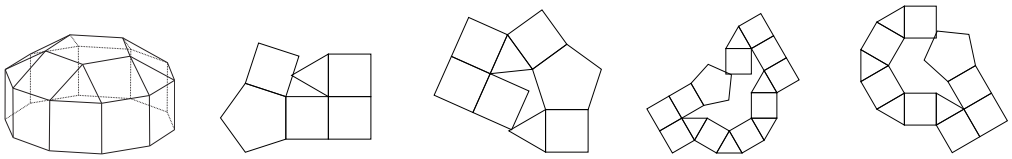

J20 (1) (2) (3) (4)

Figure A.1: List of MOPEs in J20.

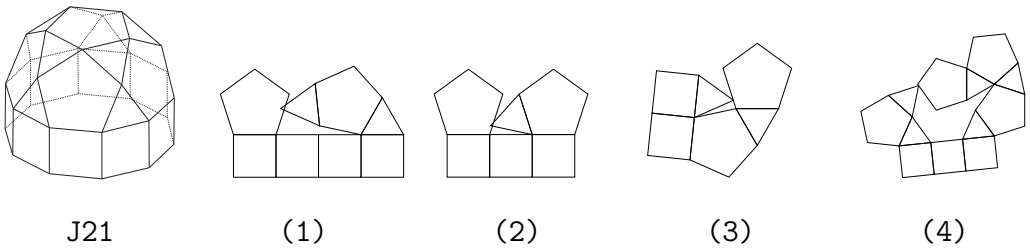

J21 (1) (2) (3) (4)

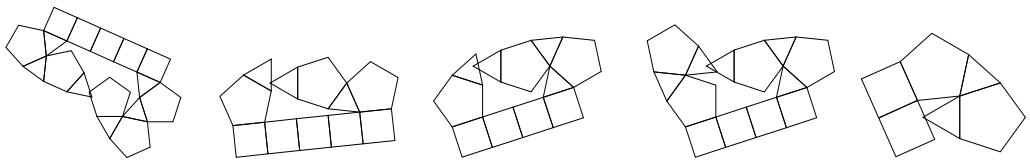

(5) (6) (7) (8) (9)

Figure A.2: List of MOPEs in J21.

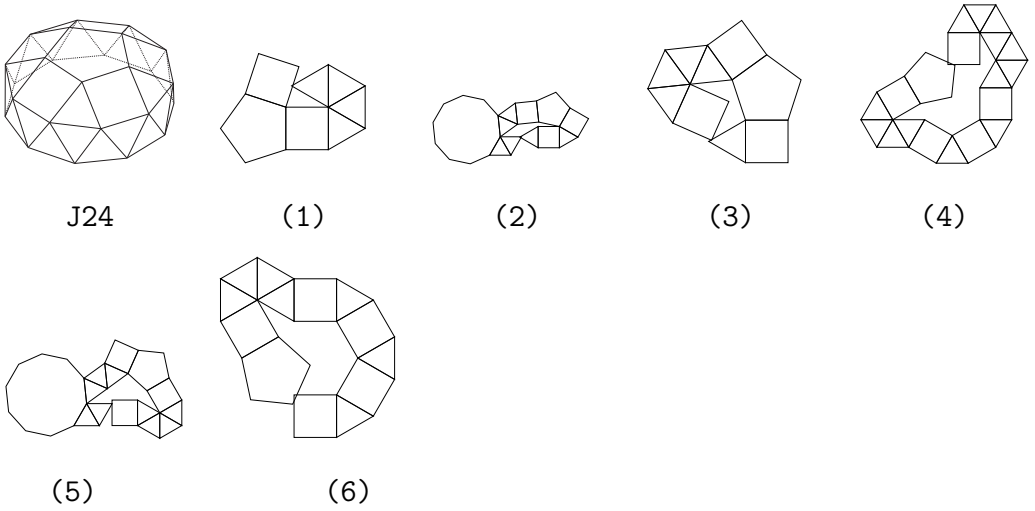

Figure A.3: List of MOPEs in J24.

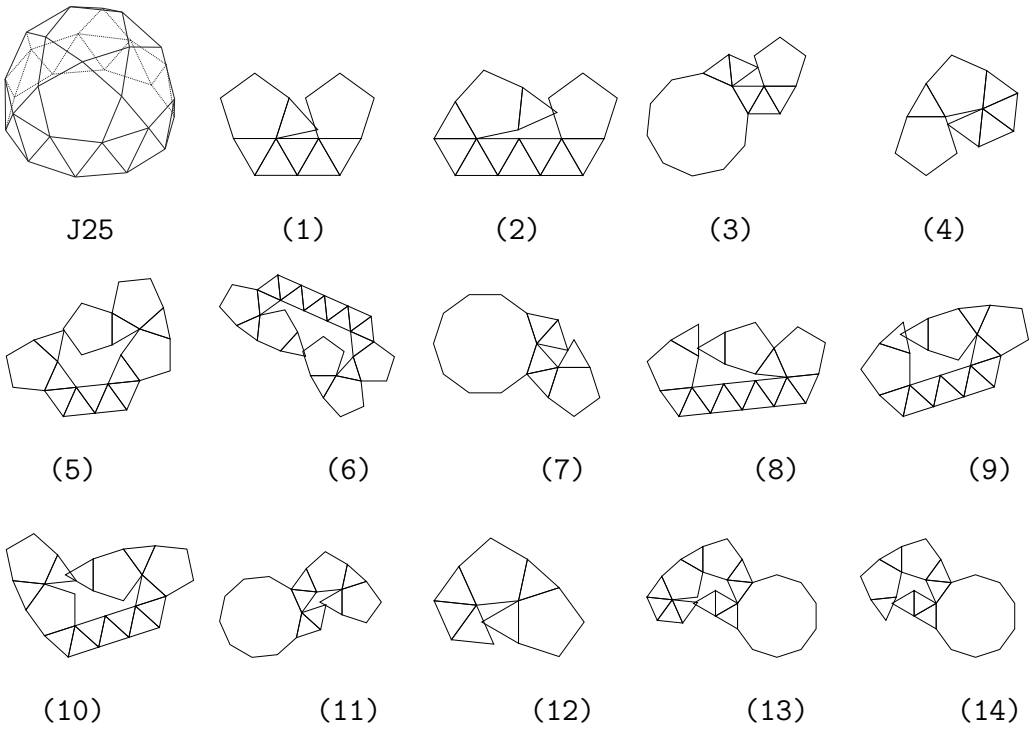

Figure A.4: List of MOPEs in J25.

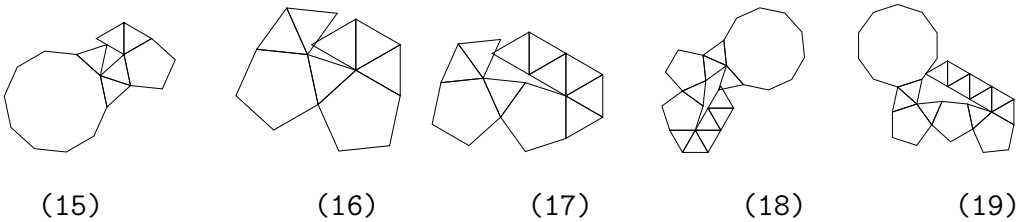

(15) (16) (17) (18) (19)

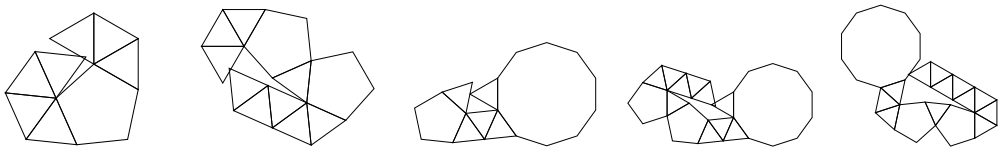

(20) (21) (22) (23) (24)

Figure A.4: List of MOPEs in J25. (continue)

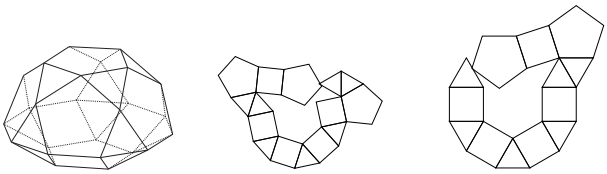

J32 (1) (2)

Figure A.5: List of MOPEs in J32.

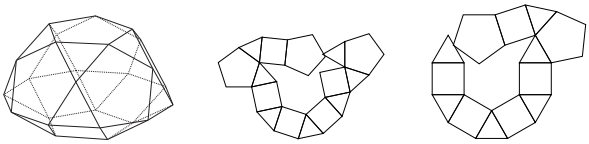

J33 (1) (2)

Figure A.6: List of MOPEs in J33.

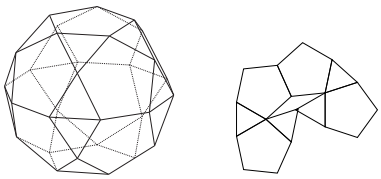

J34 (1)

Figure A.7: A MOPE in J34.

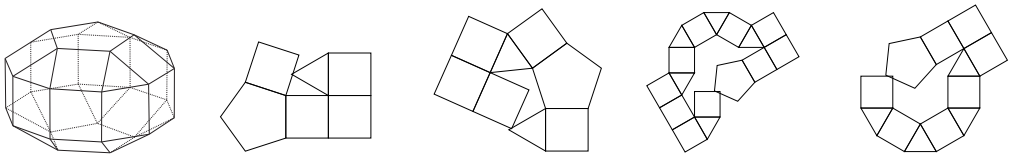

J38 (1) (2) (3) (4)

Figure A.8: List of MOPEs in J38.

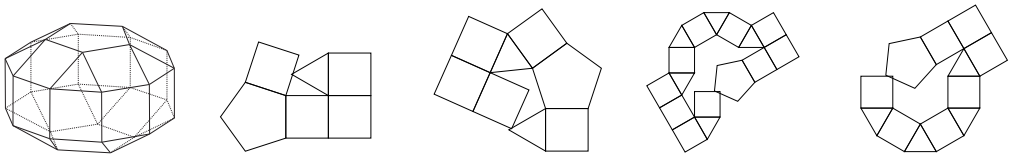

J39 (1) (2) (3) (4)

Figure A.9: List of MOPEs in J39.

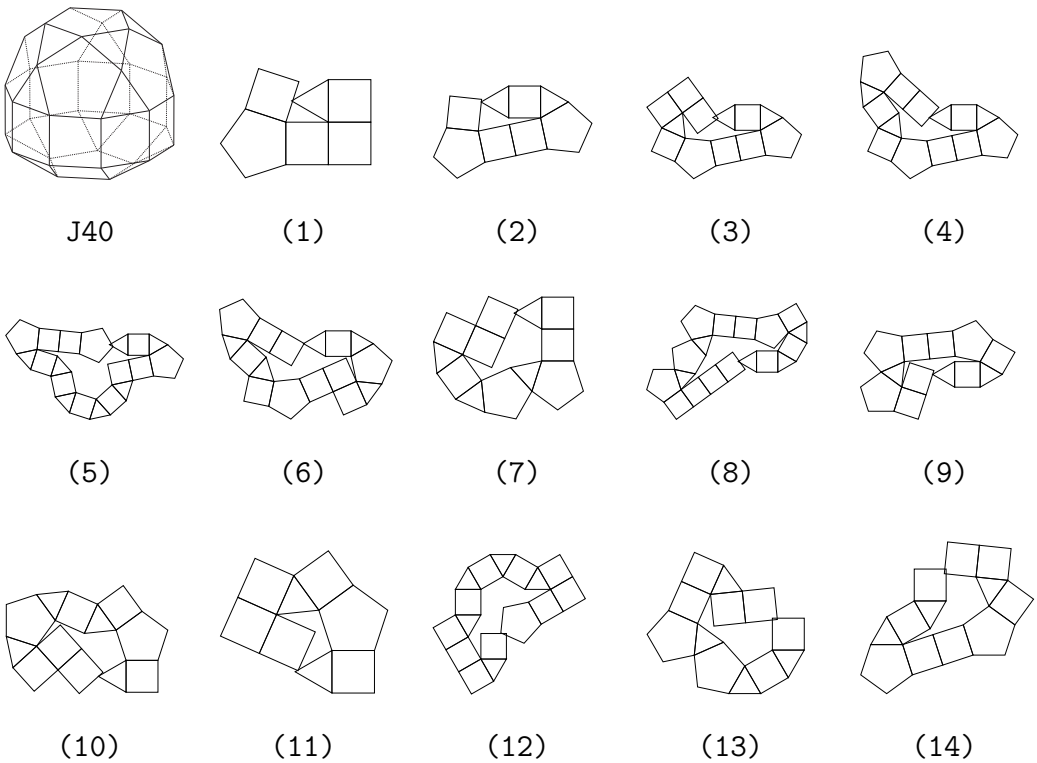

J40 (1) (2) (3) (4)

(5) (6) (7) (8) (9)

(10) (11) (12) (13) (14)

Figure A.10: List of MOPEs in J40.

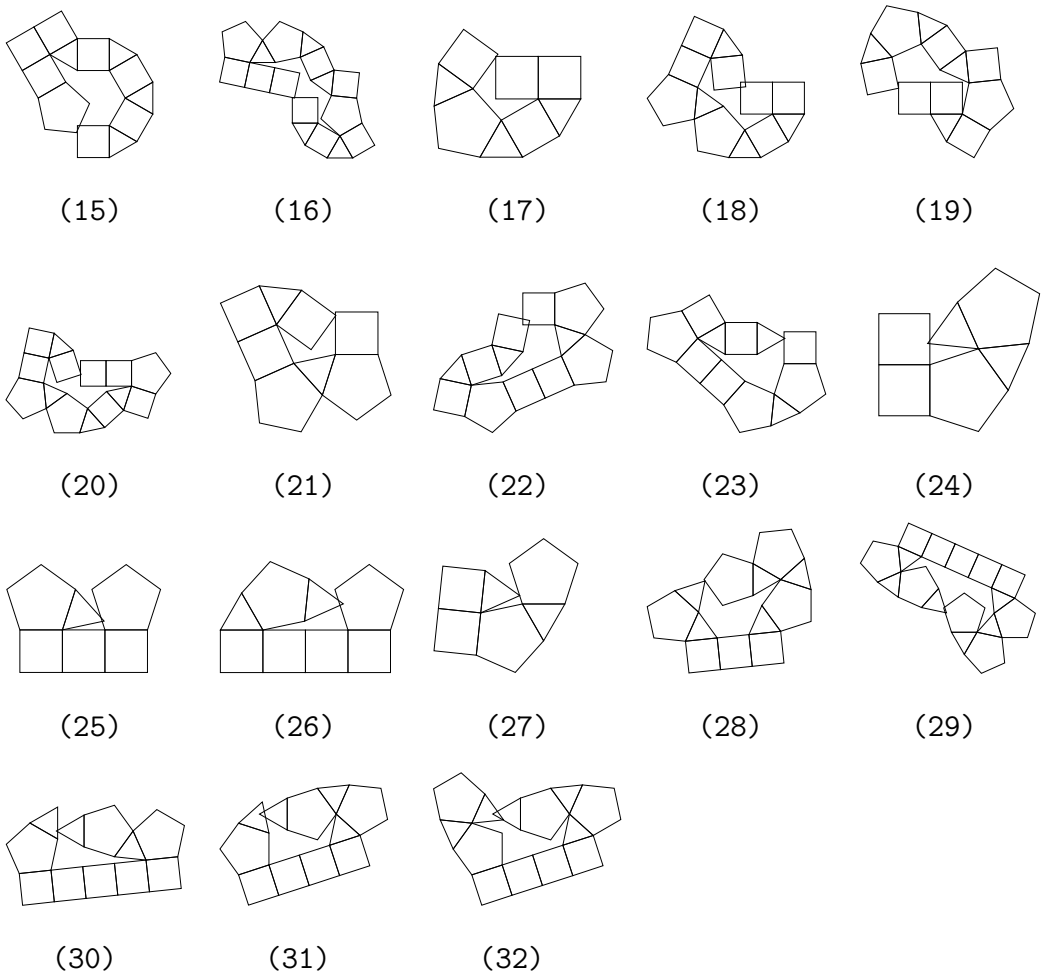

Figure A.10: List of MOPEs in J40. (continue)

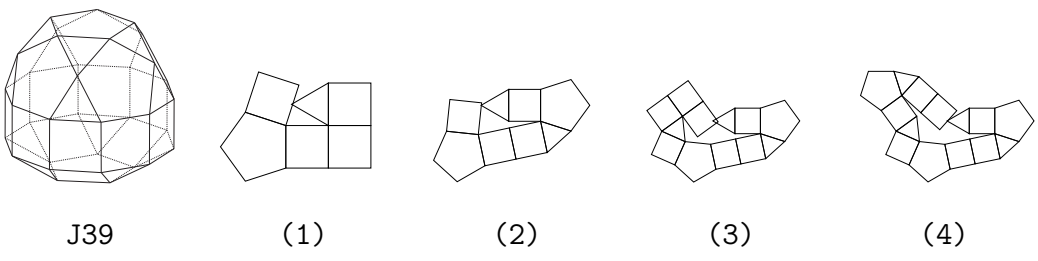

Figure A.11: List of MOPEs in J41.

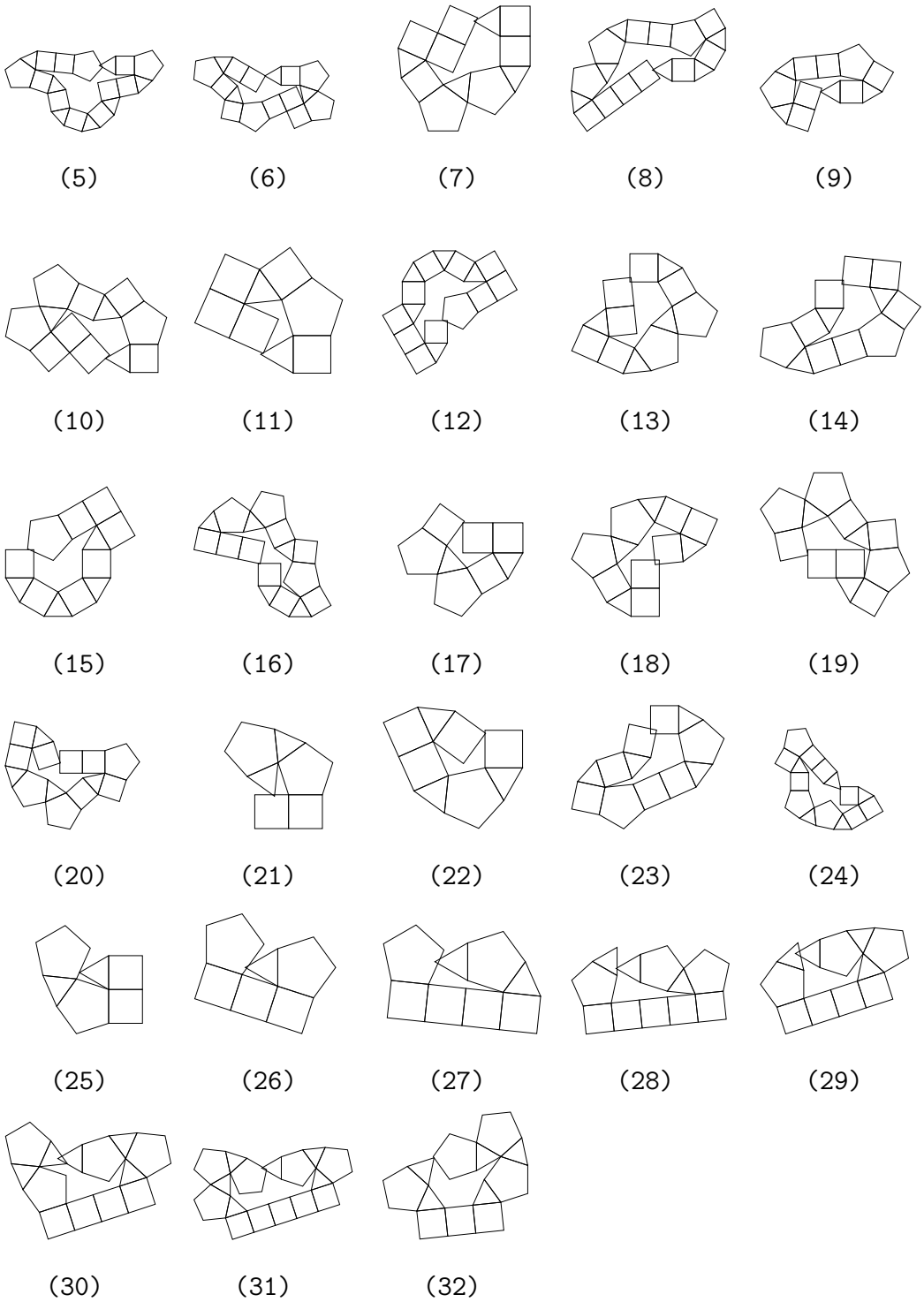

Figure A.11: List of MOPEs in J41. (continue)

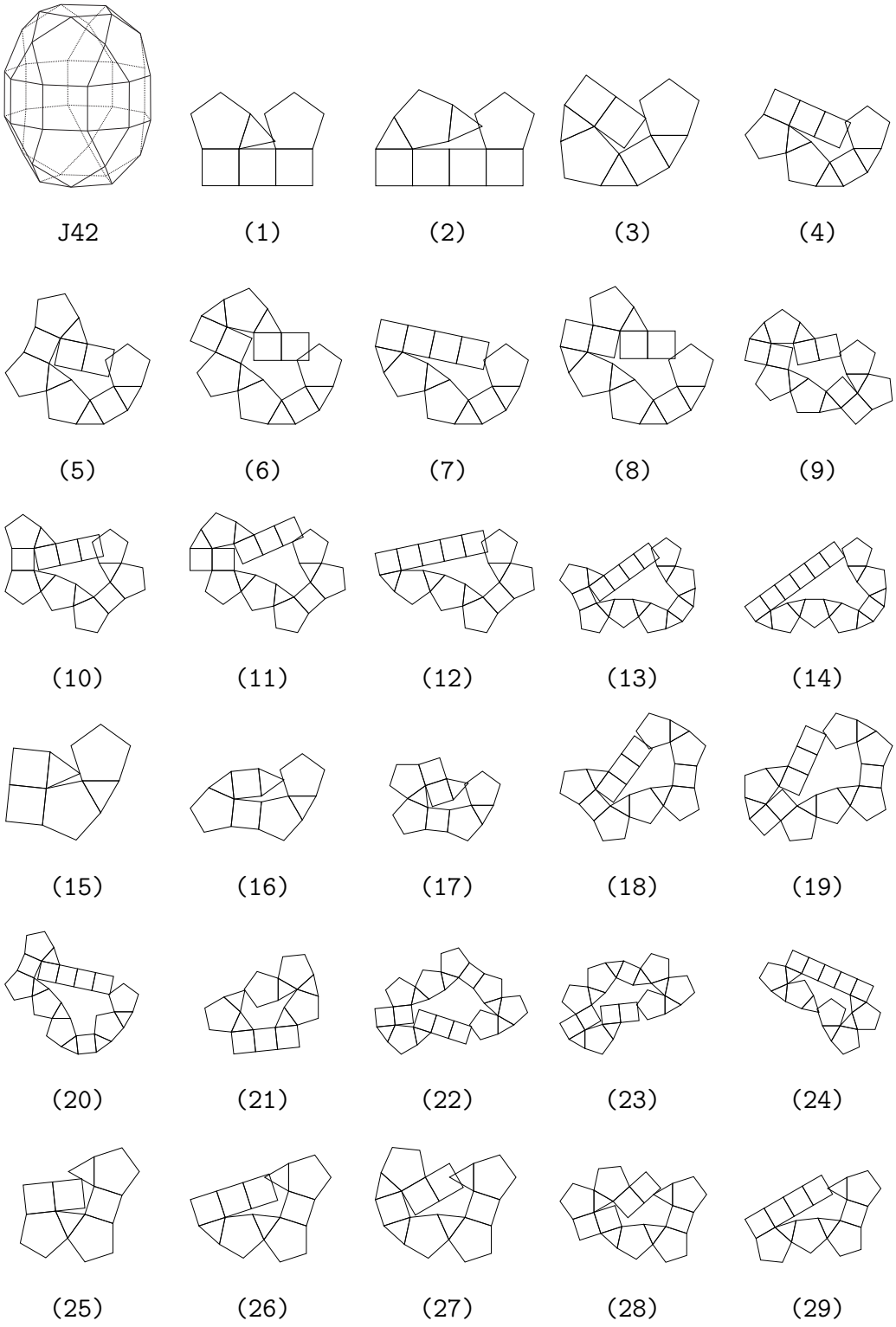

Figure A.12: List of MOPEs in J42.

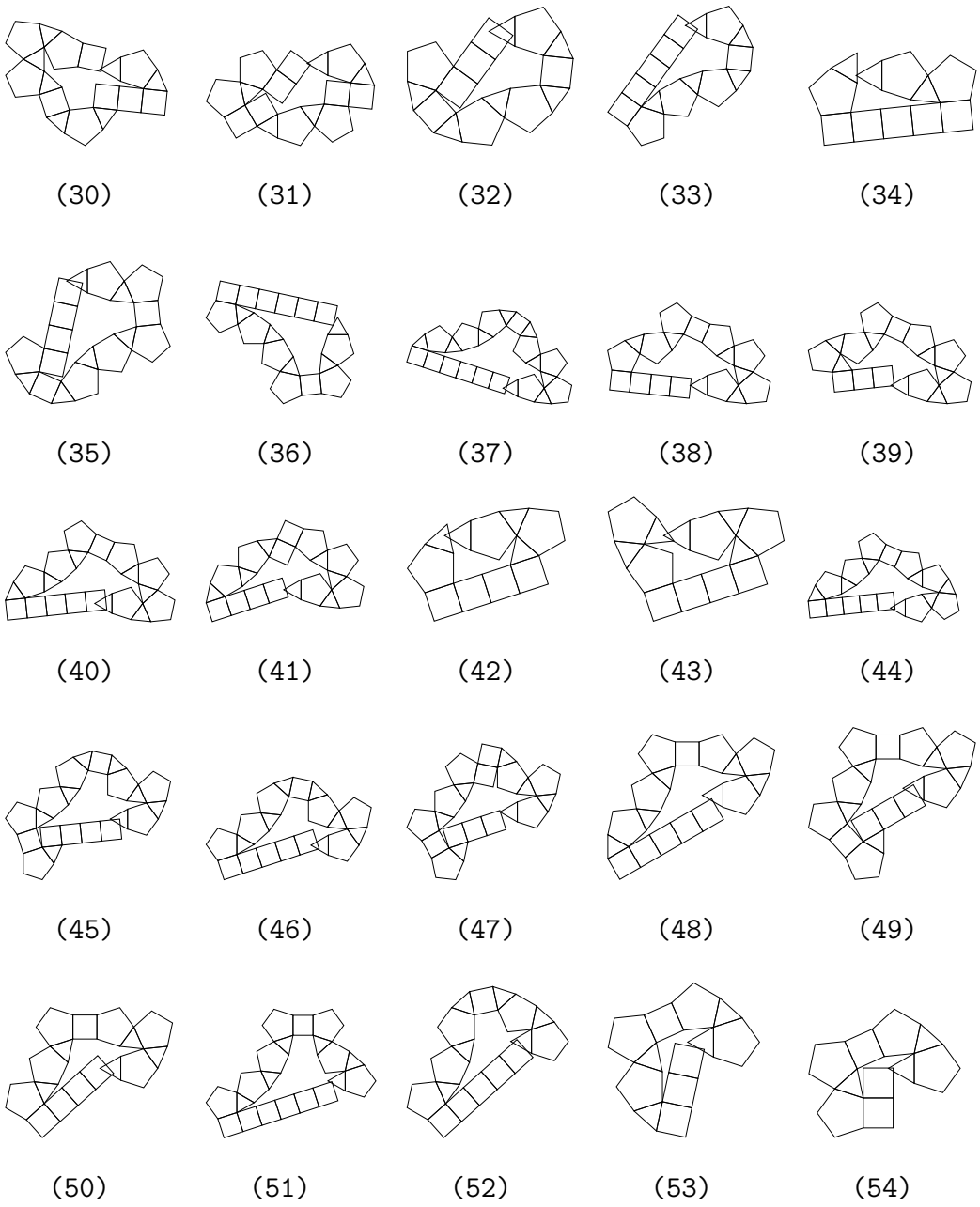

Figure A.12: List of MOPEs in J42. (continue)

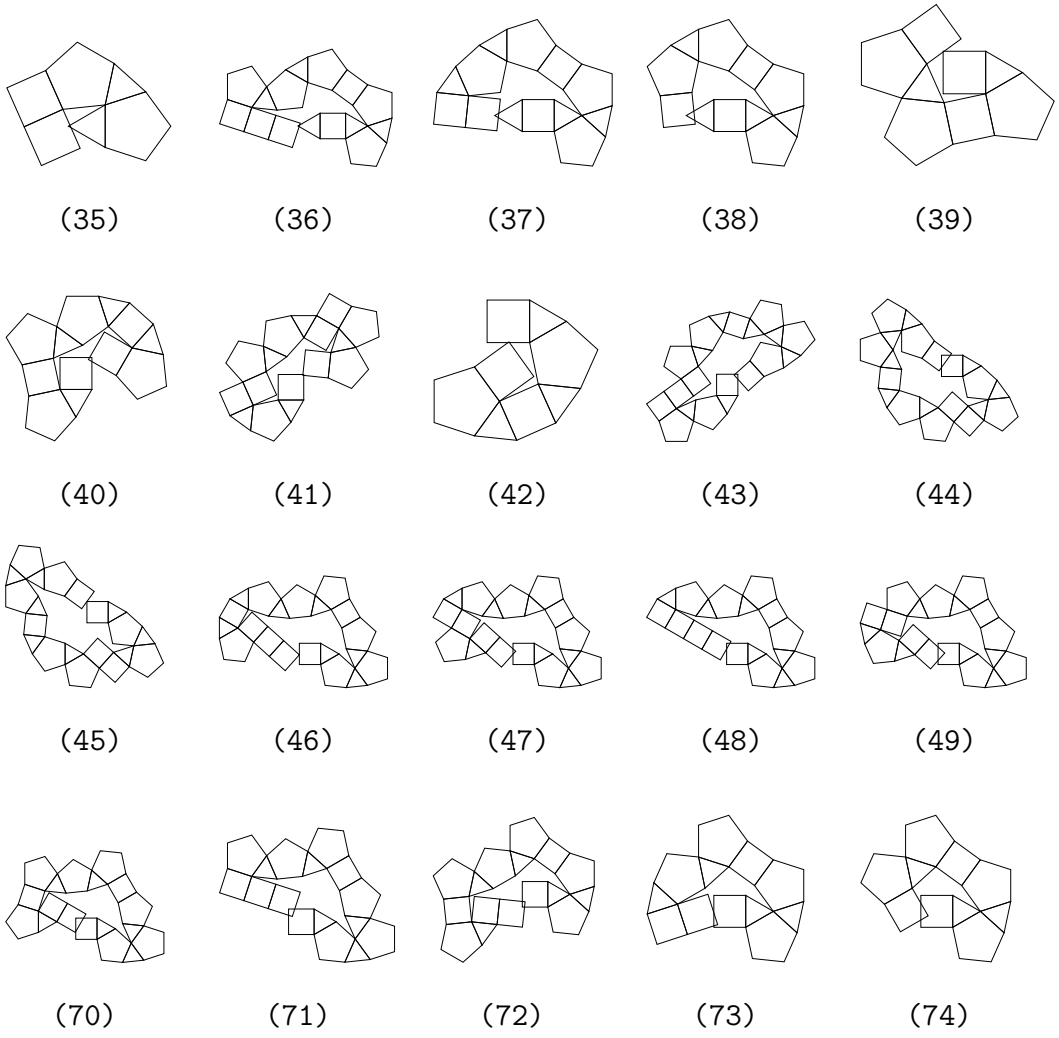

Figure A.12: List of MOPEs in J42. (continue)

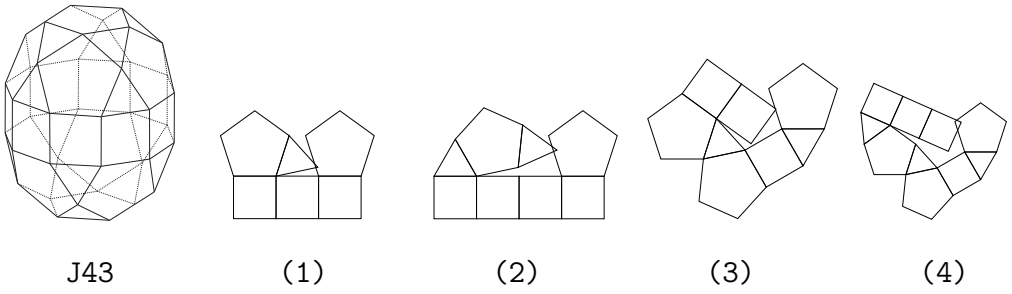

Figure A.13: List of MOPEs in J43.

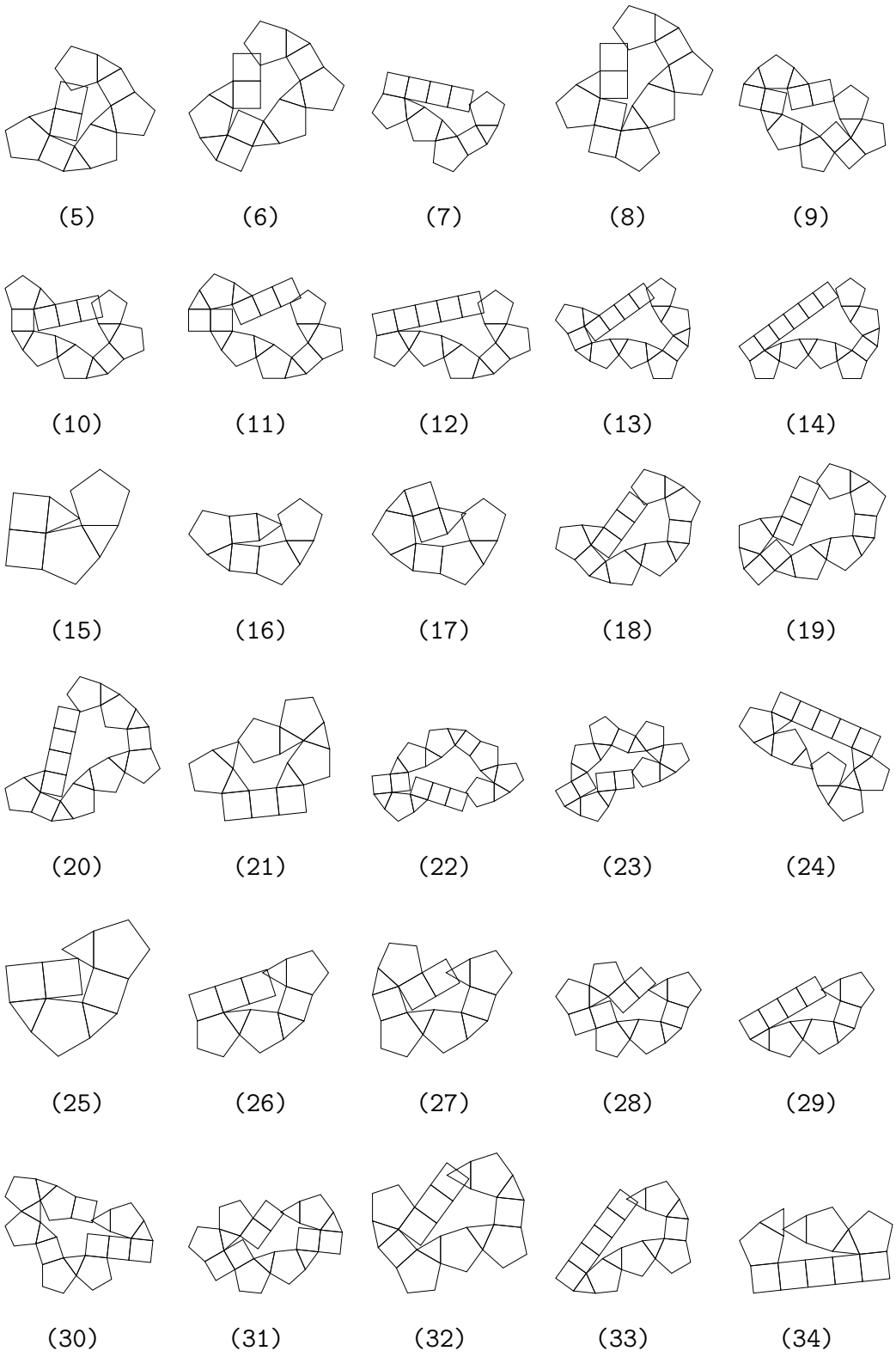

Figure A.13: List of MOPEs in J43. (continue)

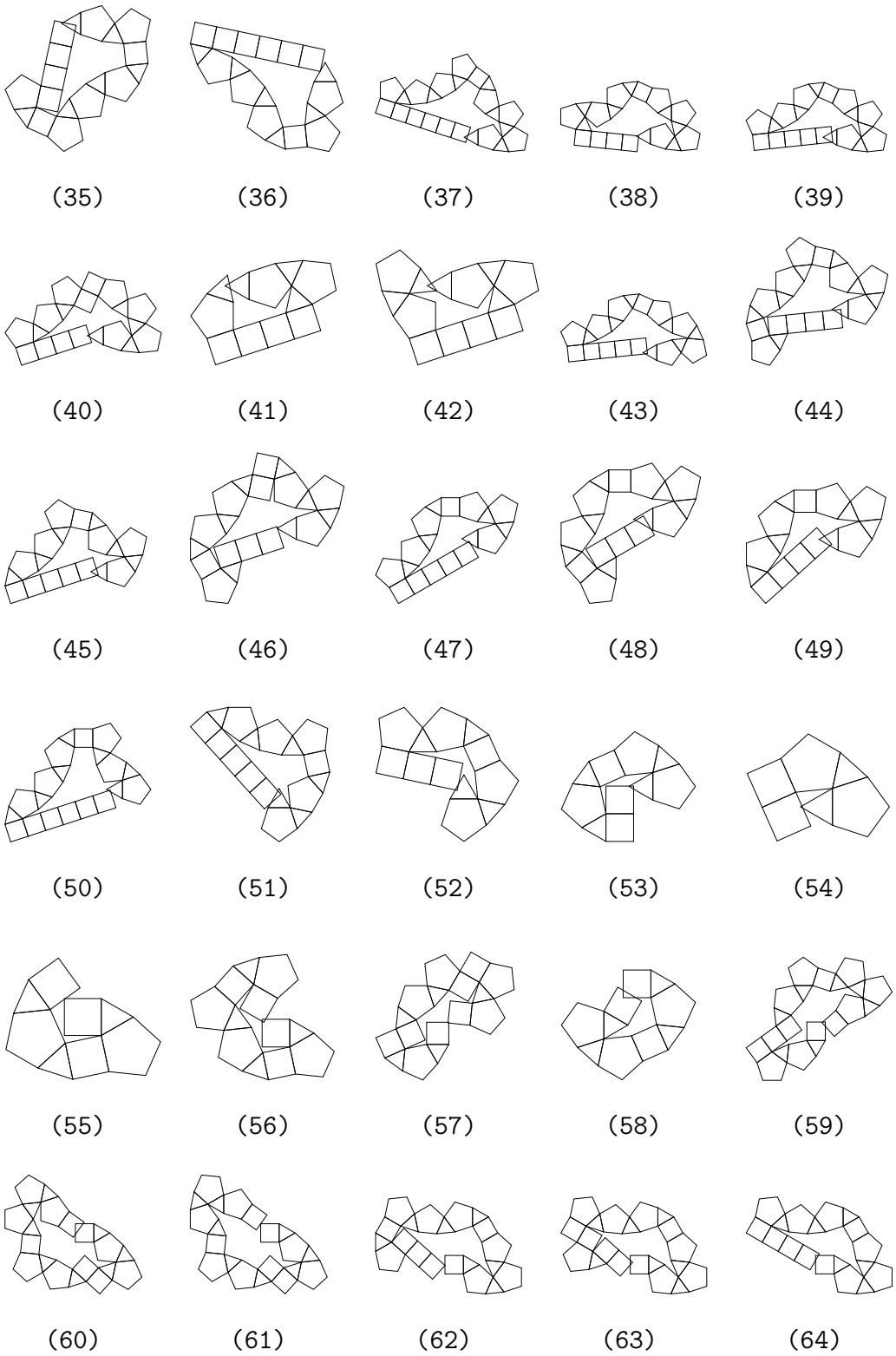

Figure A.13: List of MOPEs in J43. (continue)

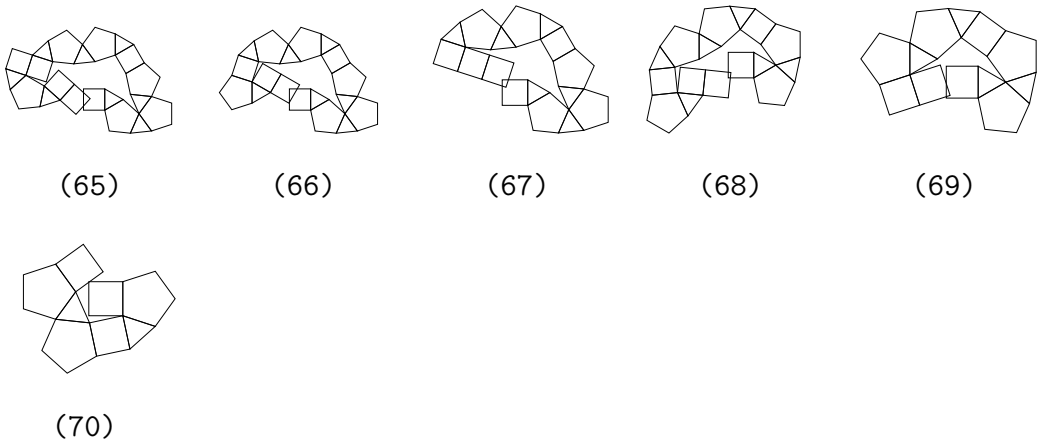

Figure A.13: List of MOPEs in J43. (continue)

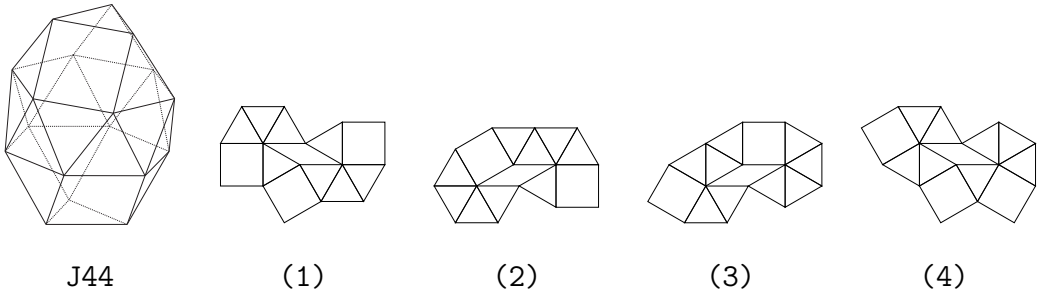

Figure A.14: List of MOPEs in J44.

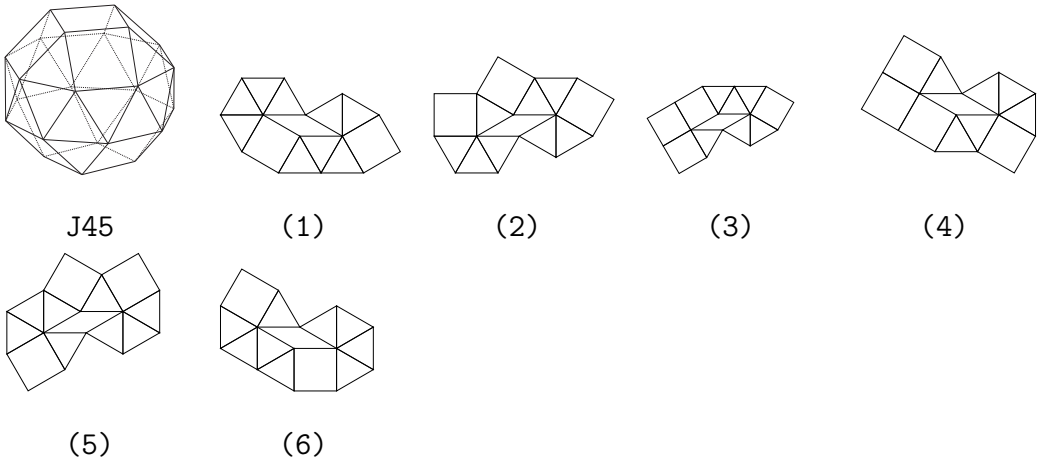

Figure A.15: List of MOPEs in J45.

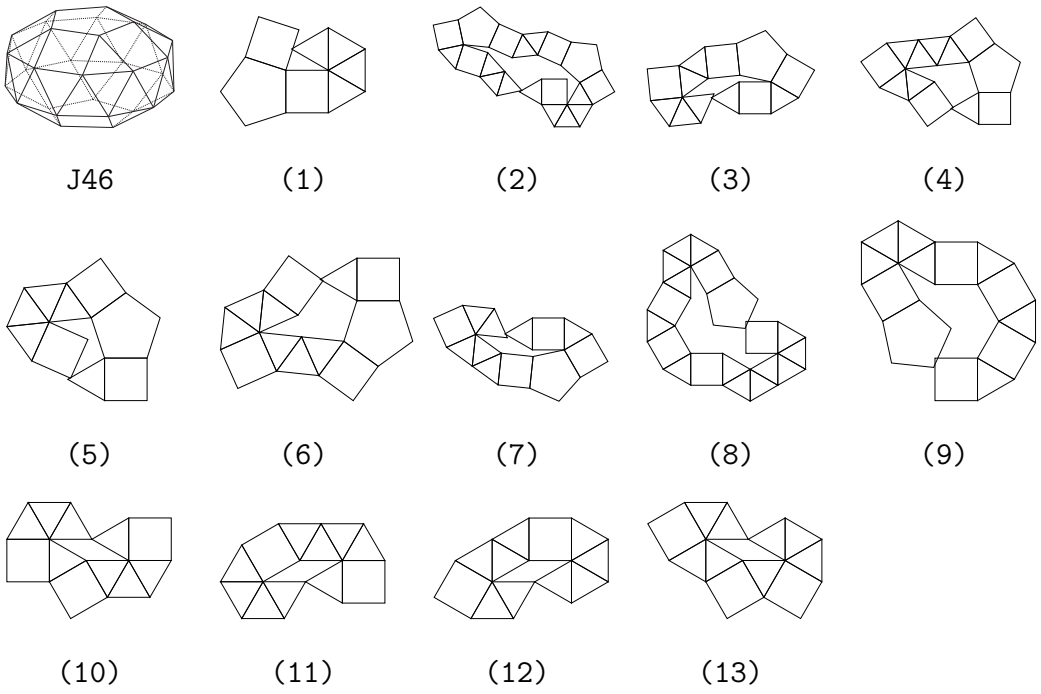

Figure A.16: List of MOPEs in J46.

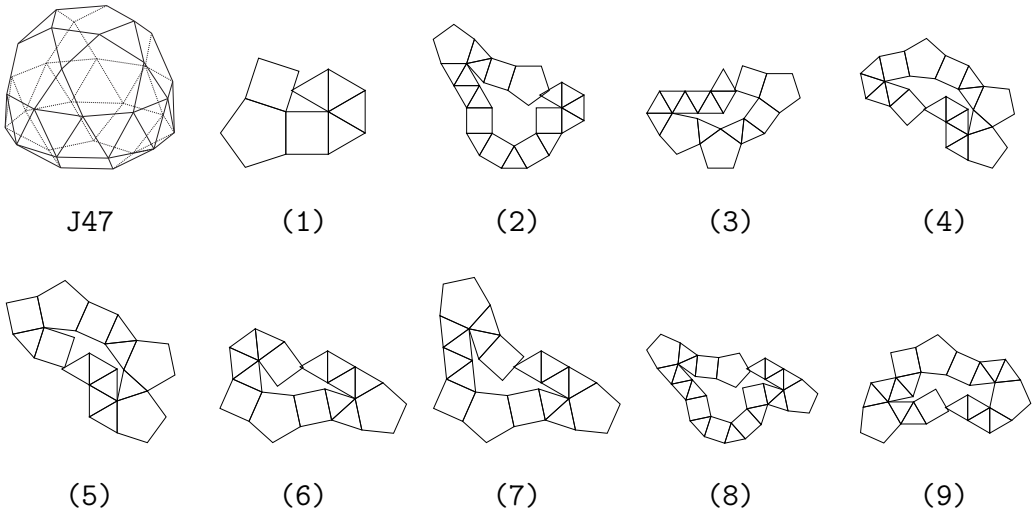

Figure A.17: List of MOPEs in J47.

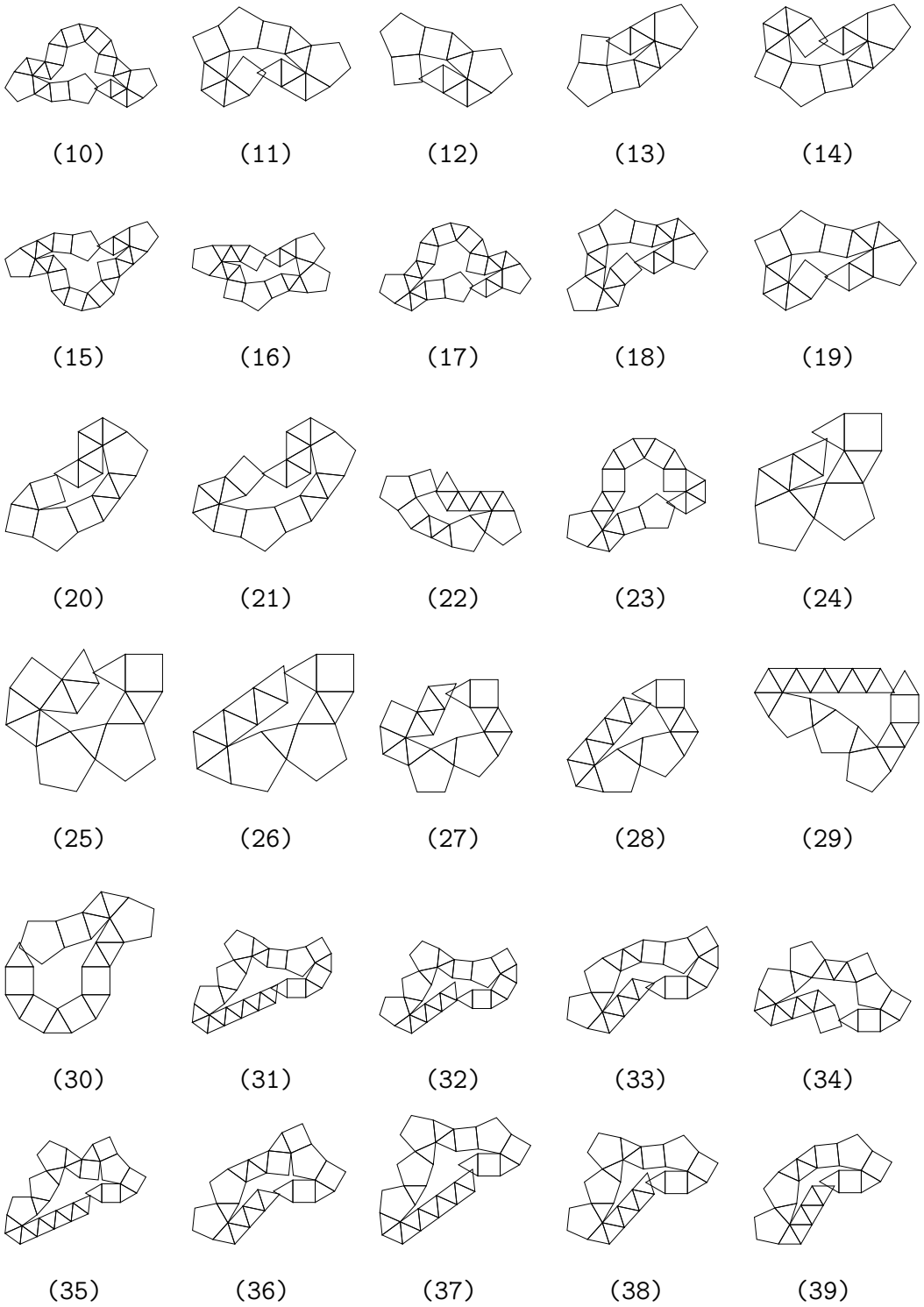

Figure A.17: List of MOPEs in J47. (continue)

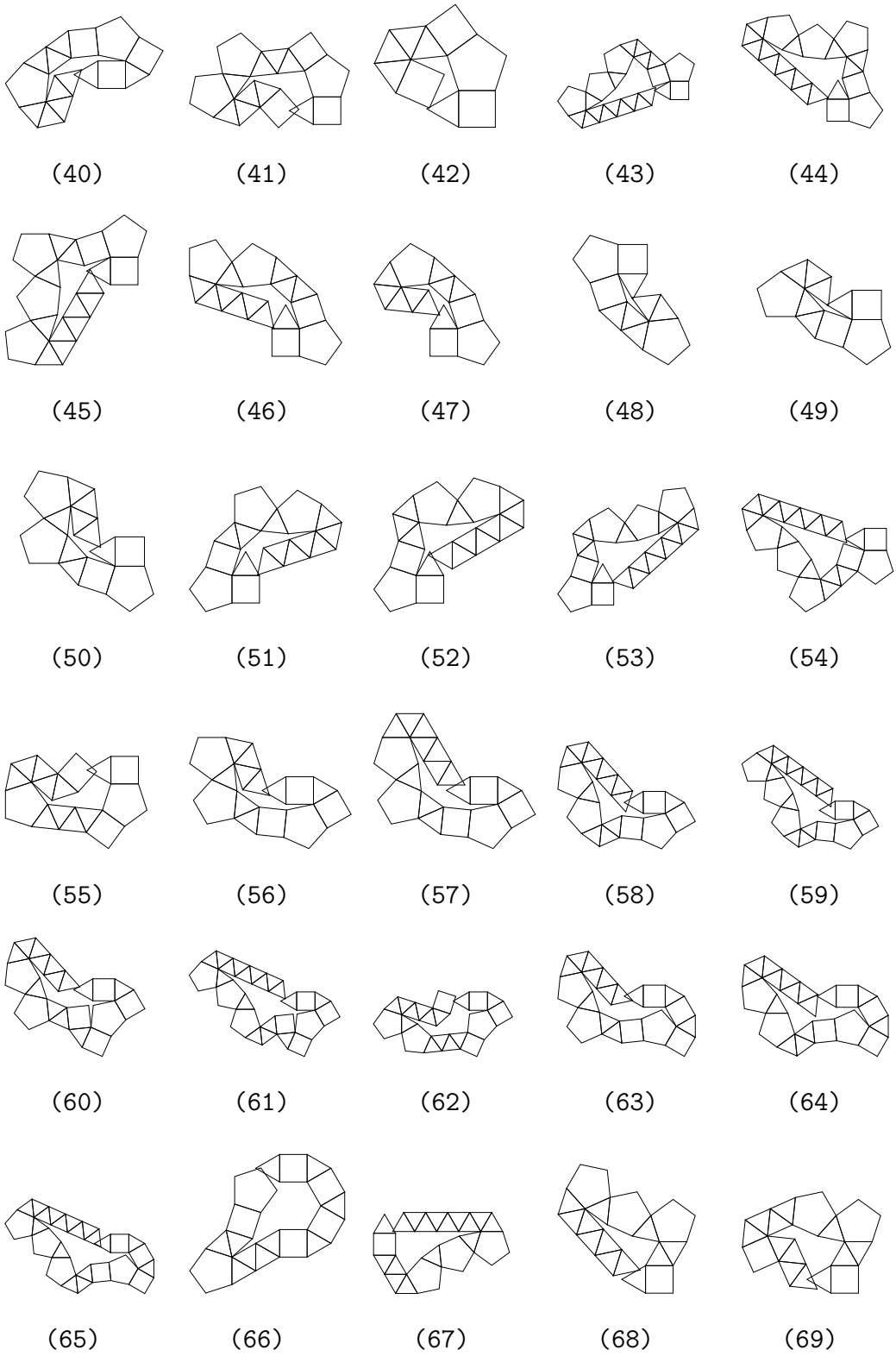

Figure A.17: List of MOPEs in J47. (continue)

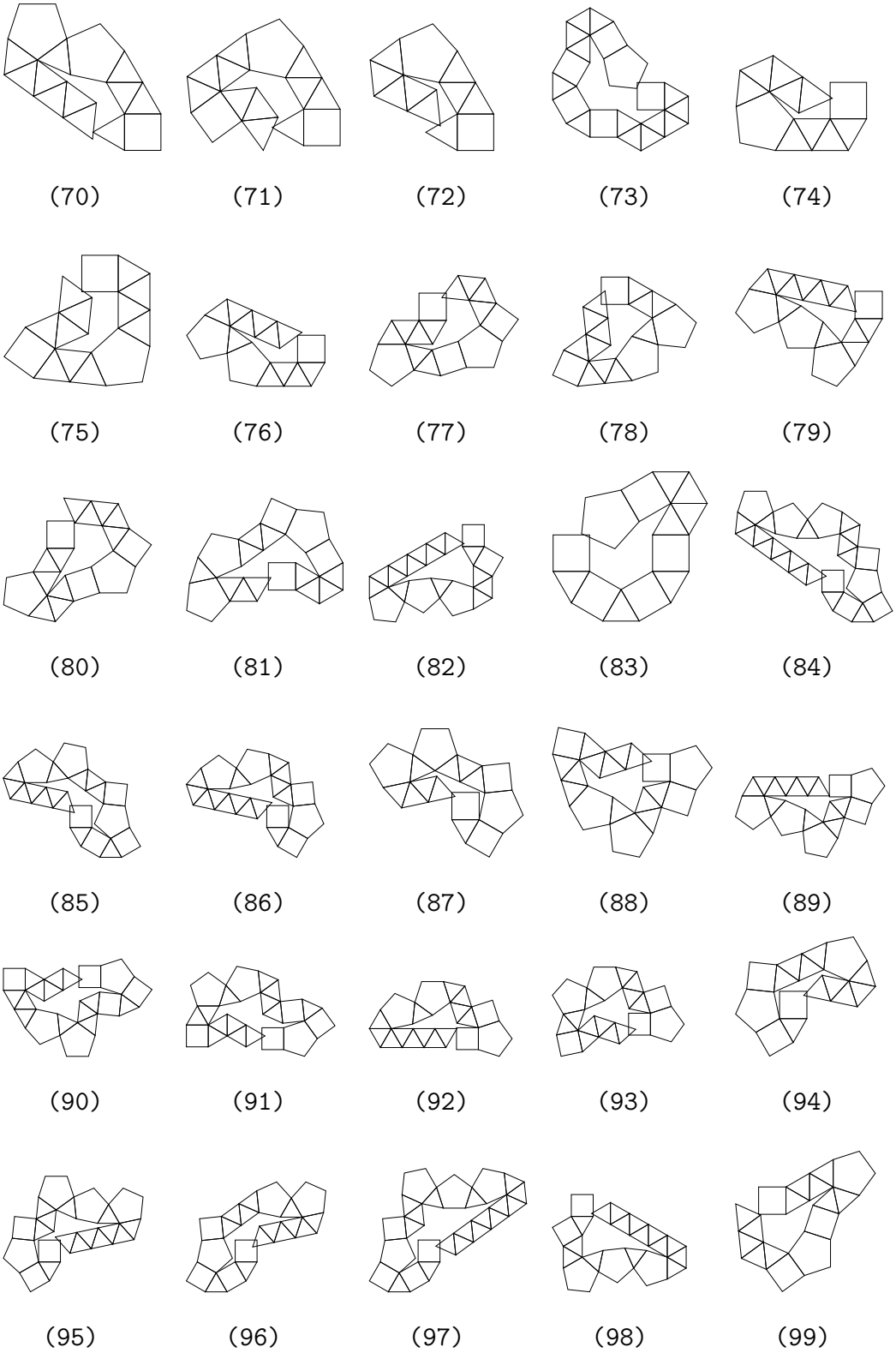

Figure A.17: List of MOPEs in J47. (continue)

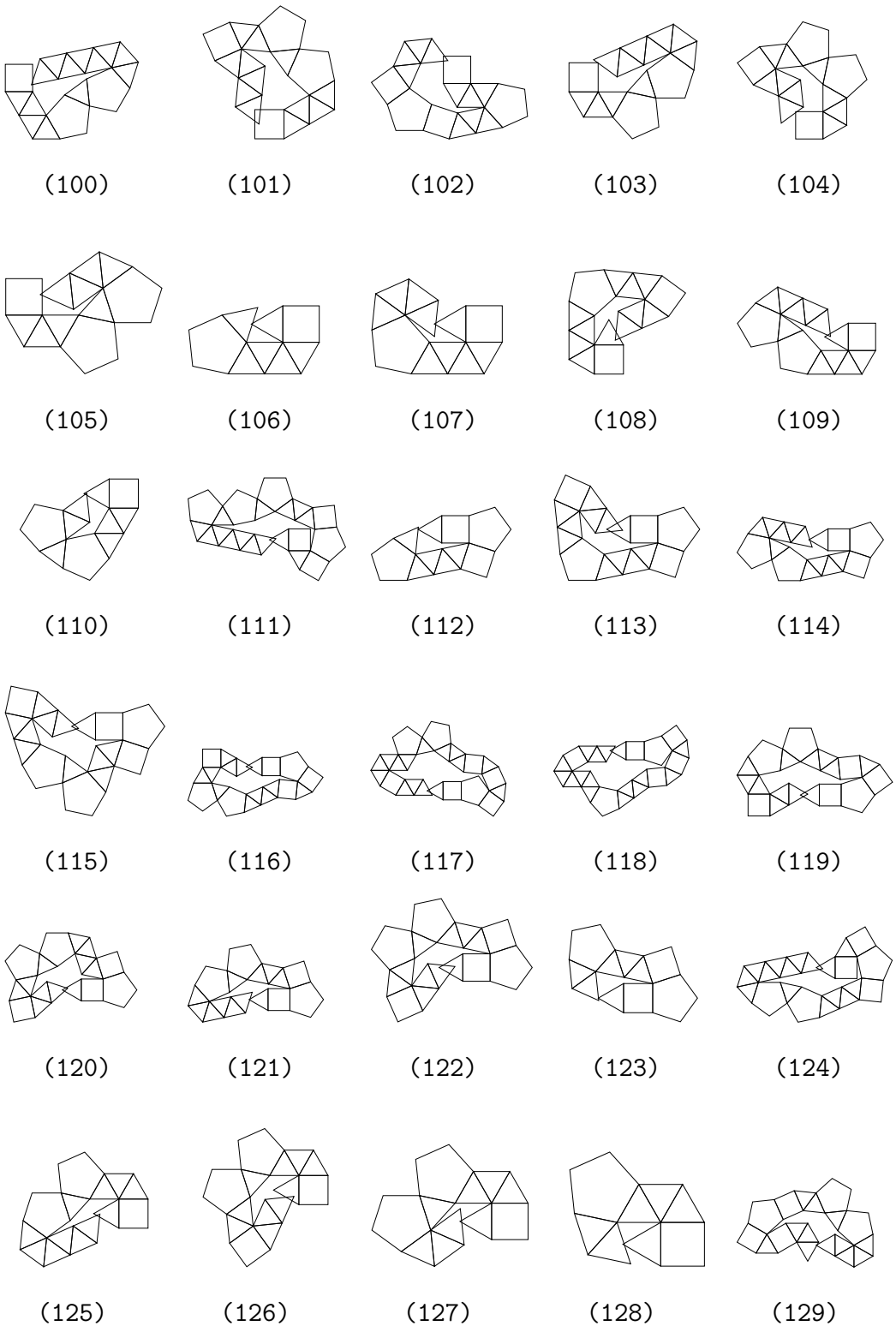

Figure A.17: List of MOPEs in J47. (continue)

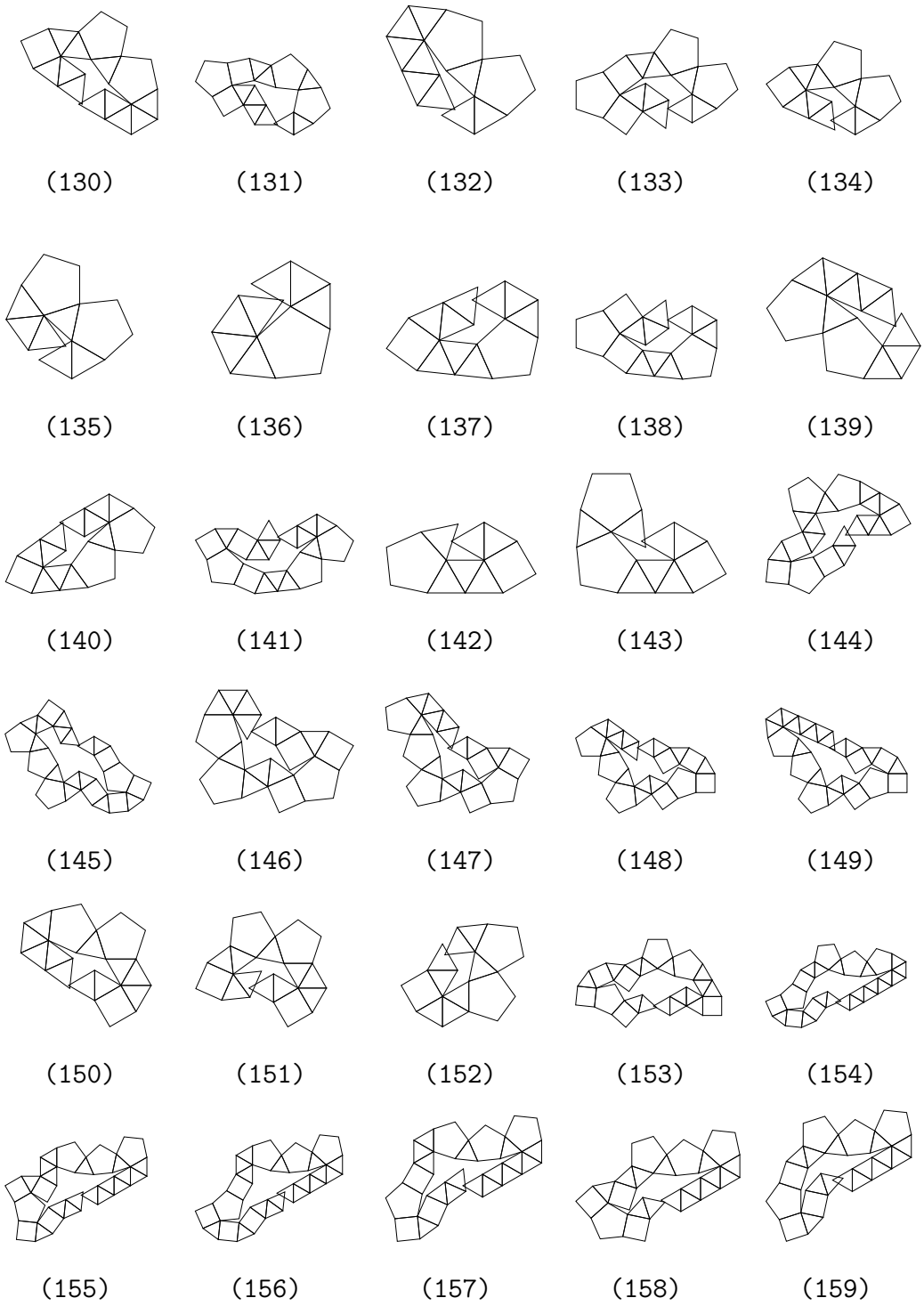

Figure A.17: List of MOPEs in J47. (continue)

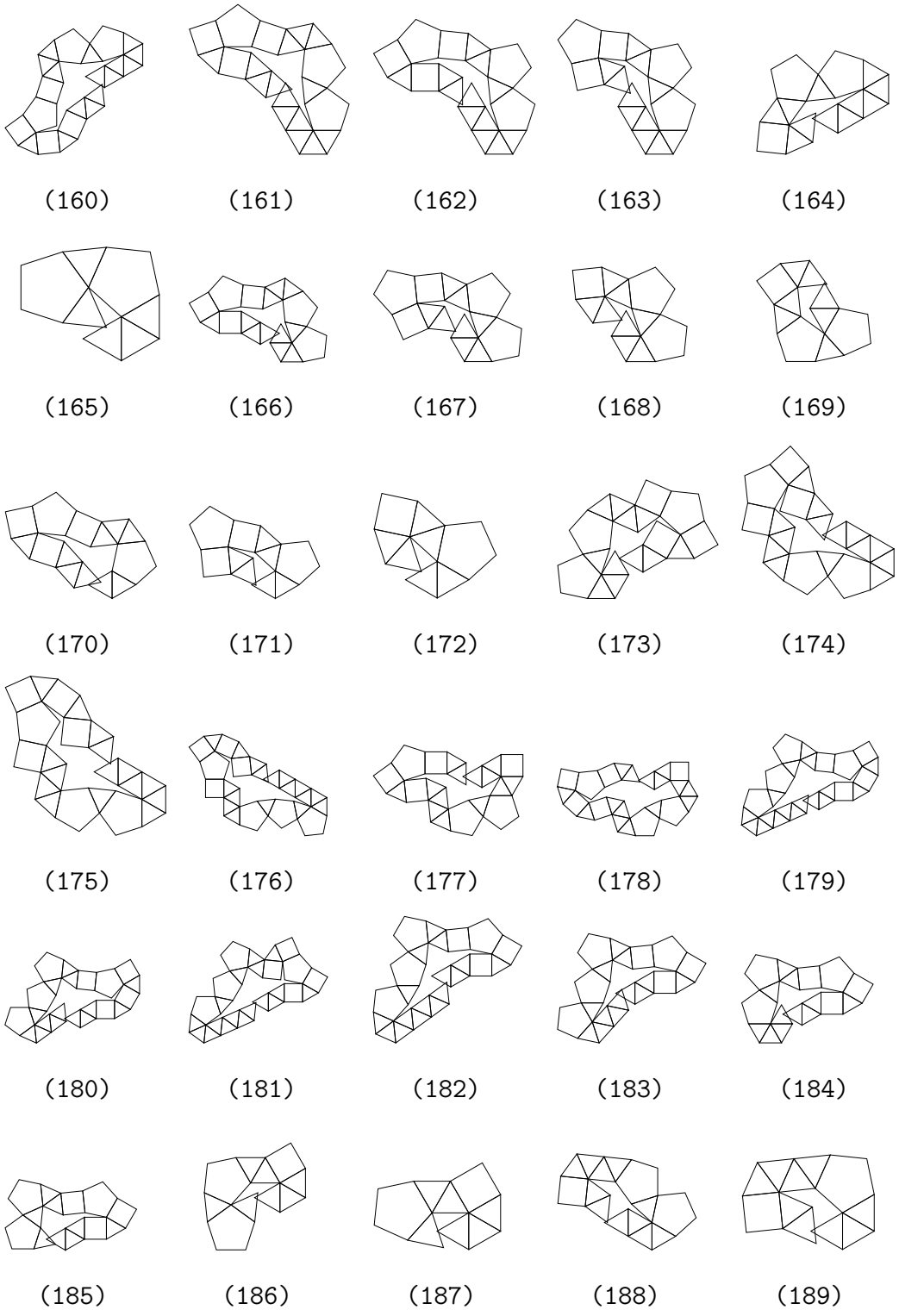

Figure A.17: List of MOPEs in J47. (continue)

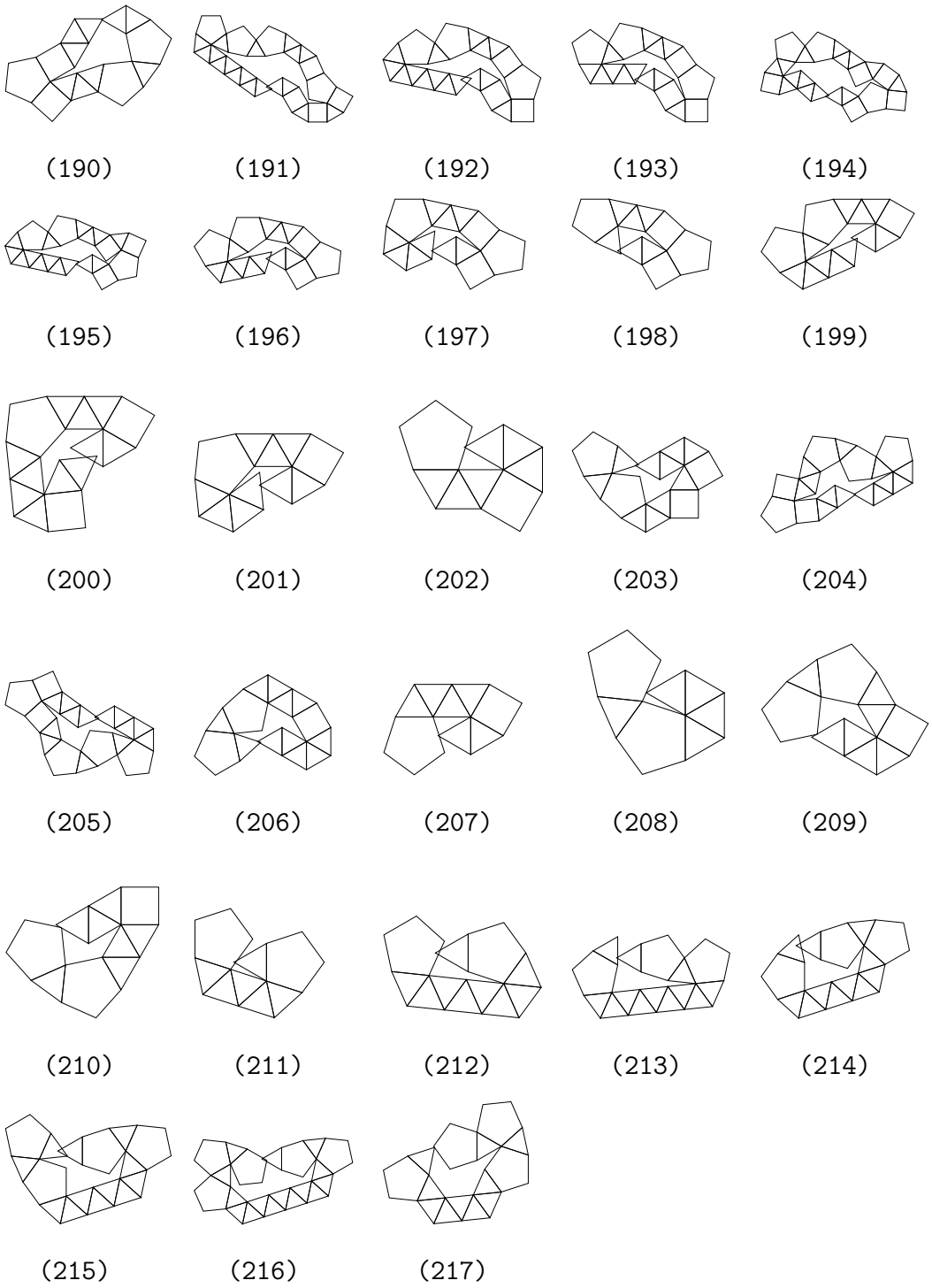

Figure A.17: List of MOPEs in J47. (continue)

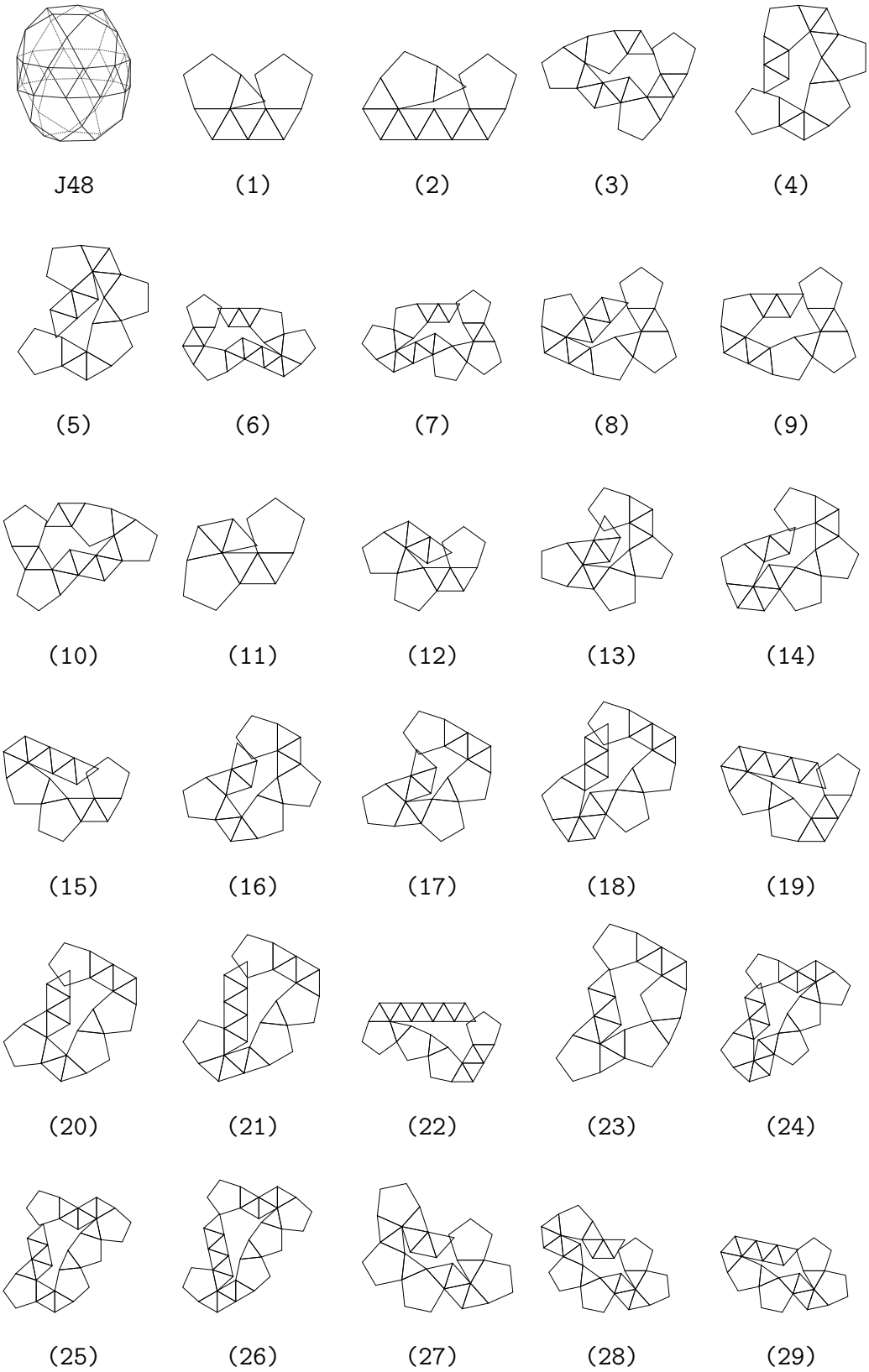

Figure A.18: List of MOPEs in J48.

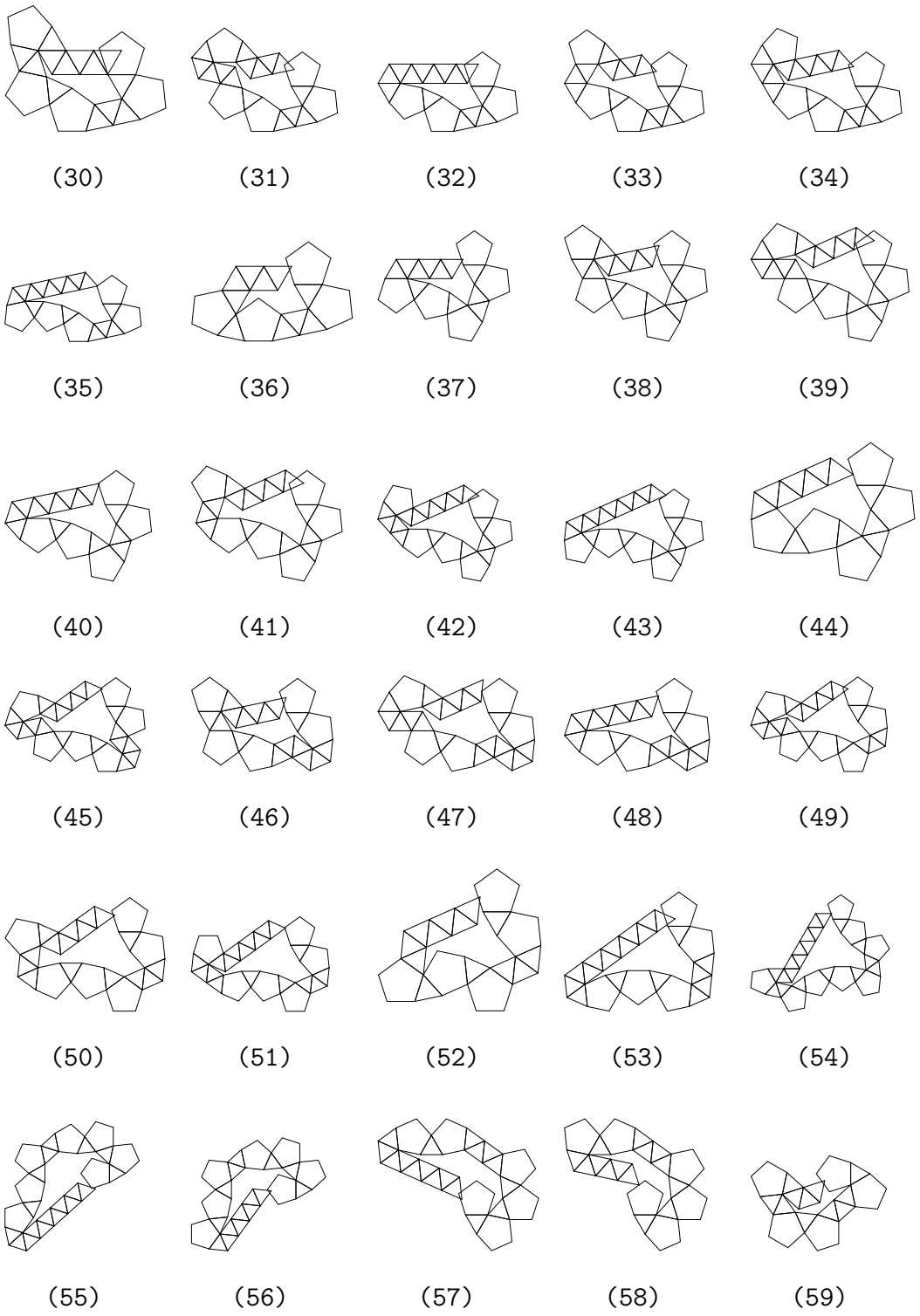

Figure A.18: List of MOPEs in J48. (continue)

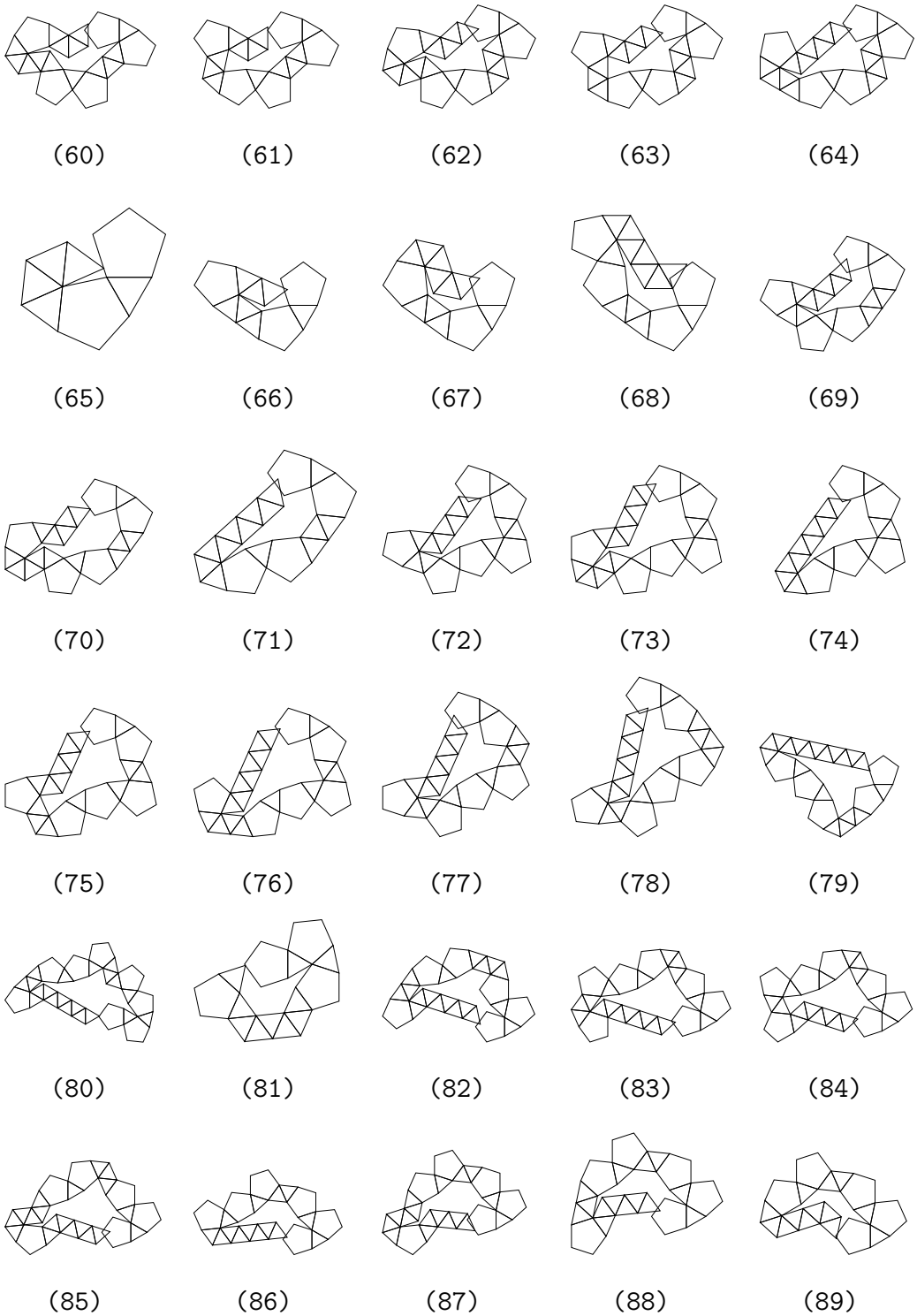

Figure A.18: List of MOPEs in J48. (continue)

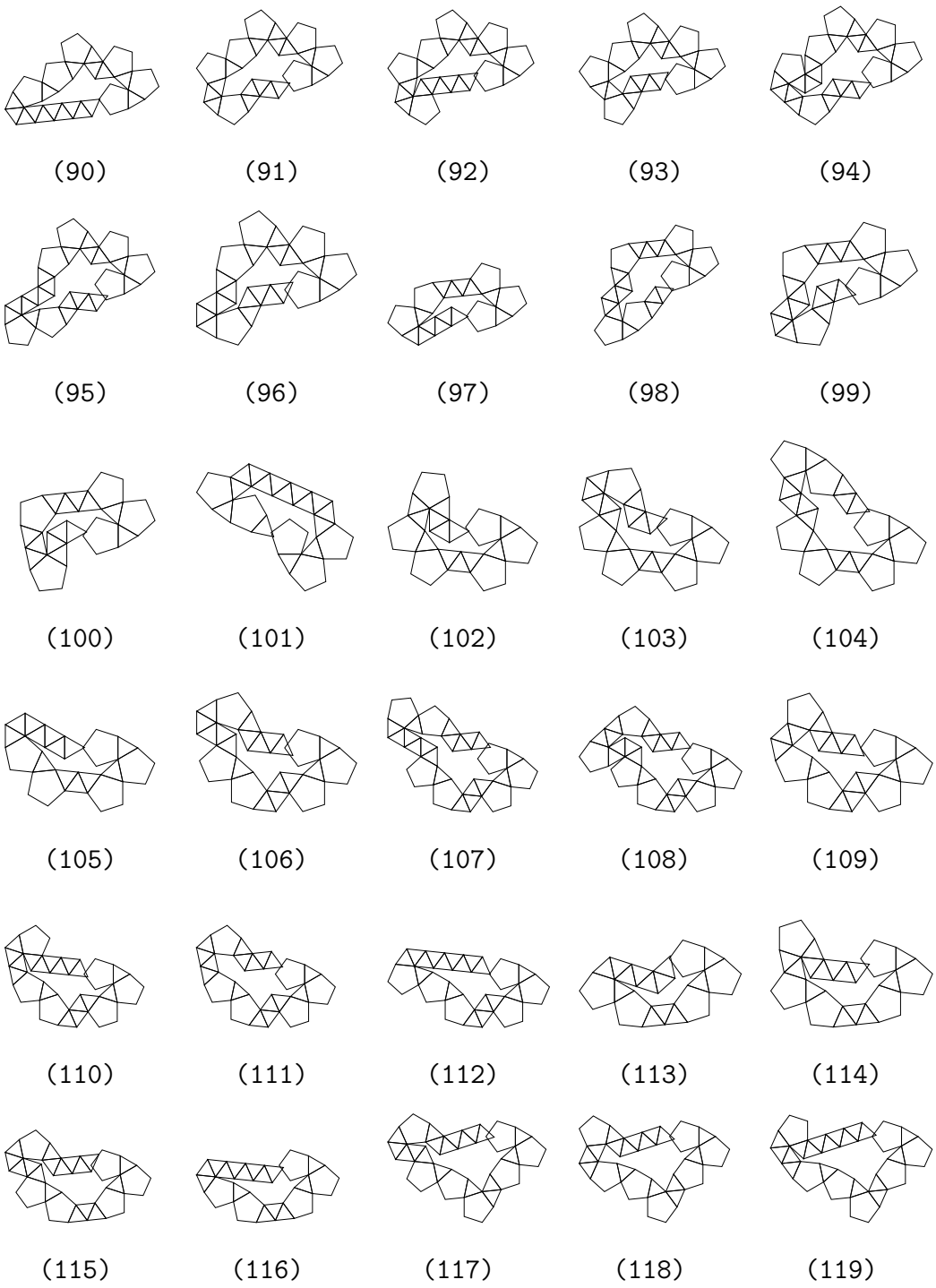

Figure A.18: List of MOPEs in J48. (continue)

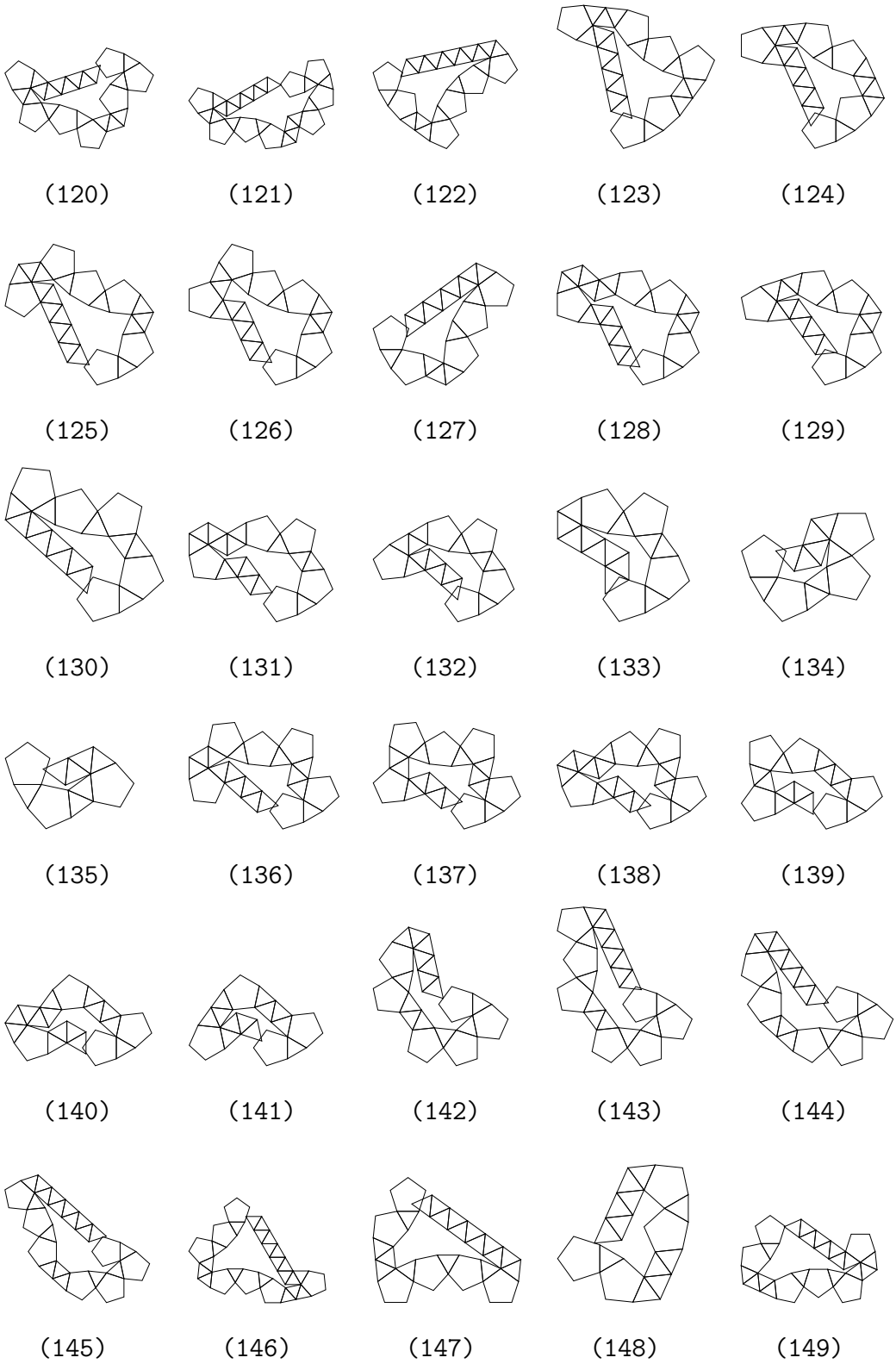

Figure A.18: List of MOPEs in J48. (continue)

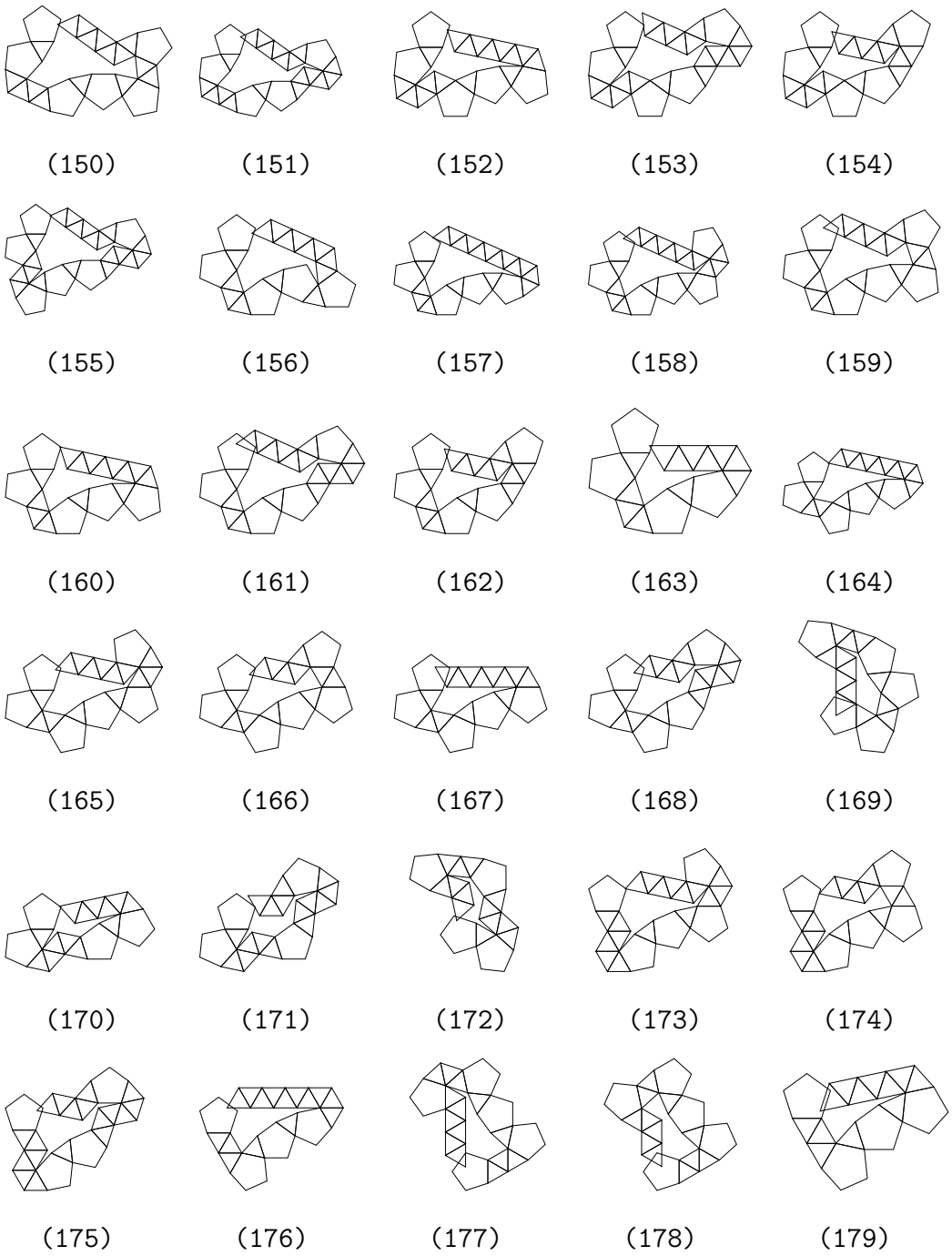

Figure A.18: List of MOPEs in J48. (continue)

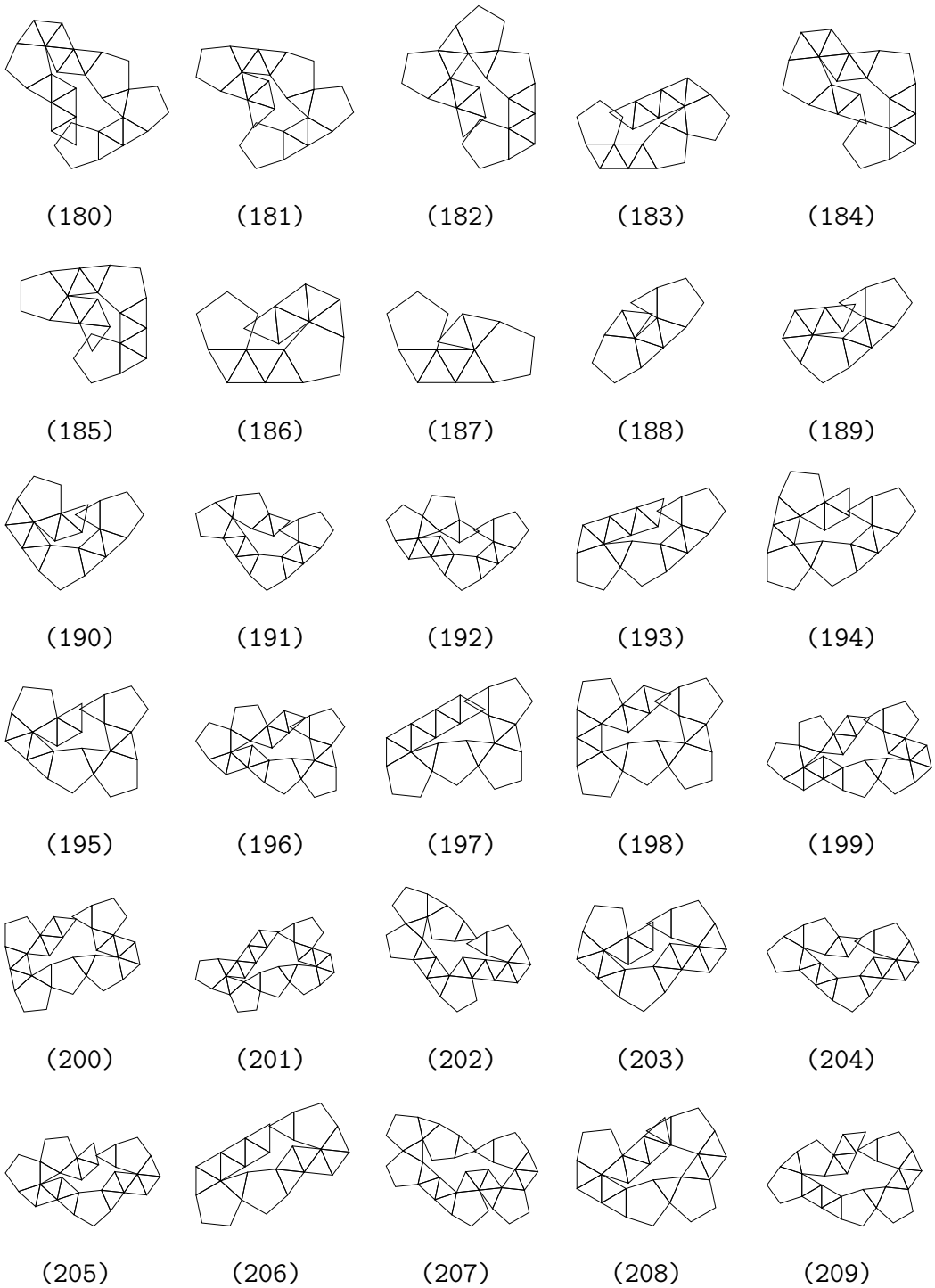

Figure A.18: List of MOPEs in J48. (continue)

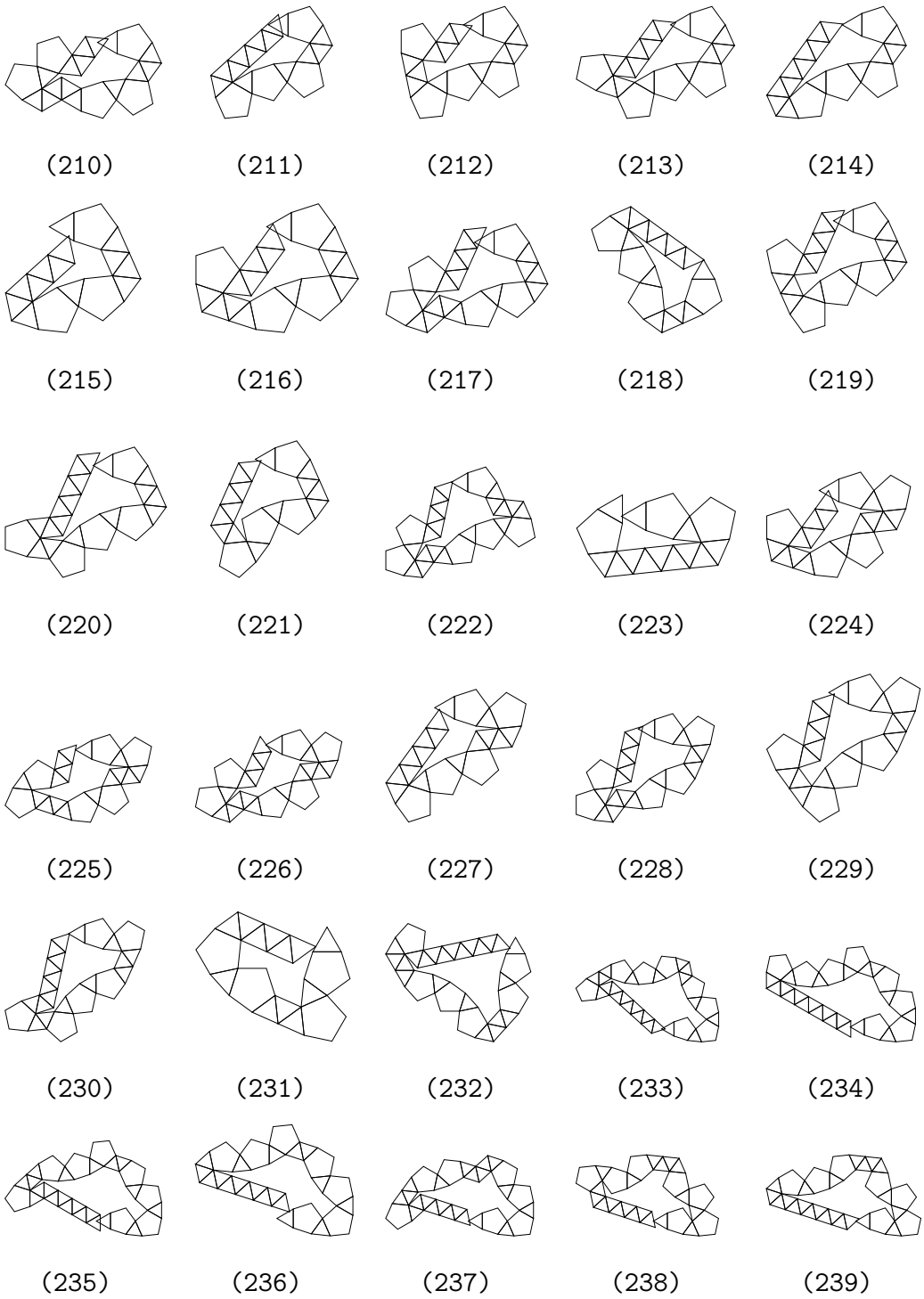

Figure A.18: List of MOPEs in J48. (continue)

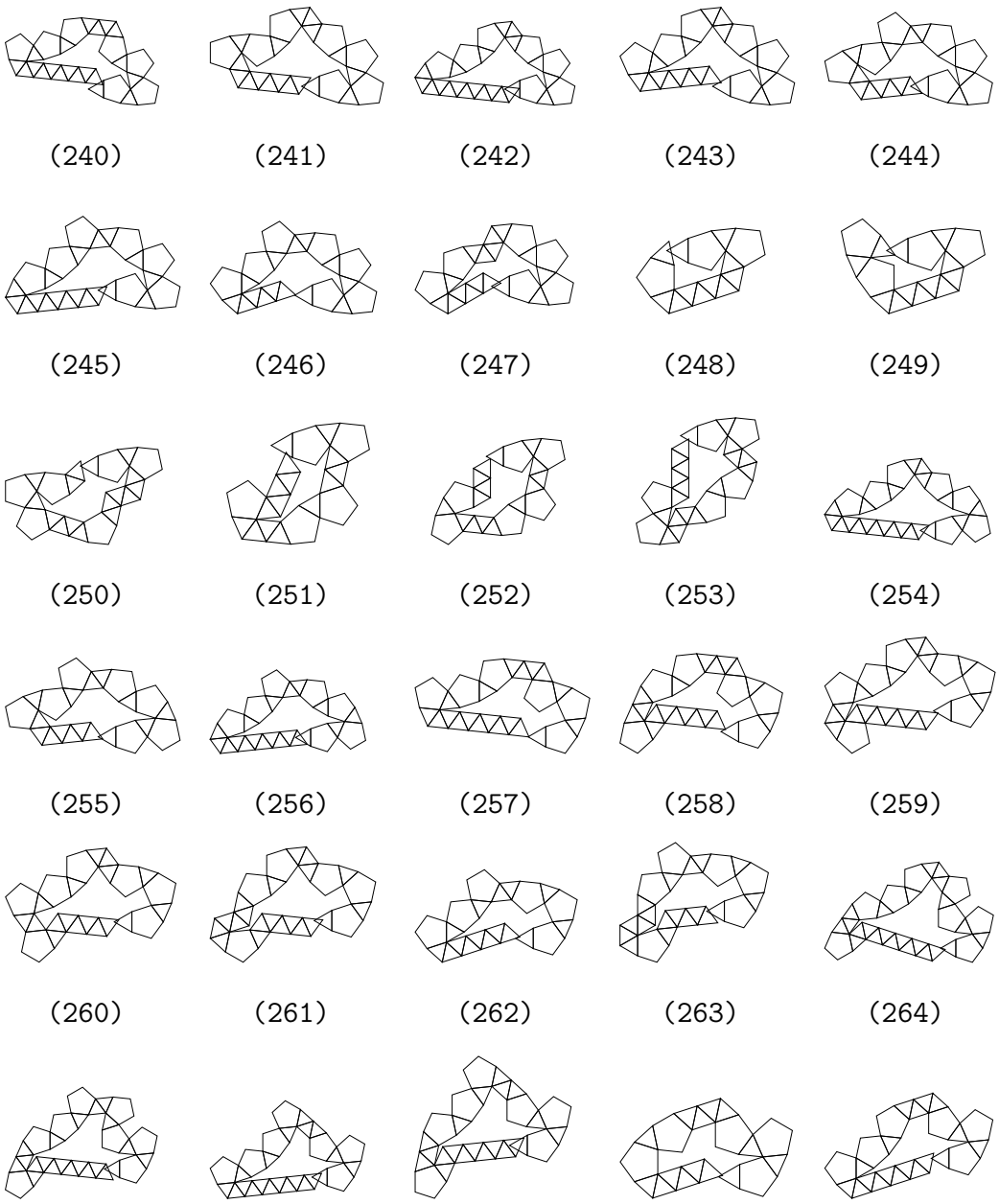

Figure A.18: List of MOPEs in J48. (continue)

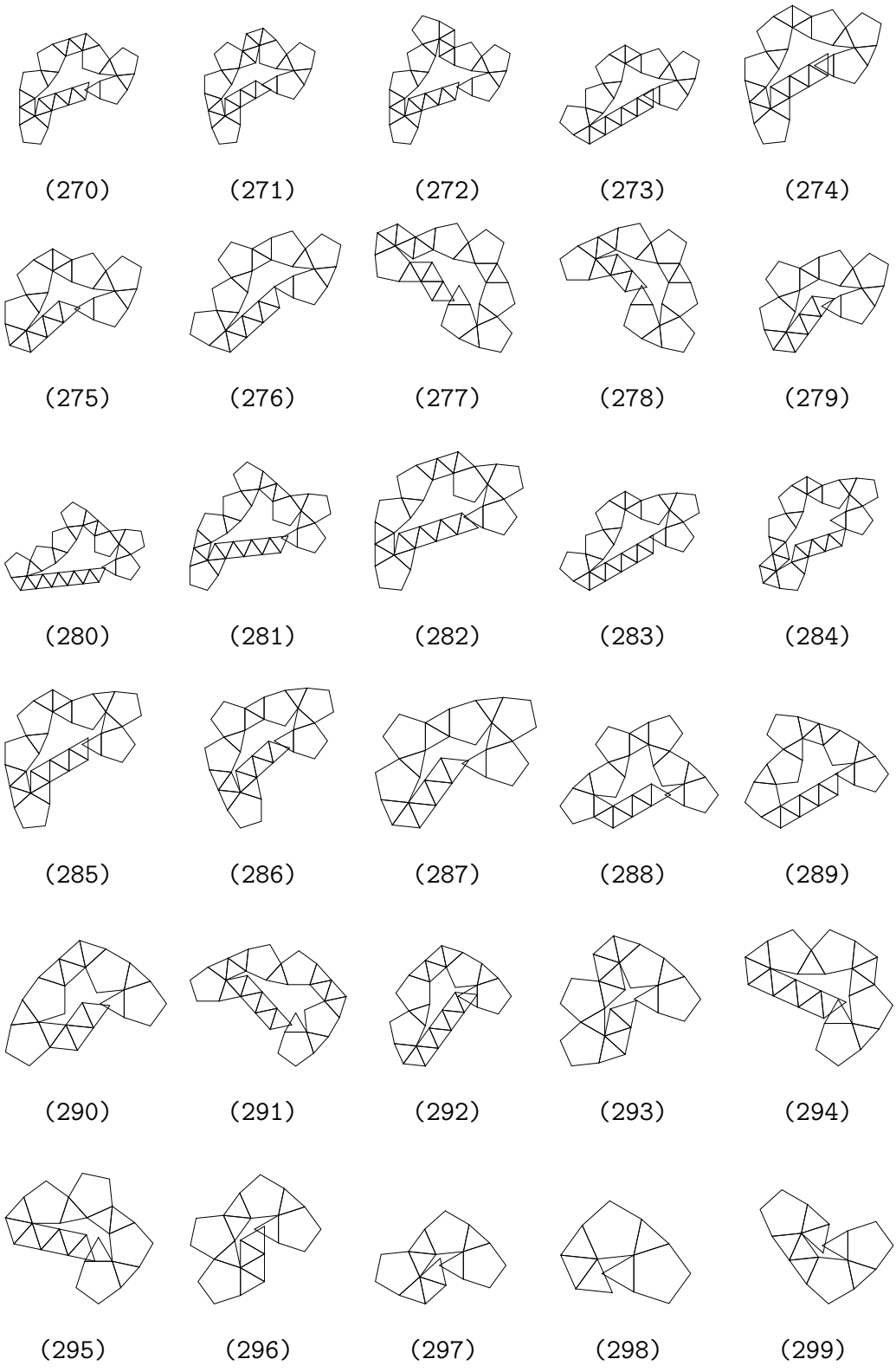

Figure A.18: List of MOPEs in J48. (continue)

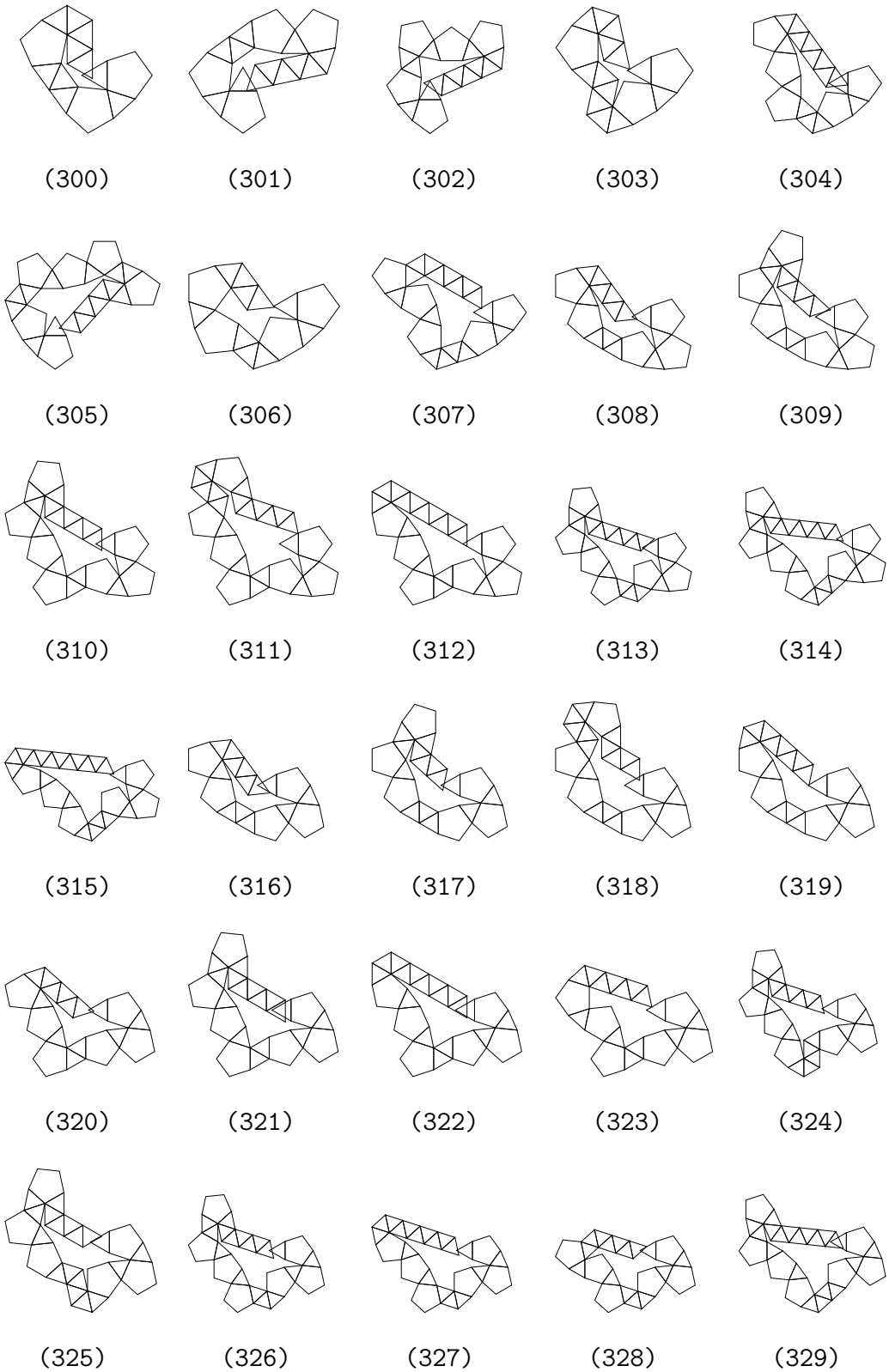

Figure A.18: List of MOPEs in J48. (continue)

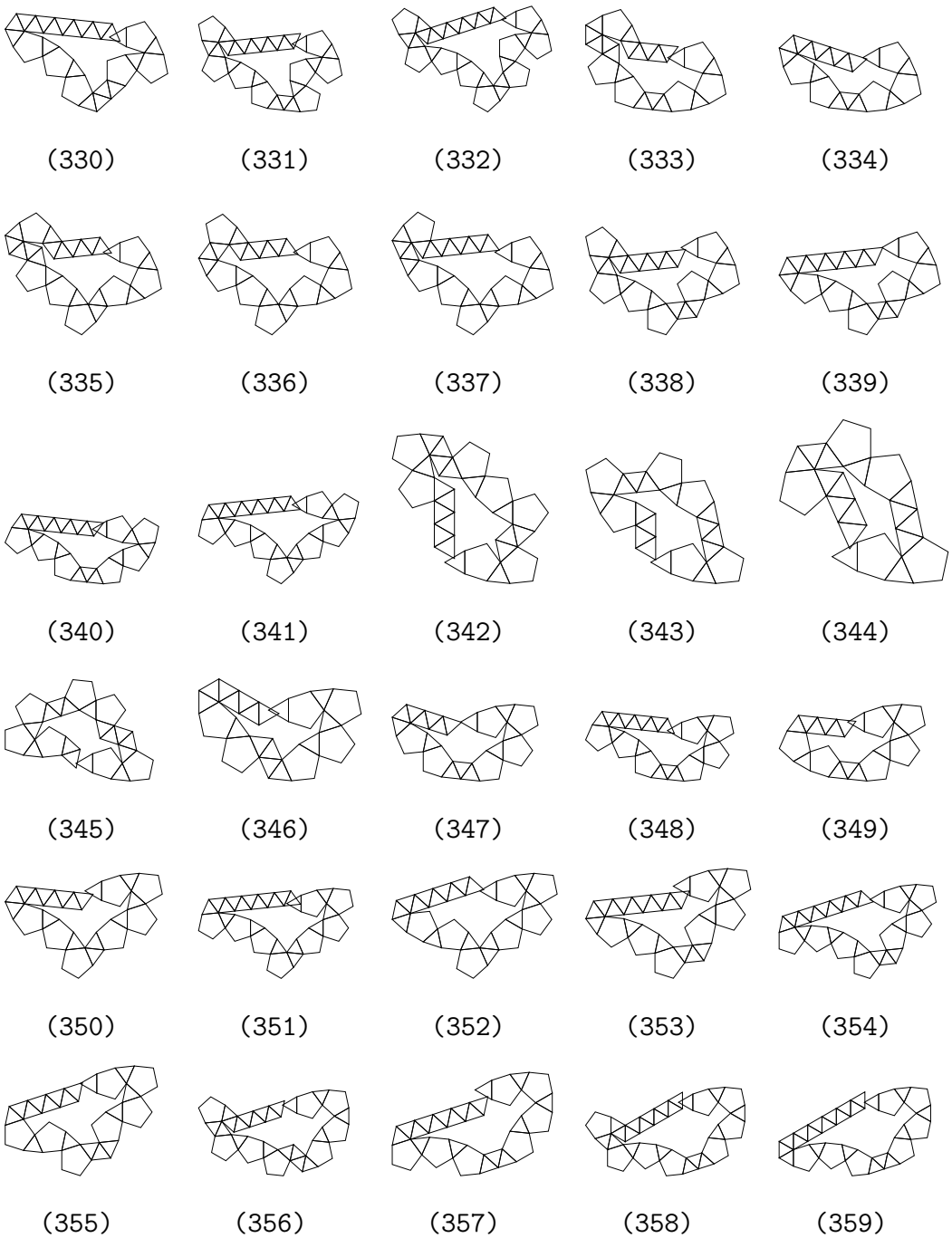

Figure A.18: List of MOPEs in J48. (continue)

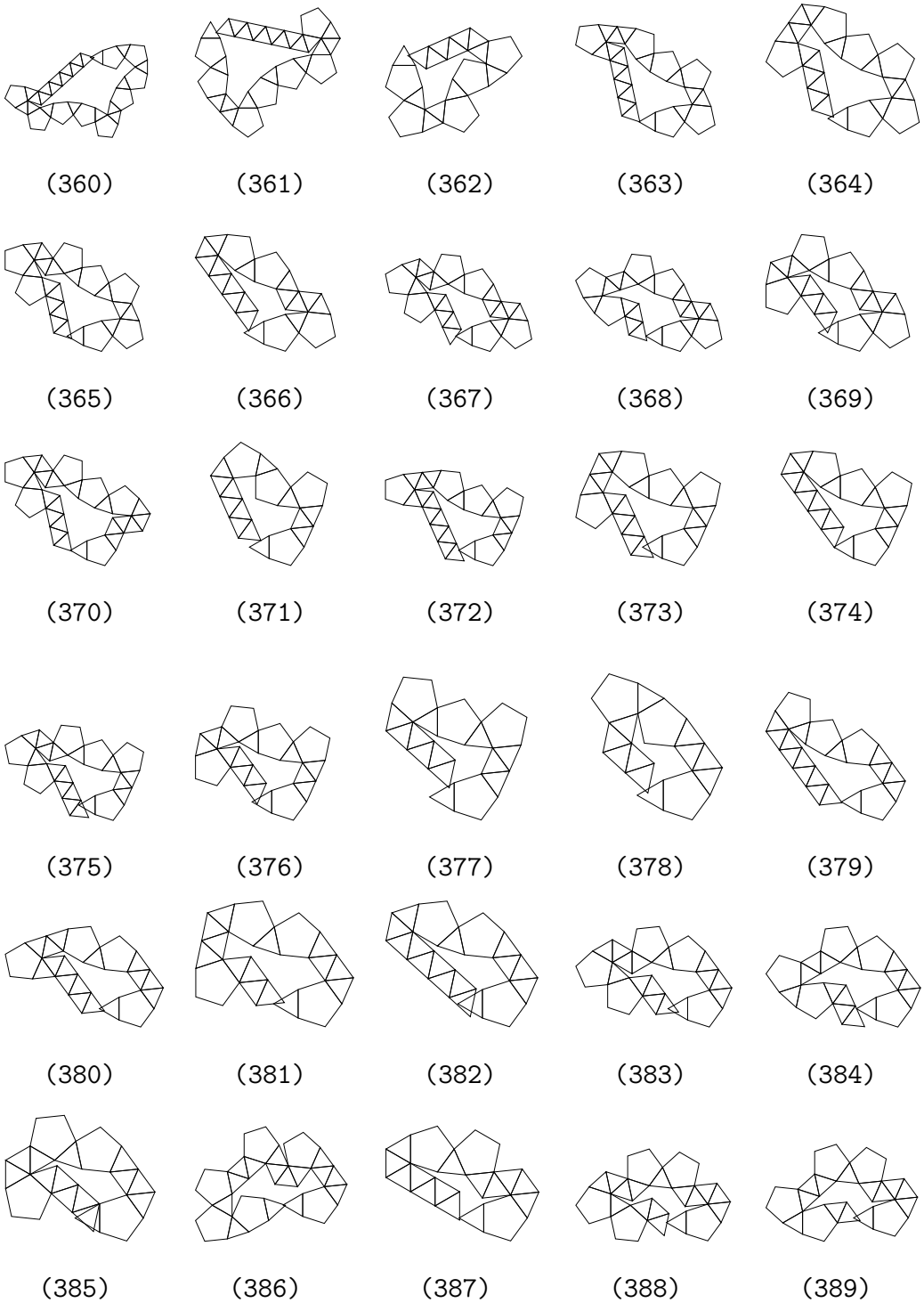

Figure A.18: List of MOPEs in J48. (continue)

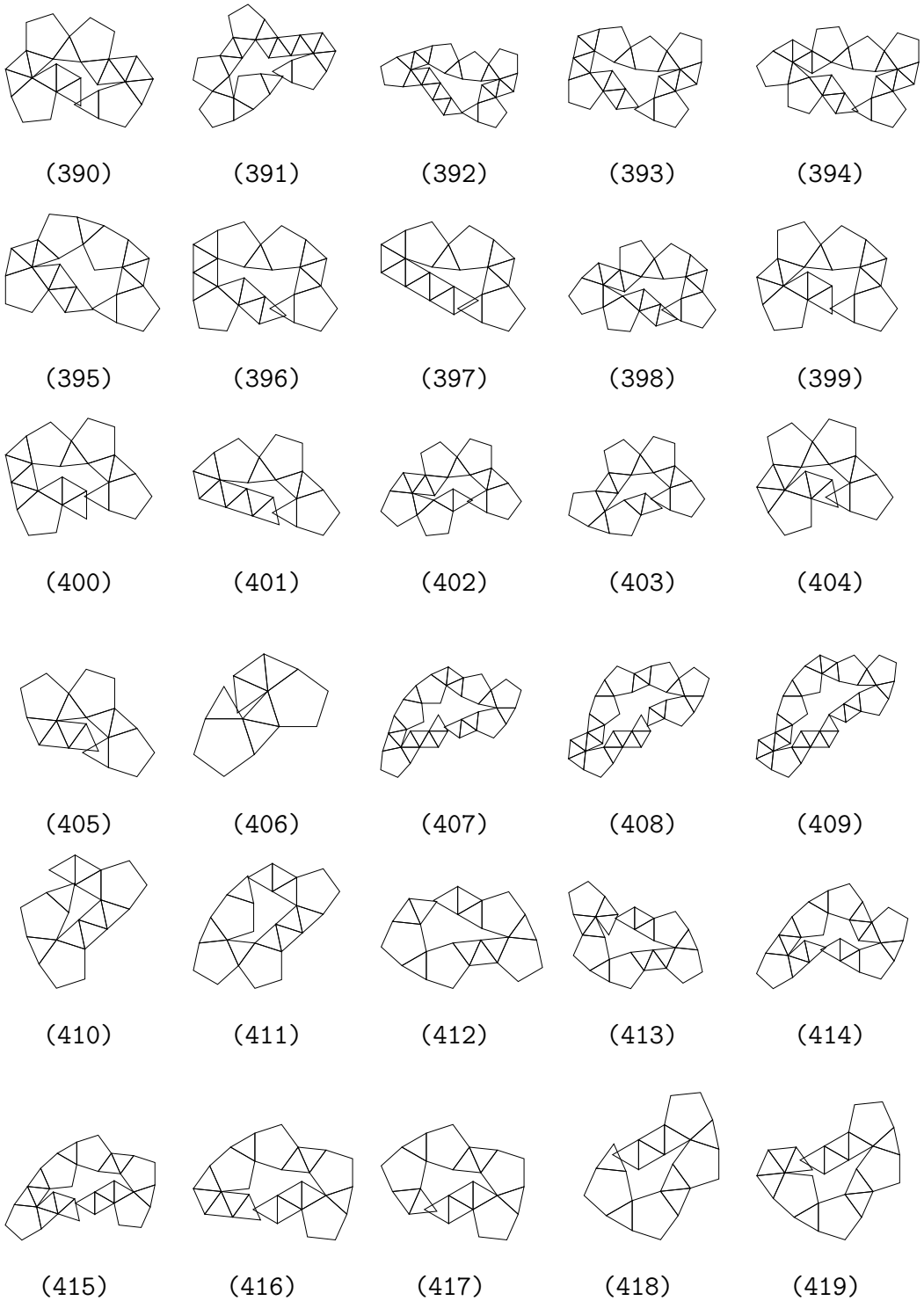

Figure A.18: List of MOPEs in J48. (continue)

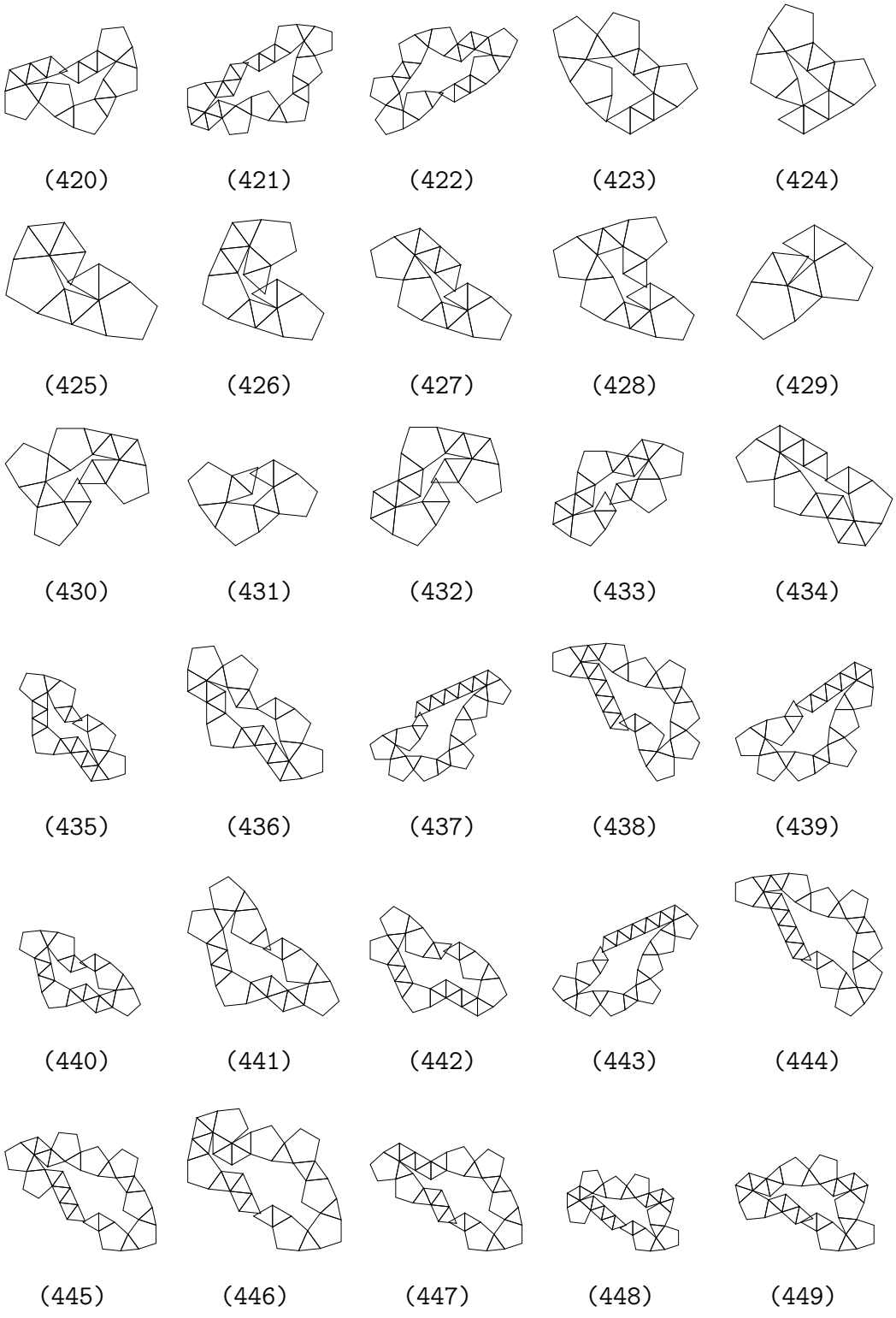

Figure A.18: List of MOPEs in J48. (continue)

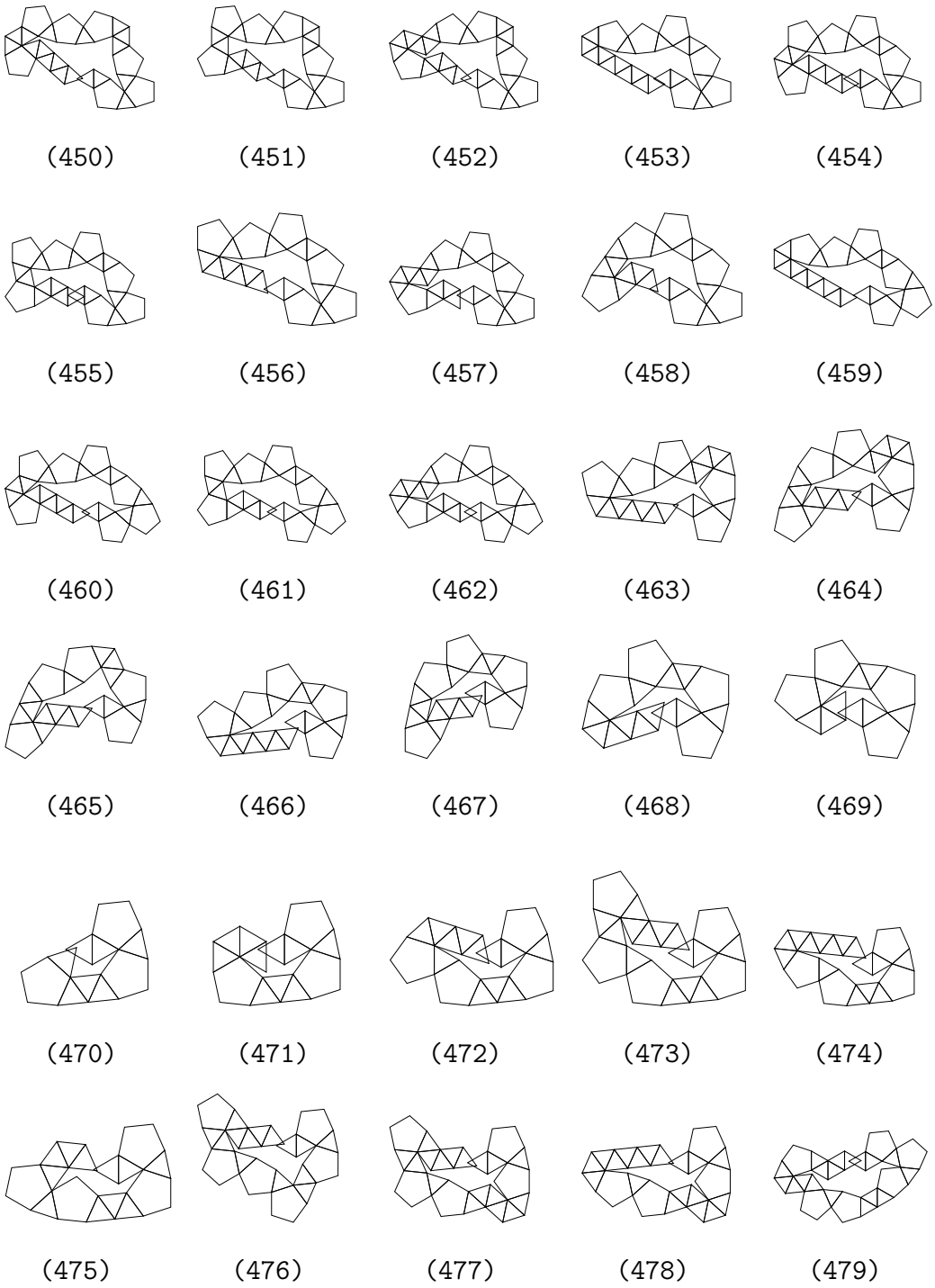

Figure A.18: List of MOPEs in J48. (continue)

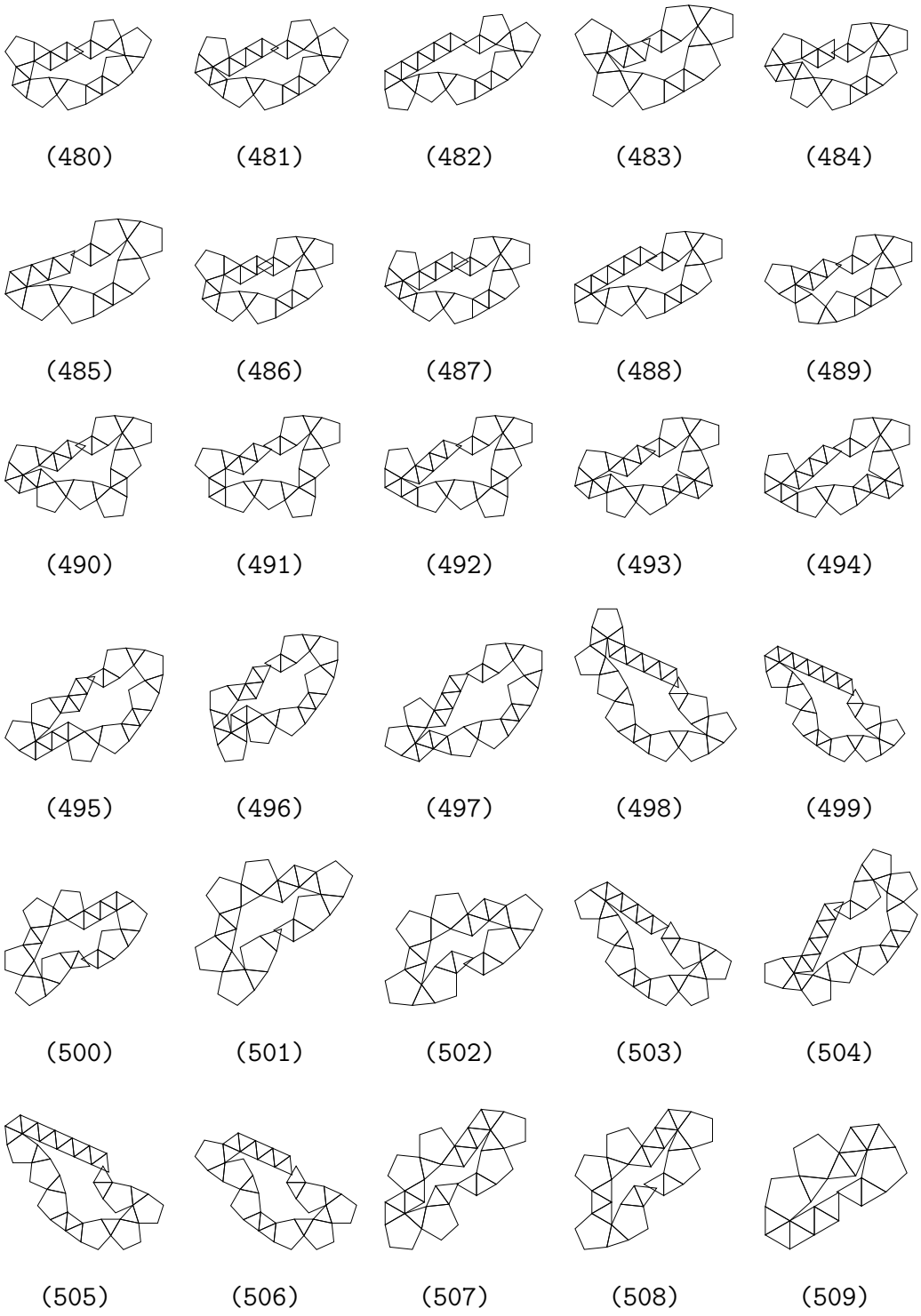

Figure A.18: List of MOPEs in J48. (continue)

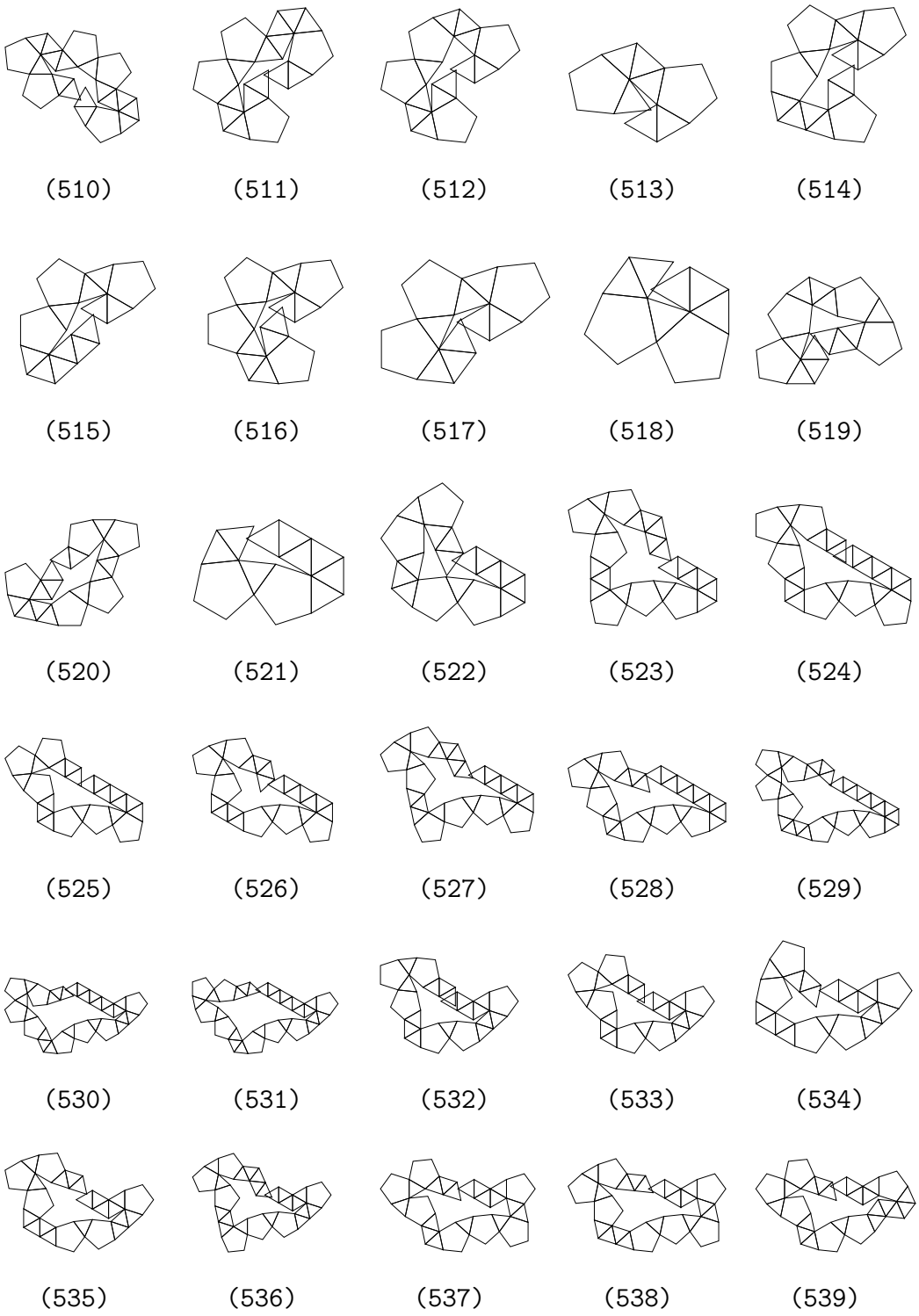

Figure A.18: List of MOPEs in J48. (continue)

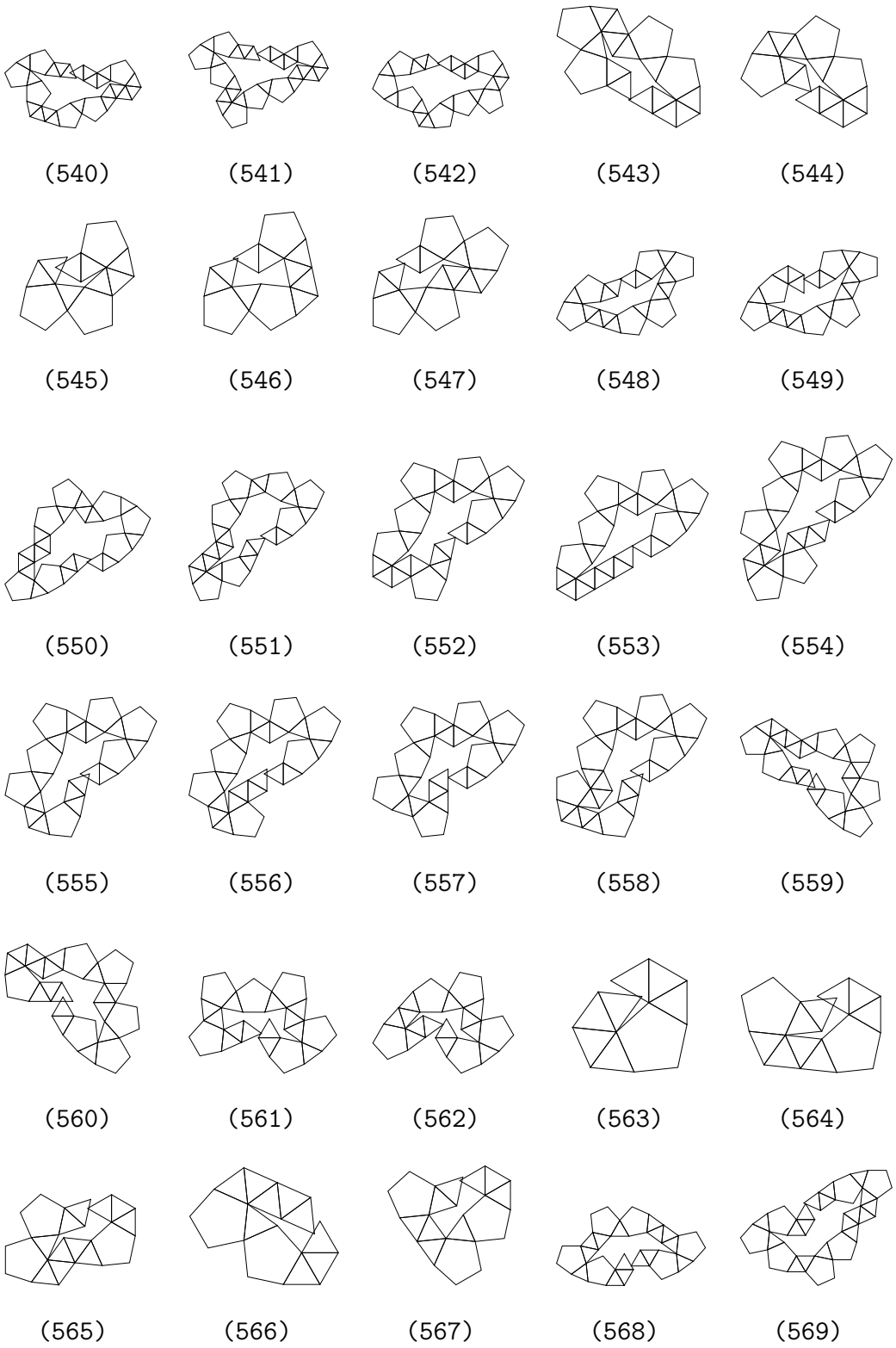

Figure A.18: List of MOPEs in J48. (continue)

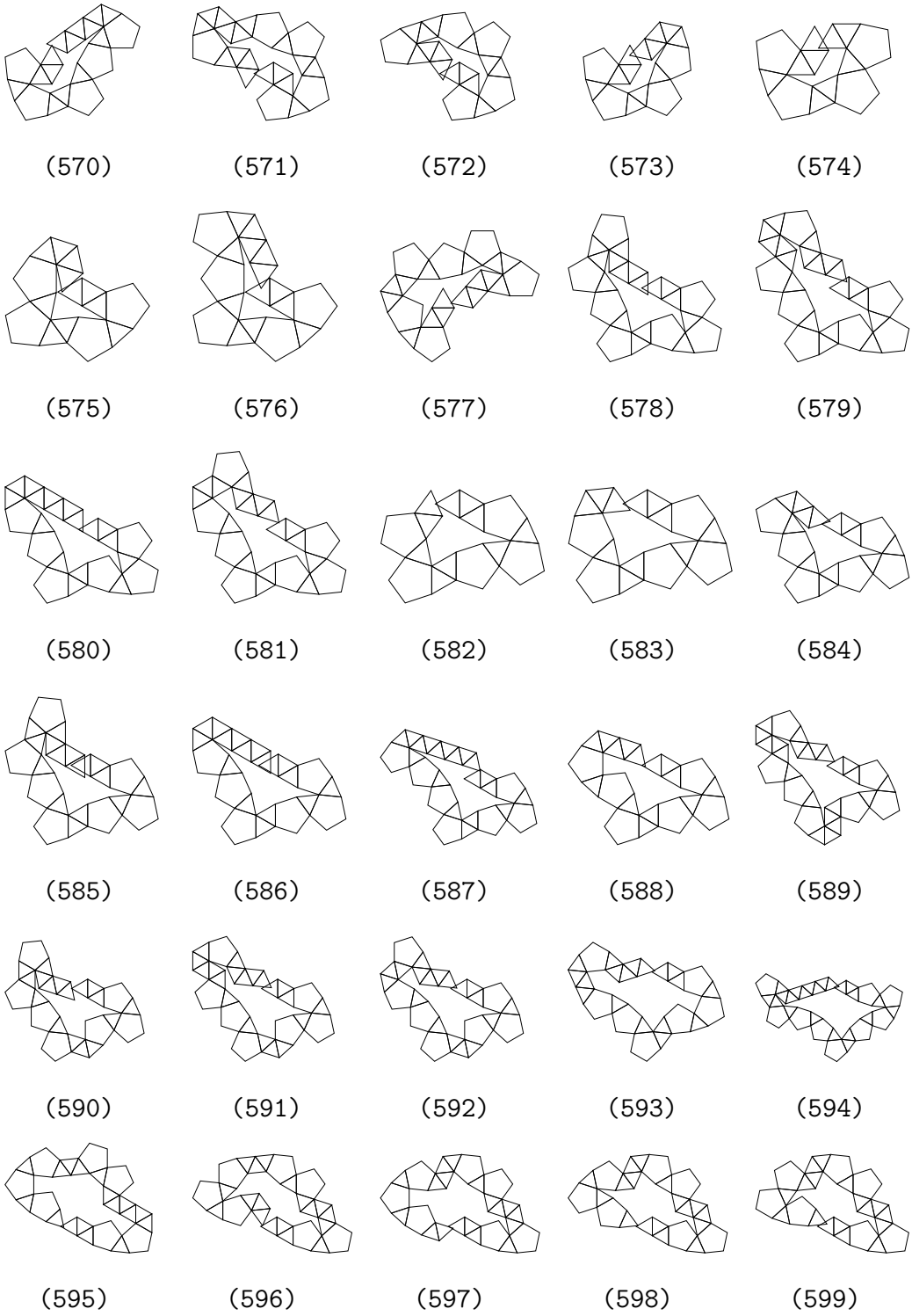

Figure A.18: List of MOPEs in J48. (continue)

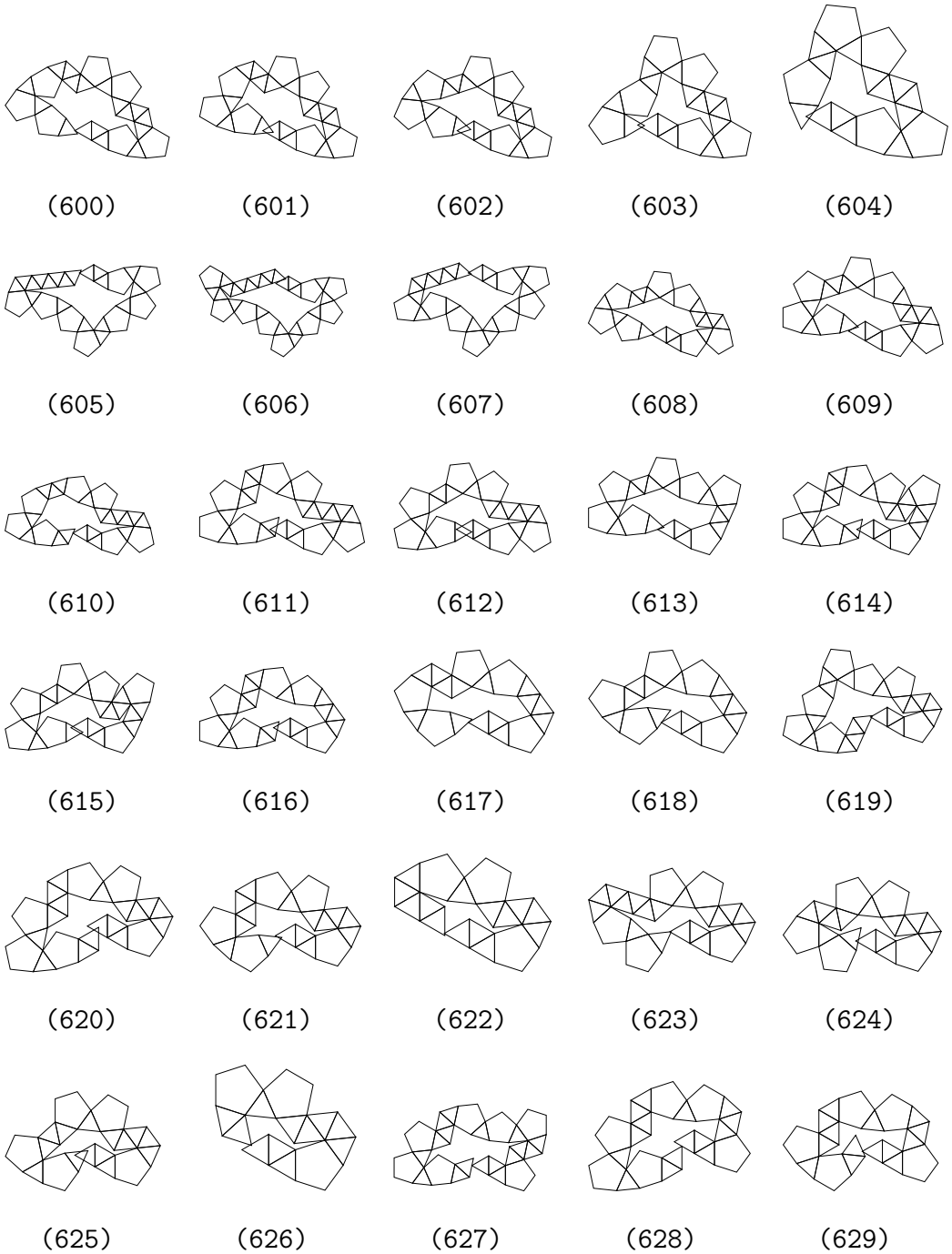

Figure A.18: List of MOPEs in J48. (continue)

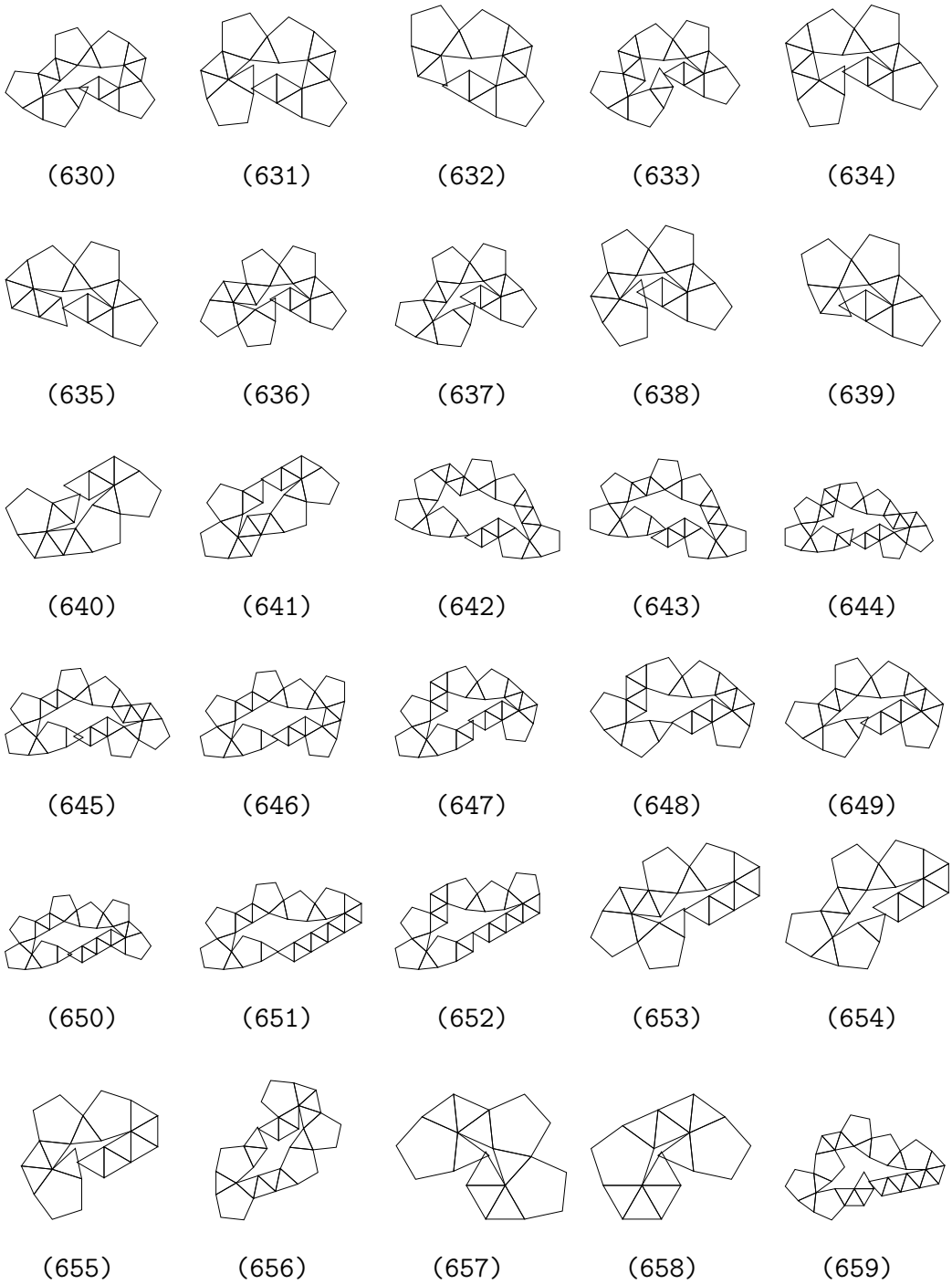

Figure A.18: List of MOPEs in J48. (continue)

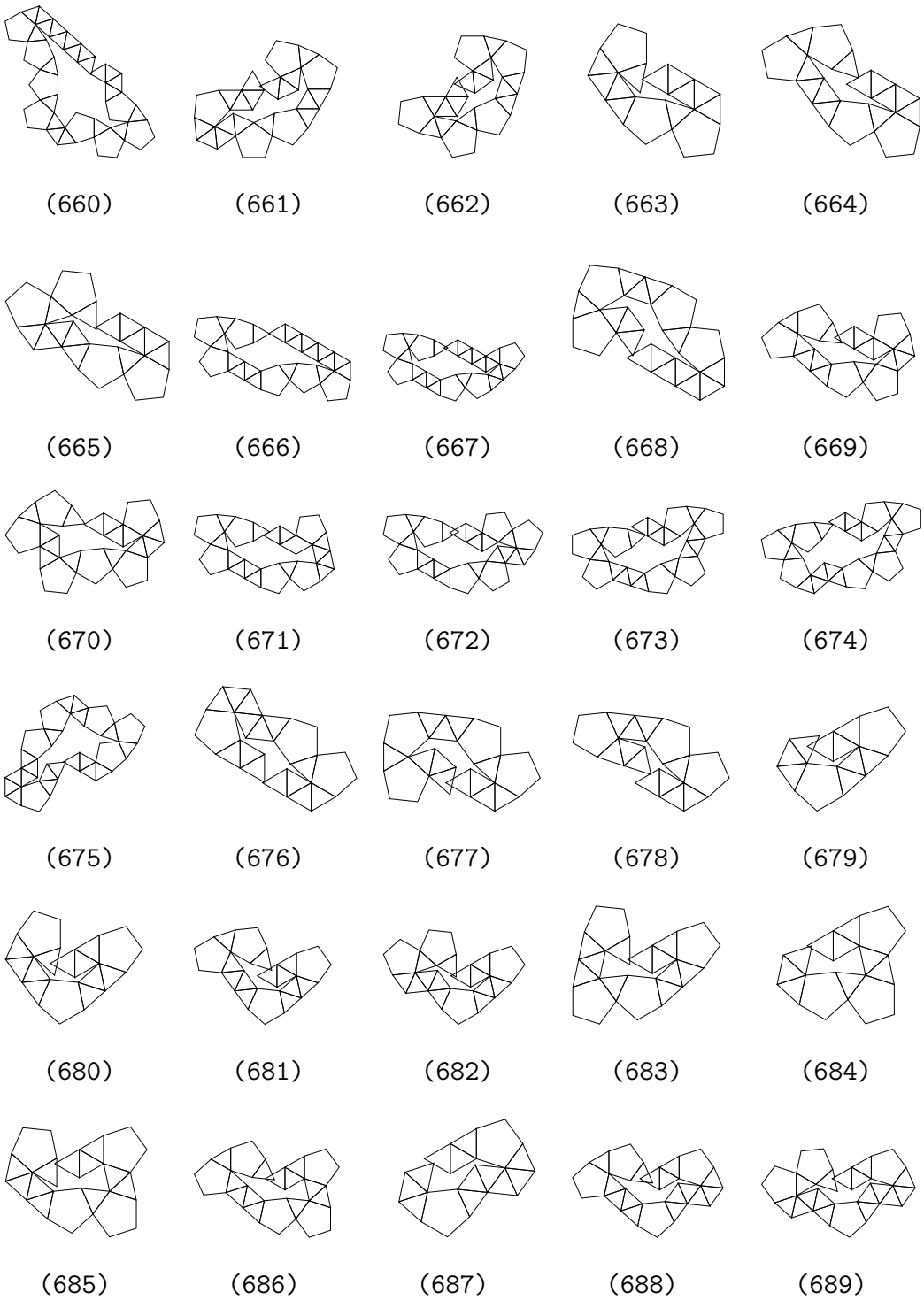

Figure A.18: List of MOPEs in J48. (continue)

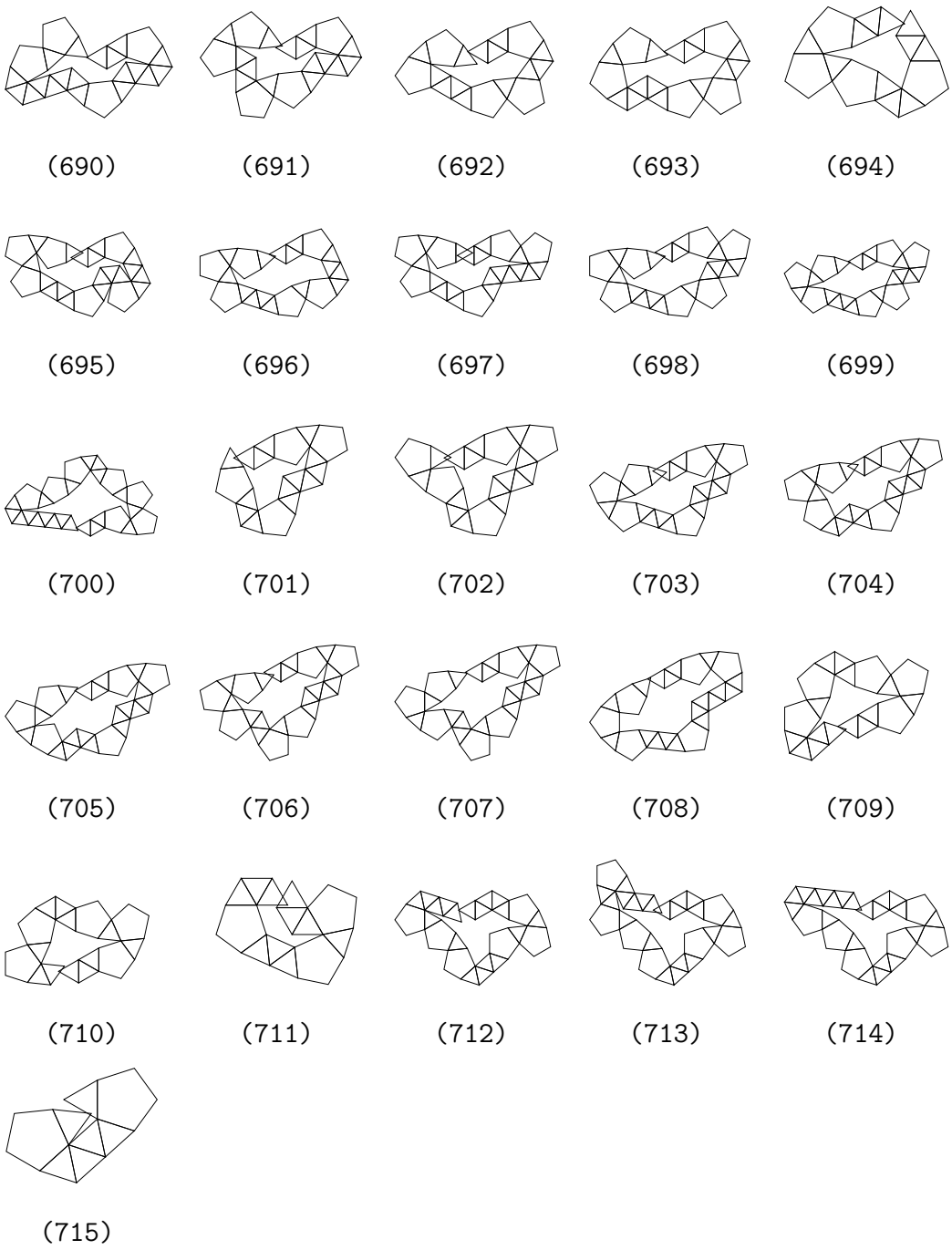

Figure A.18: List of MOPEs in J48. (continue)

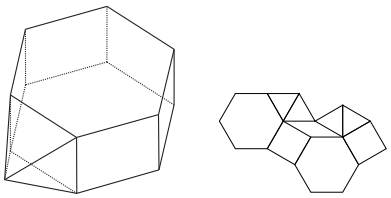

J54 (1)

Figure A.19: A MOPE in J54.

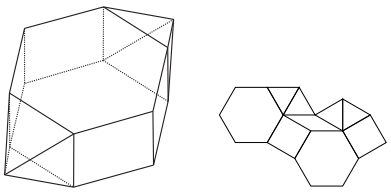

J55 (1)

Figure A.20: A MOPE in J55.

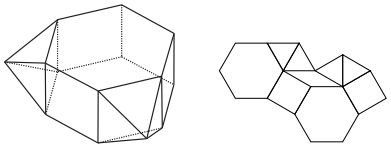

J56 (1)

Figure A.21: A MOPE in J56.

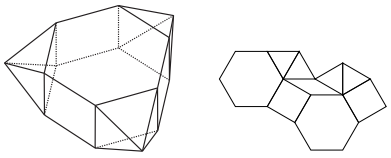

J57 (1)

Figure A.22: A MOPE in J57.

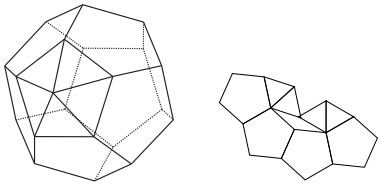

J58 (1)

Figure A.23: A MOPE in J58.

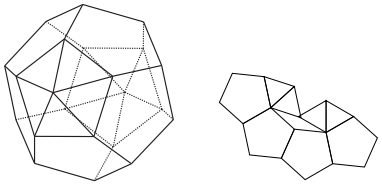

J59 (1)

Figure A.24: A MOPE in J59.

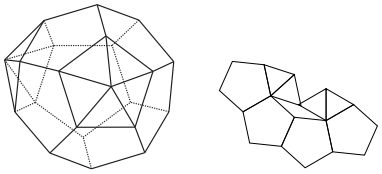

J60 (1)

Figure A.25: A MOPE in J60.

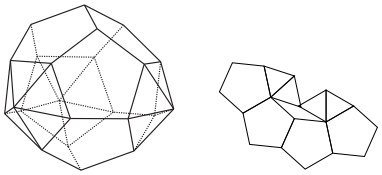

J61 (1)

Figure A.26: A MOPE in J61.

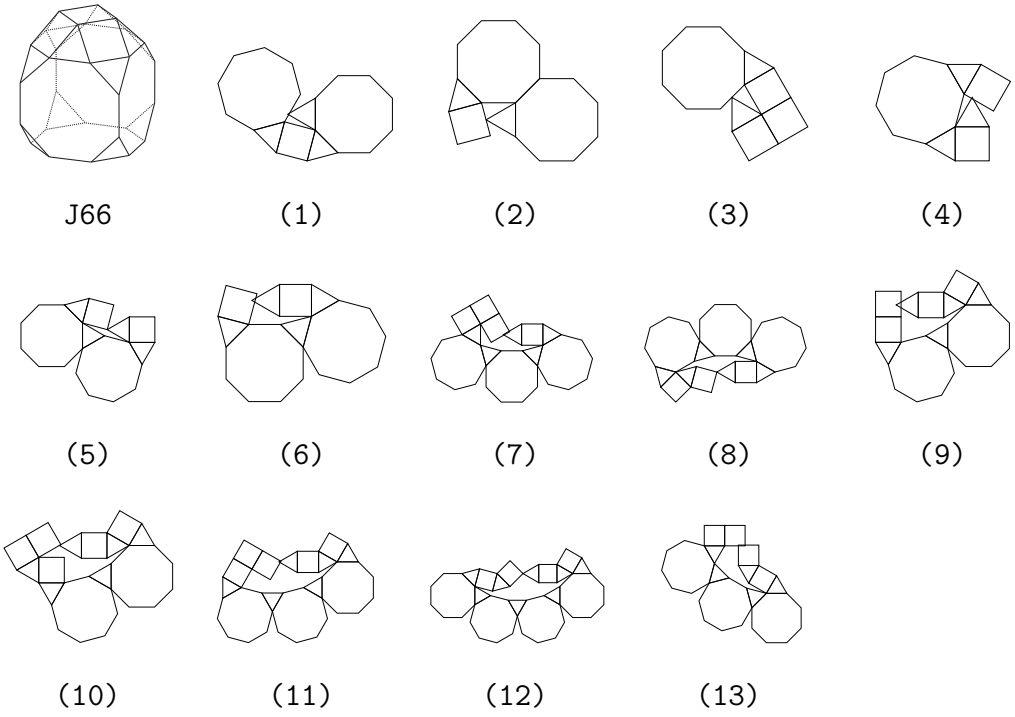

Figure A.27: List of MOPEs in J66.

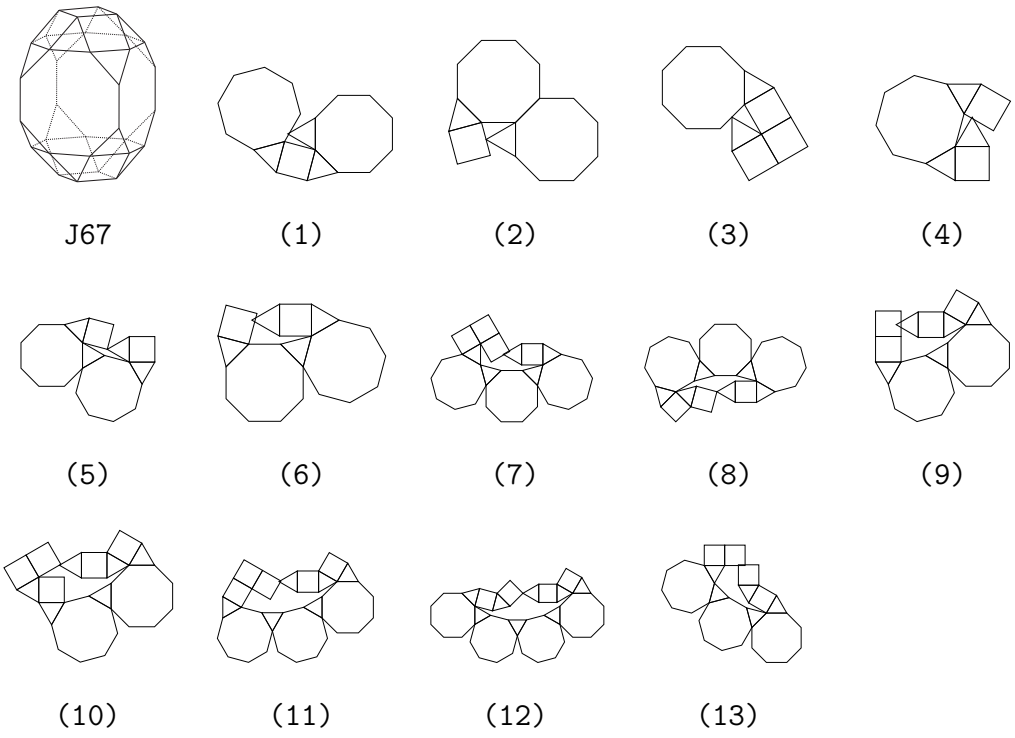

Figure A.28: List of MOPEs in J67.

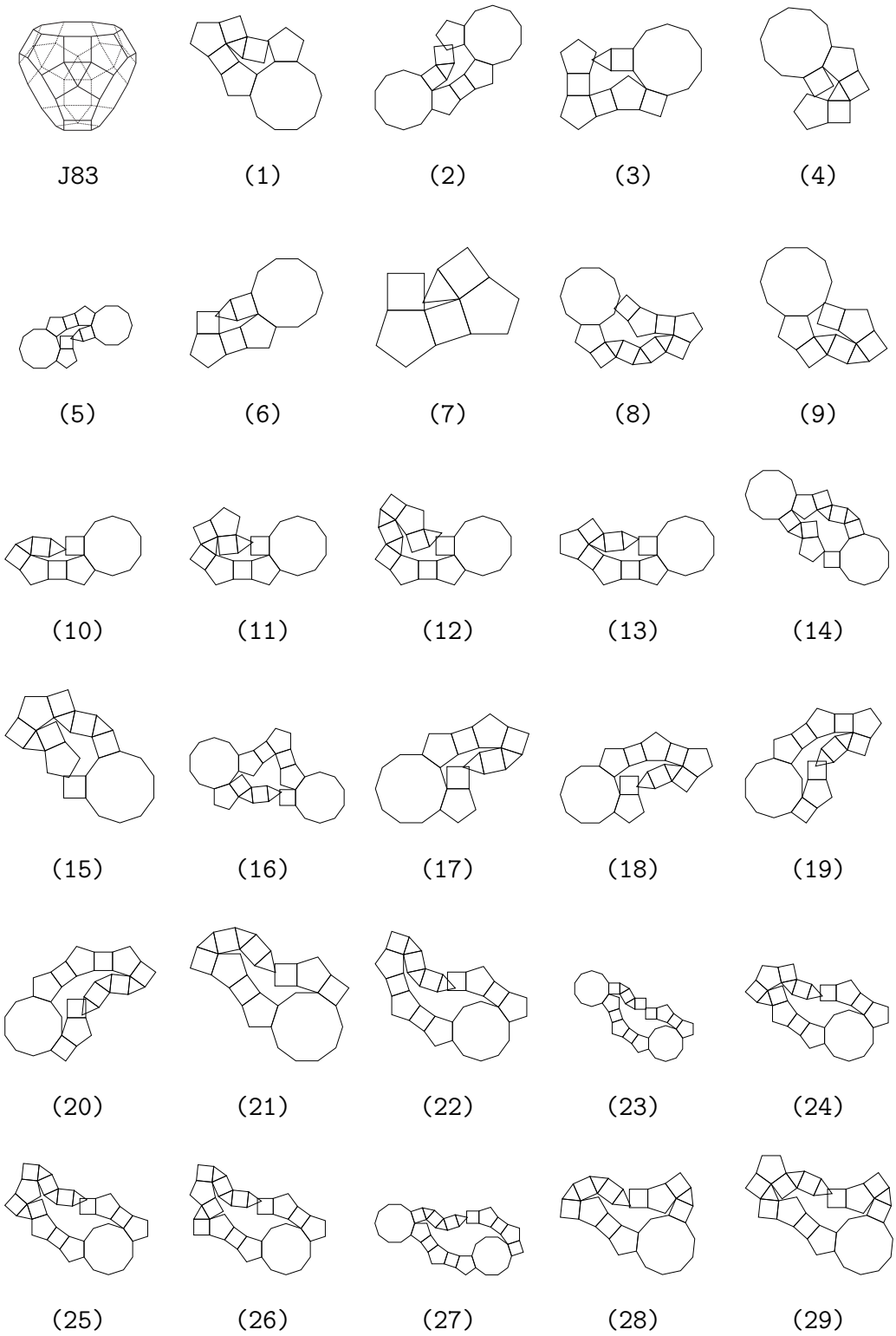

Figure A.29: List of MOPEs in J83.

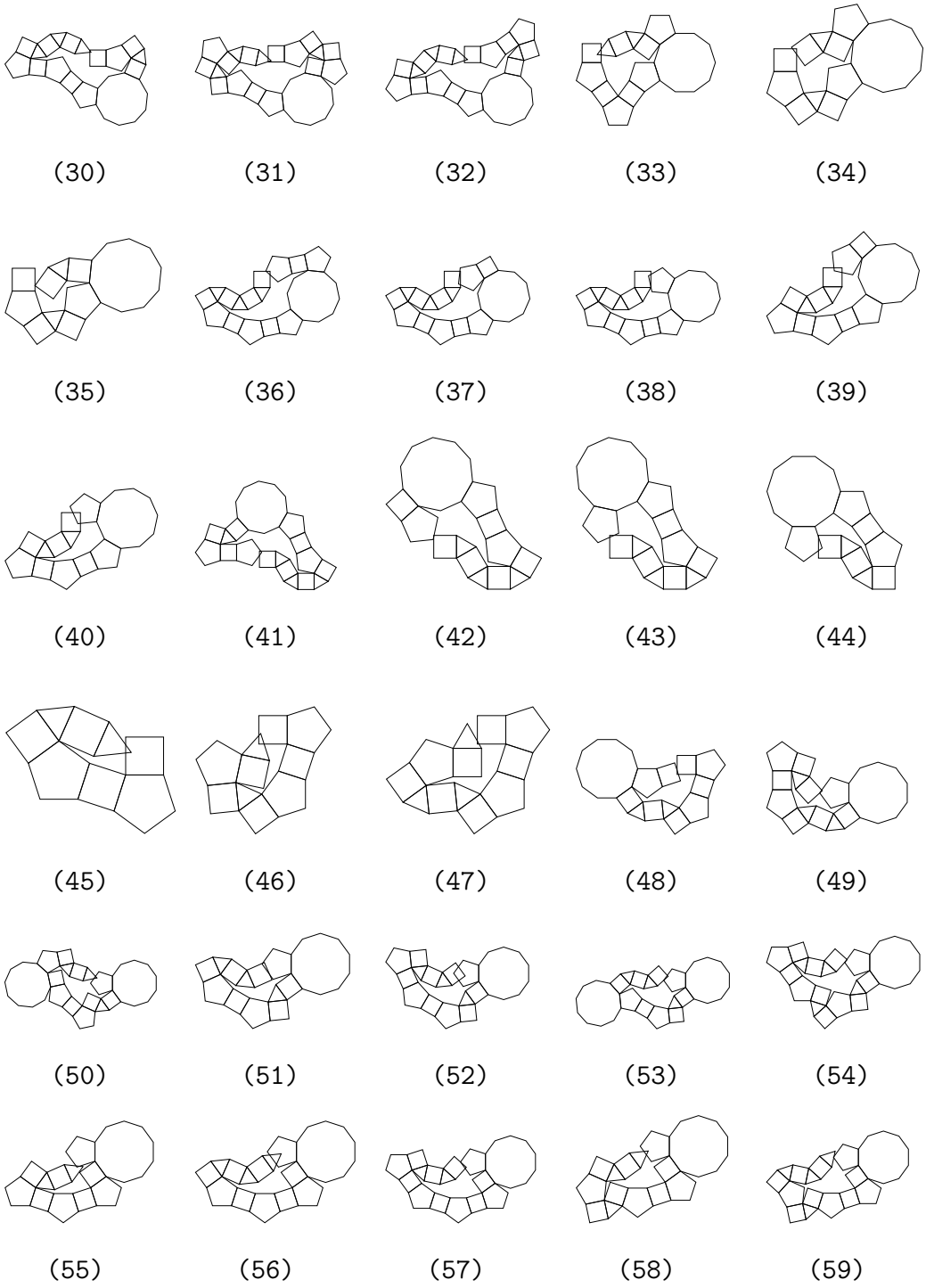

Figure A.29: List of MOPEs in J83. (continue)

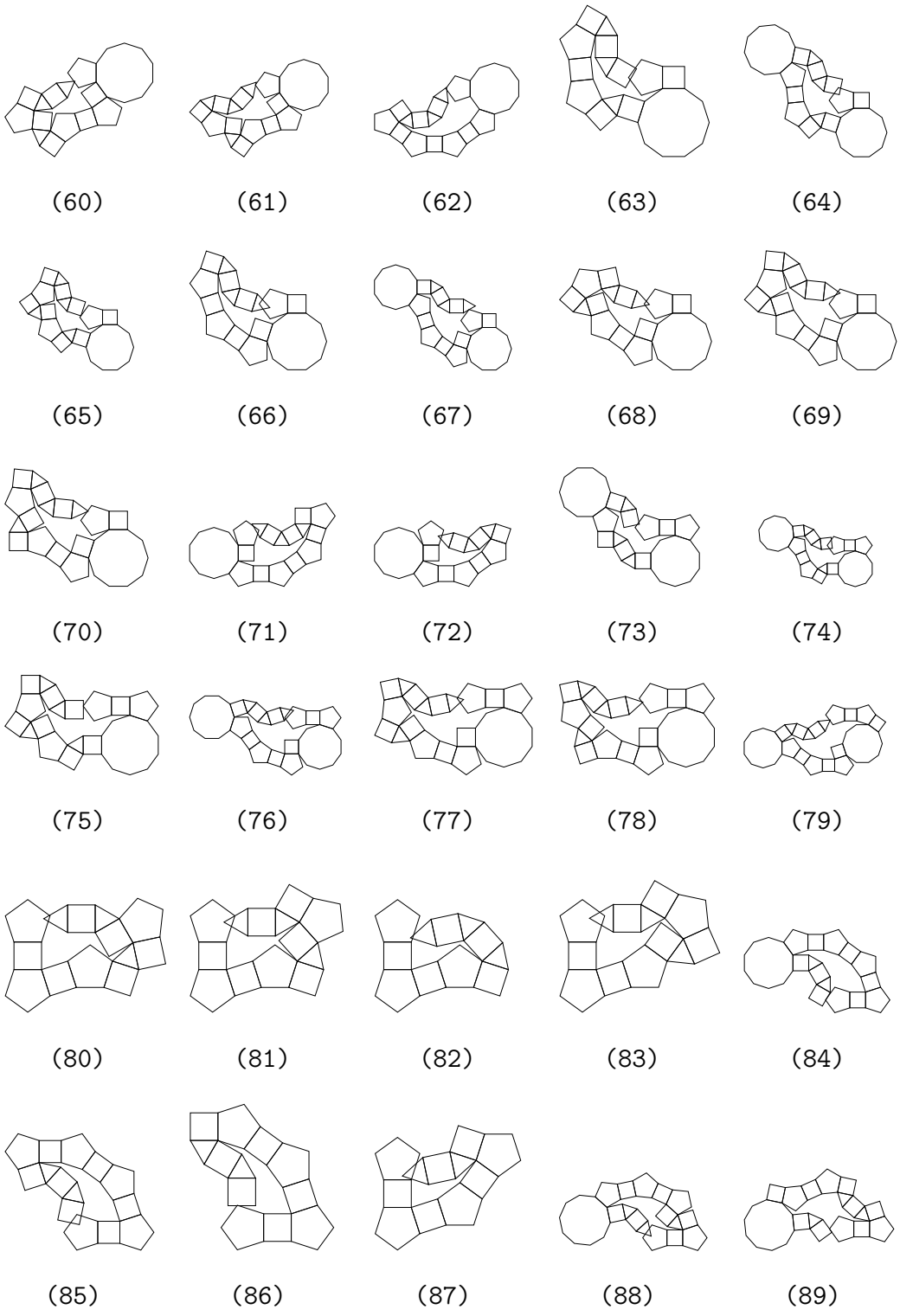

Figure A.29: List of MOPEs in J83. (continue)

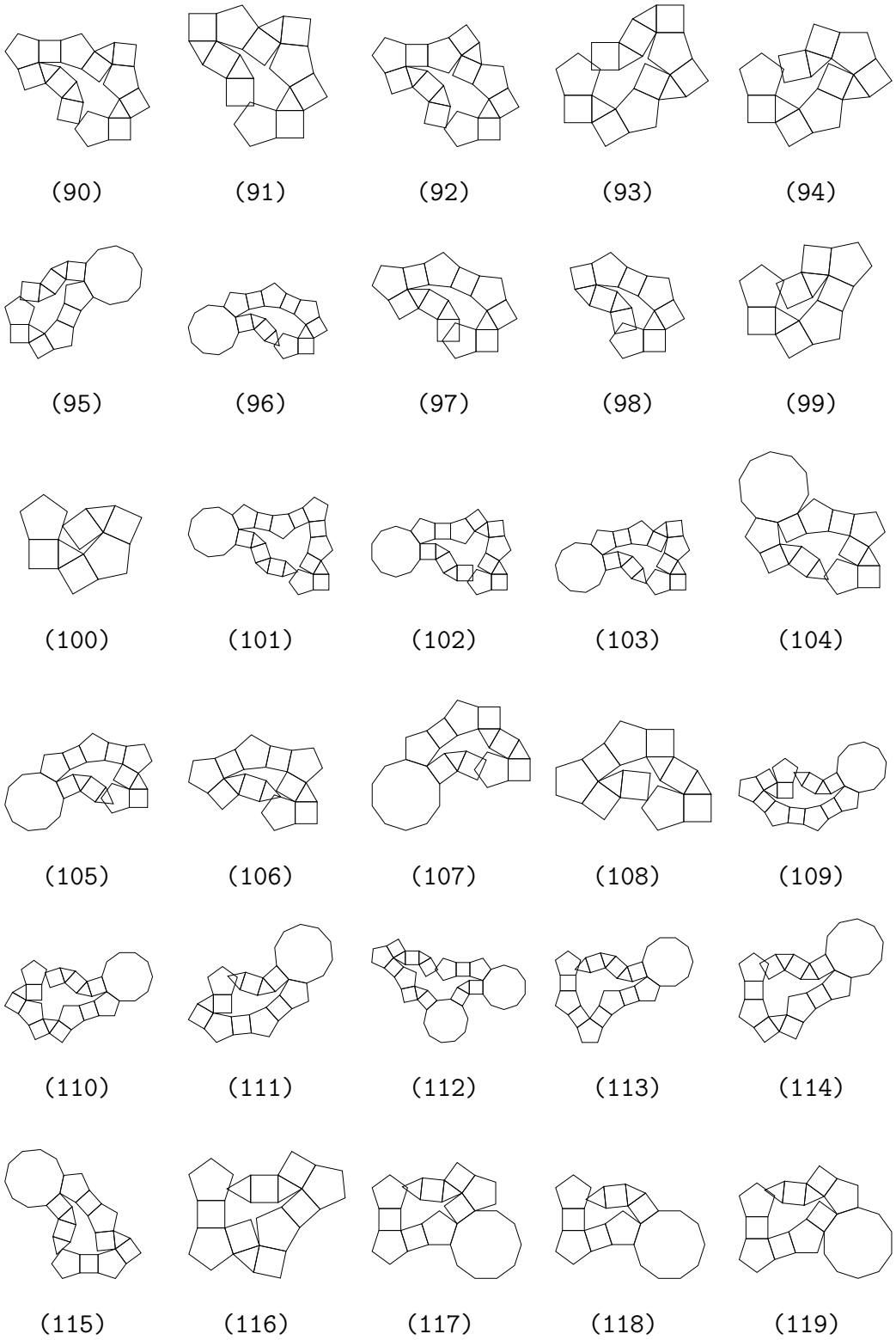

Figure A.29: List of MOPEs in J83. (continue)

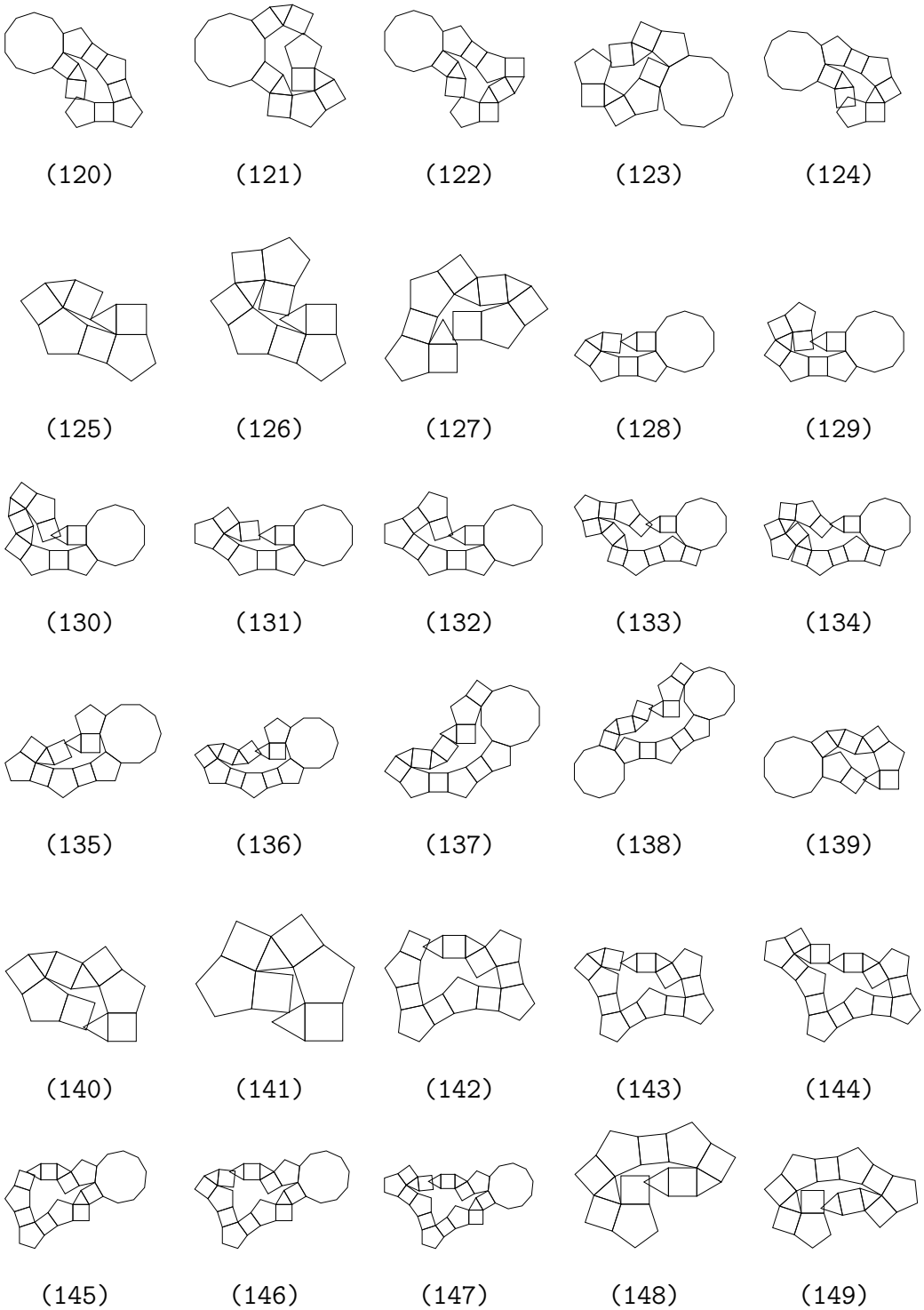

Figure A.29: List of MOPEs in J83. (continue)

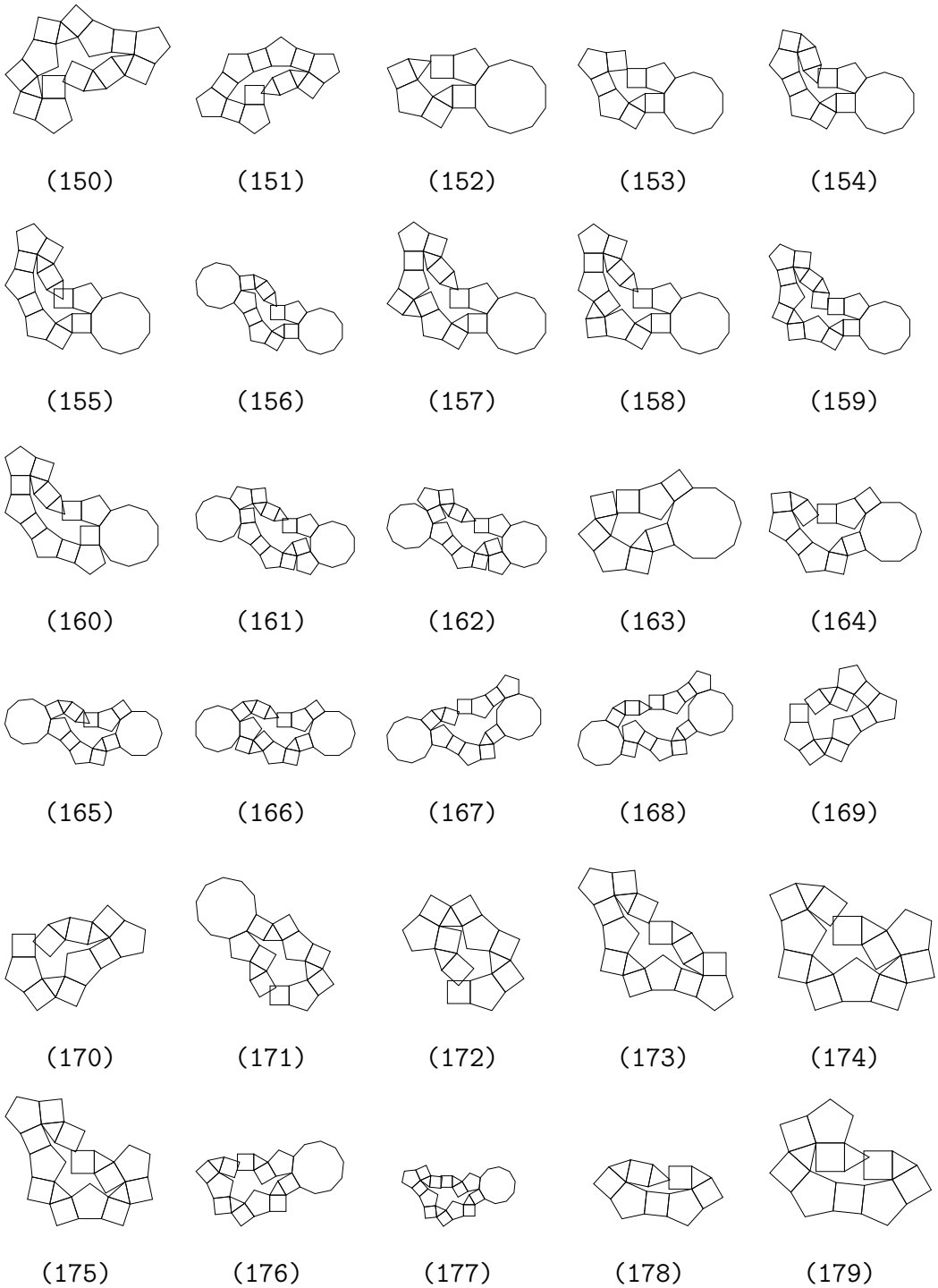

Figure A.29: List of MOPEs in J83. (continue)

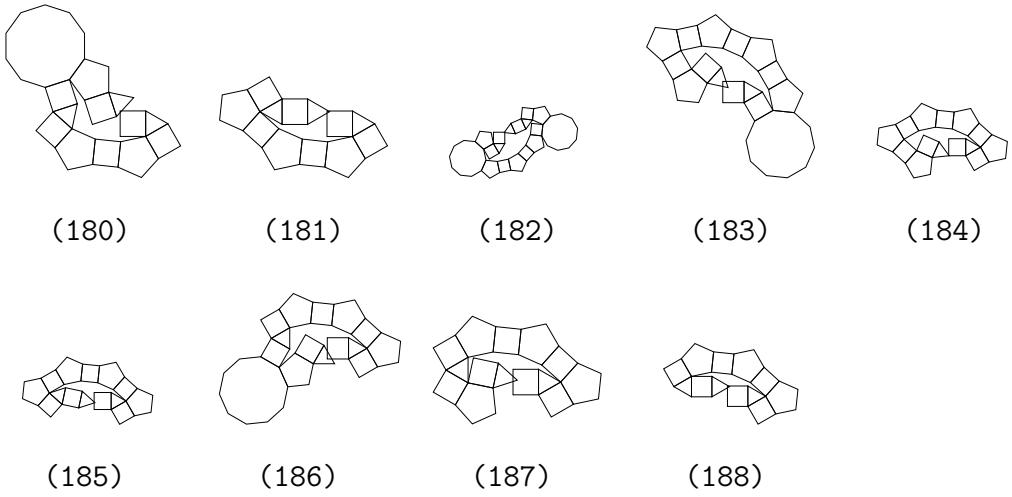

Figure A.29: List of MOPEs in J83. (continue)

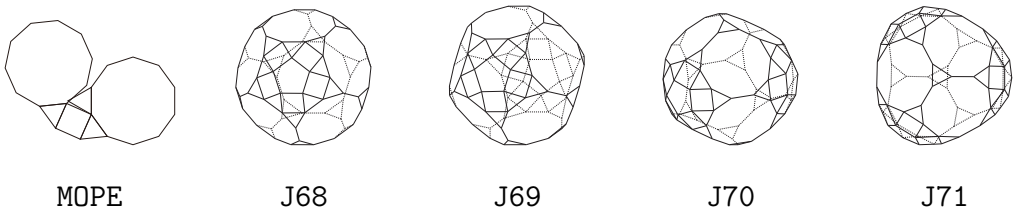

Figure A.30: An example of a common MOPE in J68 to J77.

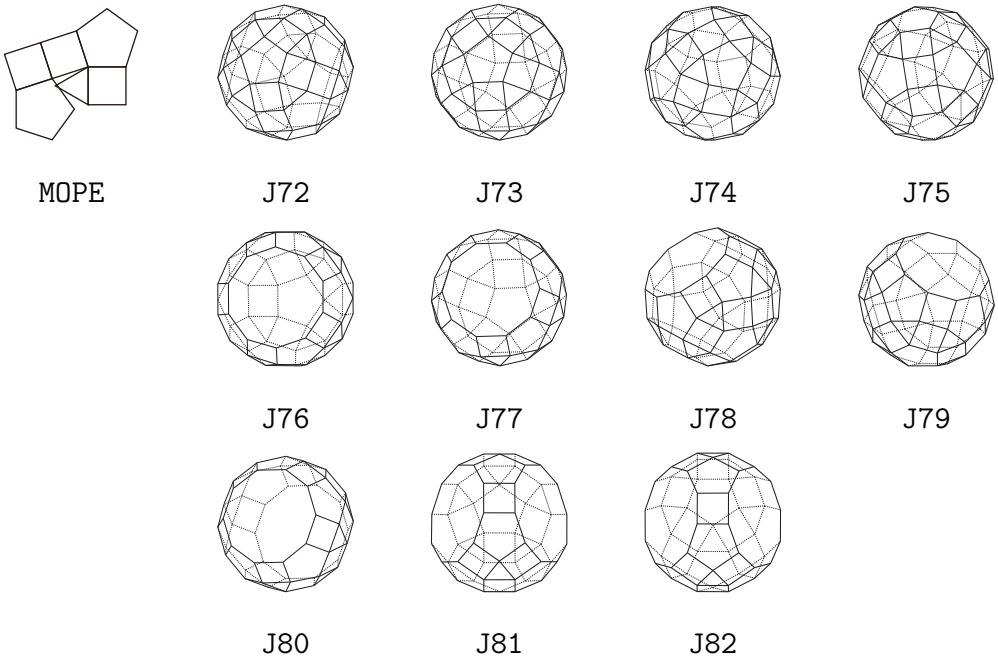

Figure A.31: An example of a common MOPE in J72 to J82.

A.2 Additional drawings for the Archimedean prisms

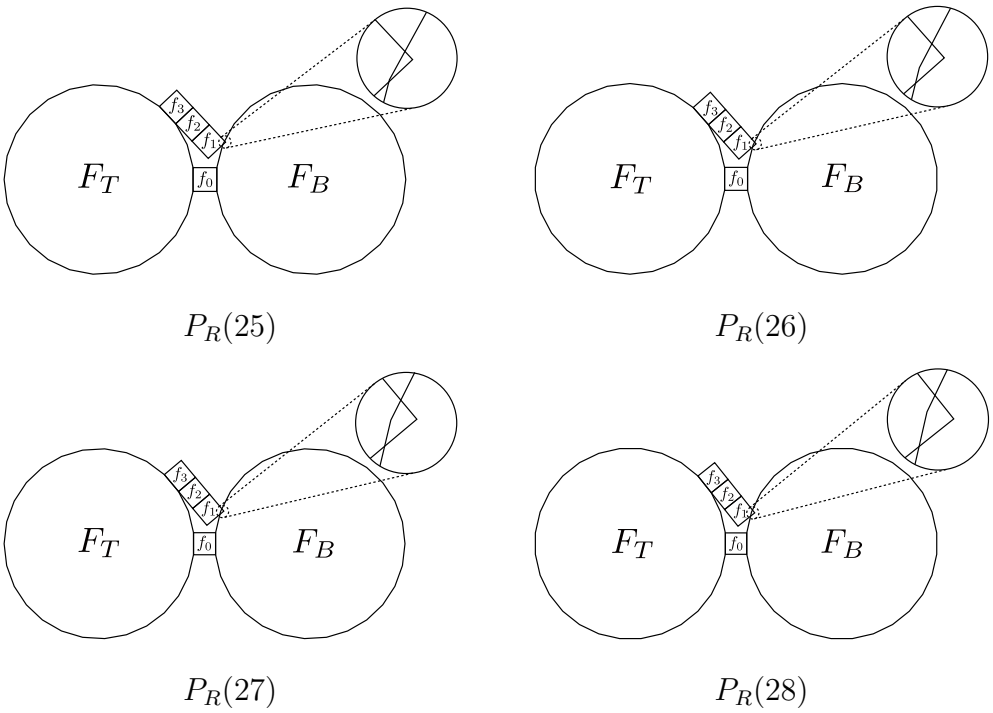

Figure A.32: Overlapping edge unfoldings in $P_R(25)$ to $P_R(28)$ consisting of faces $\{F_B, f_0, F_T, f_3, f_2, f_1\}$.

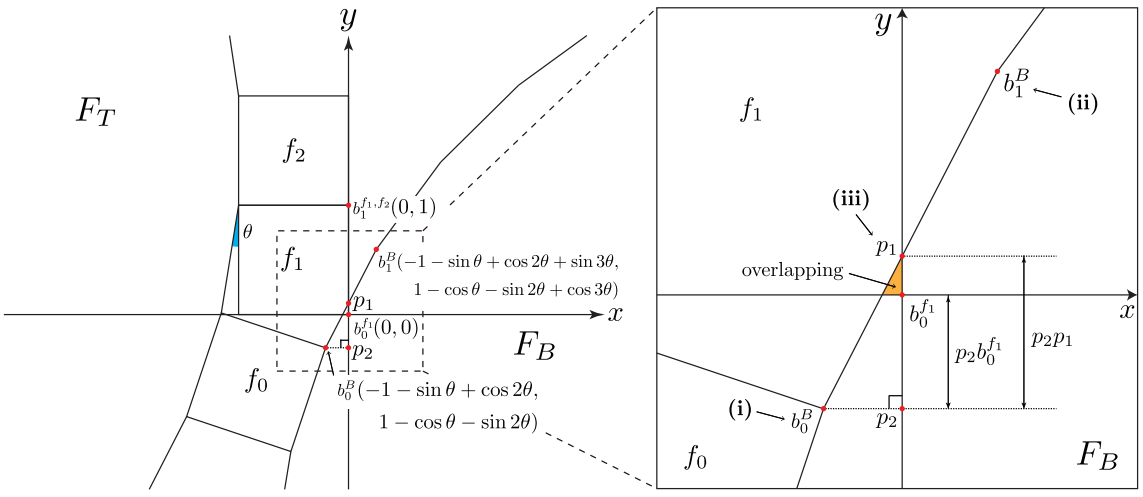

Figure A.33: Enlarged and simplified image of Figure 3.8.

A.3 Additional drawings for the Archimedean antiprisms

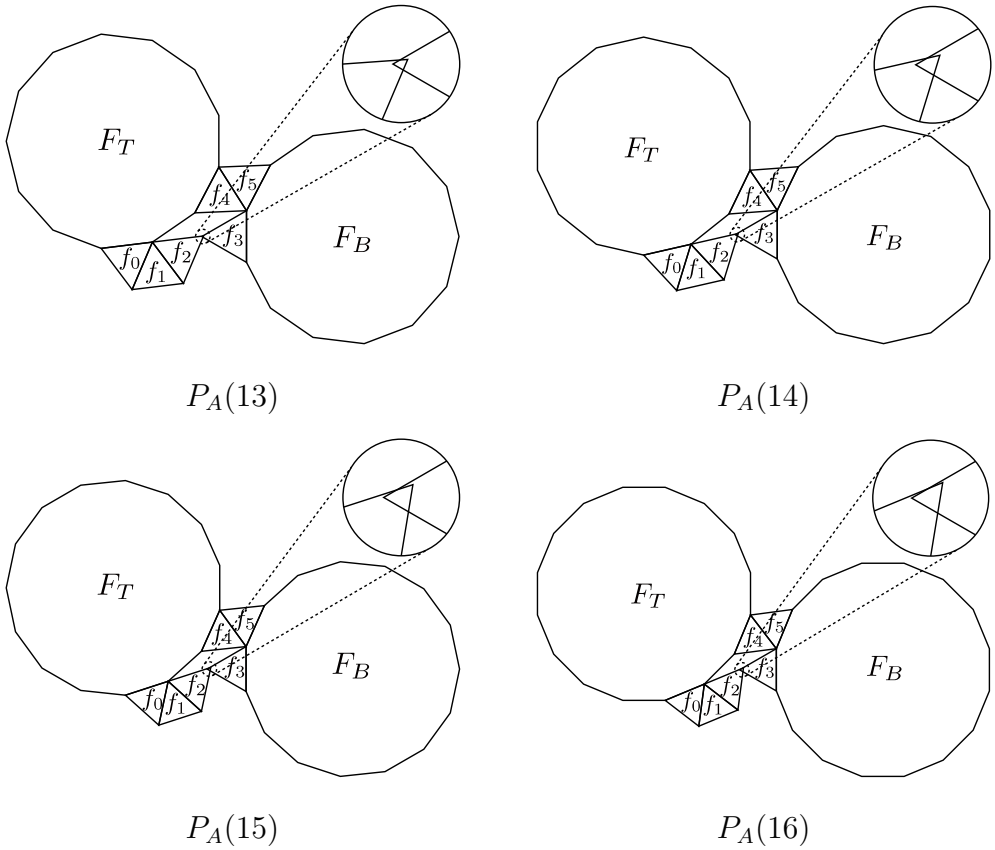

Figure A.34: Overlapping edge unfoldings in $P_A(13)$ to $P_A(16)$ consisting of faces $\{f_3, F_B, f_5, f_4, F_T, f_0, f_1, f_2\}$.

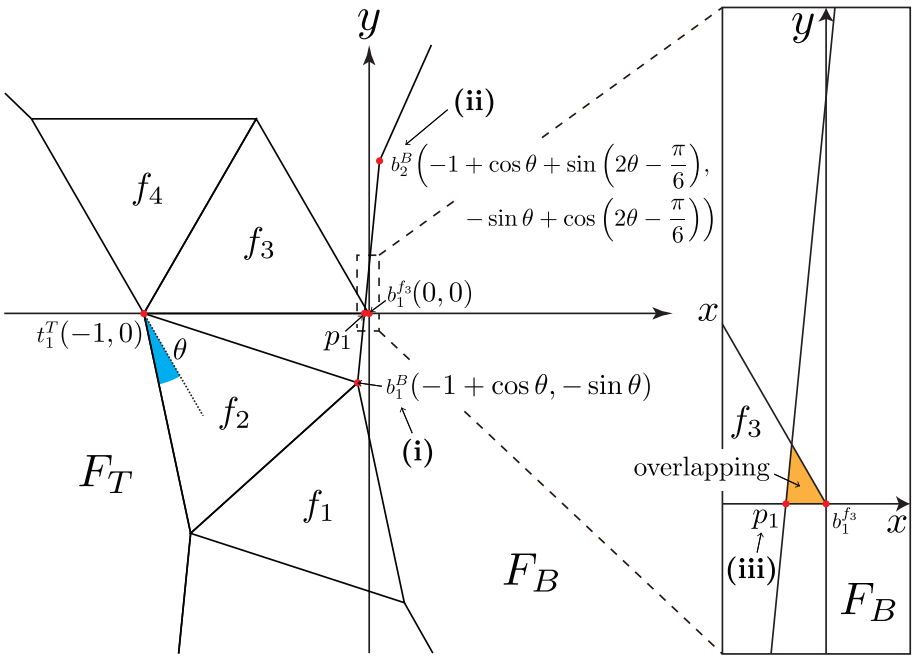

(a) The case for $19 \leq n \leq 24$

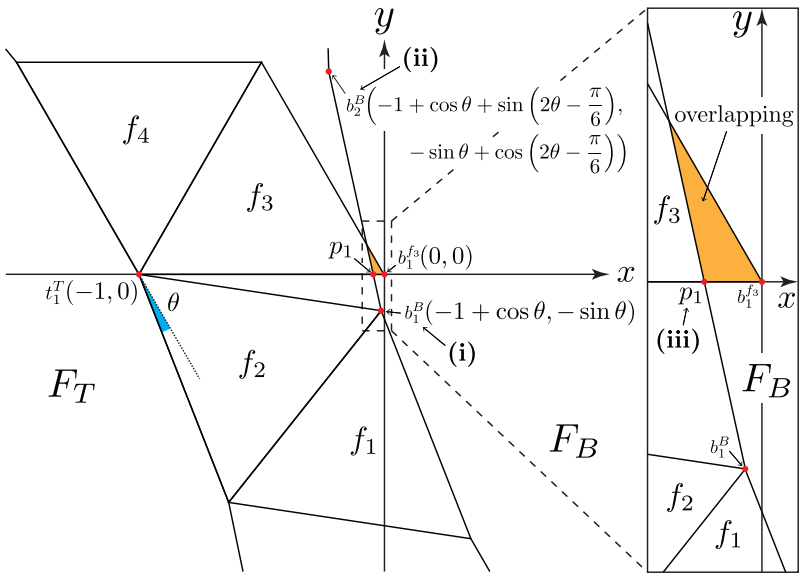

(b) The case for $n \geq 25$

Figure A.35: Enlarged and simplified image of Figure 3.12.

Appendix B

Detailed verification of boundary-boundary in touch

In this chapter, we present a method to check boundary-boundary in touch using coordinate transformations. Let's consider a linkage, as shown in Figure B.1, where each edge has unit length and consists of $k+1$ joints. We set the coordinate of p_0 to $(0,0)$ and label the vertices from p_1 to p_k. We also set the coordinate of p_1 to $(1,0)$. Here, the joint angles are represented as $(\theta_1, \theta_2, \ldots, \theta_{k-1})$ and range from $-\pi$ to π. A positive angle indicates counterclockwise rotation, while a negative angle indicates clockwise rotation. For a given point p, the coordinates $x(p)$ and $y(p)$ denote its x and y coordinates, respectively. The coordinates of the point $p_i = (x(p_i), y(p_i))$ can be calculated using the following equation:

$$\begin{bmatrix} x(p_i) \\ y(p_i) \\ 1 \end{bmatrix} = \begin{bmatrix} \cos\theta_1 & -\sin\theta_1 & 1 \\ \sin\theta_1 & \cos\theta_1 & 0 \\ 0 & 0 & 1 \end{bmatrix} \begin{bmatrix} \cos\theta_2 & -\sin\theta_2 & 1 \\ \sin\theta_2 & \cos\theta_2 & 0 \\ 0 & 0 & 1 \end{bmatrix} \ldots \begin{bmatrix} \cos\theta_{k-1} & -\sin\theta_{k-1} & 1 \\ \sin\theta_{k-1} & \cos\theta_{k-1} & 0 \\ 0 & 0 & 1 \end{bmatrix} \begin{bmatrix} 1 \\ 0 \\ 1 \end{bmatrix} \quad \text{(B.1)}$$

To illustrate, we consider J66-(8) as shown in Figure A.27. We label the points counterclockwise as $p_0, p_1, \ldots, p_8$, as shown in Figure B.2. Here, each edge has a length of 1 and joint angles are $(\theta_1, \theta_2, \theta_3, \theta_4, \theta_5, \theta_6, \theta_7) = \left(-\frac{\pi}{6}, \frac{11\pi}{12}, \frac{\pi}{12}, \frac{\pi}{12}, \frac{\pi}{12}, \frac{11\pi}{12}, -\frac{\pi}{6}\right)$. Our goal is to confirm that the coordinate of p_8 is $(0,0)$. Using equation (B.1), we calculate it as follows:

$$\begin{bmatrix} x(p_8) \\ y(p_8) \\ 1 \end{bmatrix} = \begin{bmatrix} \cos\left(-\frac{\pi}{6}\right) & -\sin\left(-\frac{\pi}{6}\right) & 1 \\ \sin\left(-\frac{\pi}{6}\right) & \cos\left(-\frac{\pi}{6}\right) & 0 \\ 0 & 0 & 1 \end{bmatrix} \ldots \begin{bmatrix} \cos\left(-\frac{\pi}{6}\right) & -\sin\left(-\frac{\pi}{6}\right) & 1 \\ \sin\left(-\frac{\pi}{6}\right) & \cos\left(-\frac{\pi}{6}\right) & 0 \\ 0 & 0 & 1 \end{bmatrix} \begin{bmatrix} 1 \\ 0 \\ 1 \end{bmatrix} = \begin{bmatrix} 0 \\ 0 \\ 1 \end{bmatrix}$$

Since the coordinate of p_8 is $(0,0)$, this confirms that p_0 and p_8 are vertex-vertex in touch.

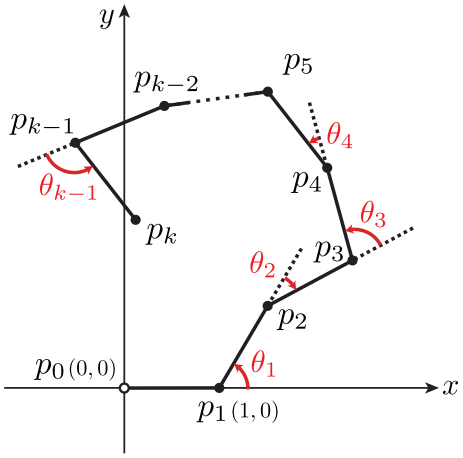

Figure B.1: Example of a linkage with arbitrary joint angles and unit edge lengths of 1.

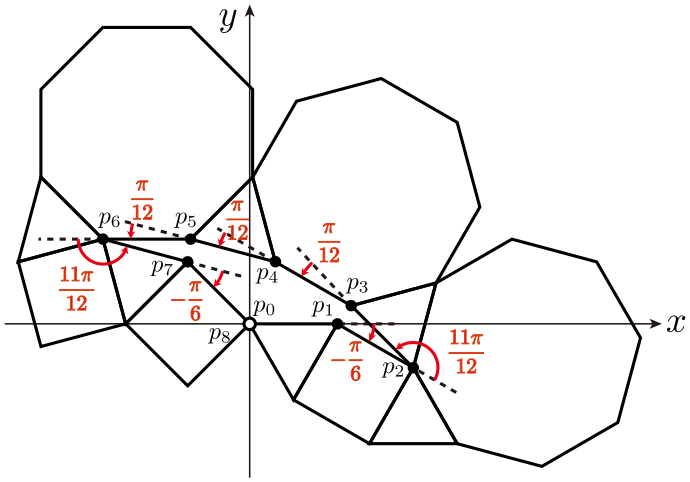

Figure B.2: Verifying that J66-(8) in Figure A.27 has vertex-vertex in touch.

Appendix C

Additional proofs

C.1 Proof of Claim 3.7

Proof. **(The coordinates of b_0^B)** Let p_3 be the intersection point of the perpendicular line from point t_1^T to the x-axis and the perpendicular line from point t_0^T to the y-axis. The coordinate of point t_0^T is $(-1-\sin\theta, 1-\cos\theta)$ since $\triangle t_1^T p_3 t_0^T$ is a right triangle with an oblique side of length 1. Let p_4 be the intersection point of the auxiliary line drawn parallel to the y-axis with respect to point t_0^T and the auxiliary line extending the line segment $b_1^{f_1,f_2} t_1^T$ in the direction of t_1^T, p_5 be the intersection point of the auxiliary line drawn perpendicular to the line segment $t_0^T b_0^B$ at point t_0^T and the line segment $t_1^T p_3$, and p_6 be the intersection point of the perpendicular line from point b_0^B to the x-axis and the perpendicular line from point t_0^T to the y-axis. The angle $\angle t_1^T t_0^T p_4$ is θ since $t_0^T p_4 // p_3 t_1^T$, $\angle p_5 t_0^T t_1^T$ is θ since it is the exterior angle of F_T, $\angle p_3 t_0^T p_5$ is $\pi/2 - 2\theta$ since $\angle p_3 t_0^T p_4$ is a right angle, and $\angle b_0^B t_0^T p_6$ is 2θ since $\angle b_0^B t_0^T p_5$ is a right angle. As a result, the coordinate of point b_0^B is $(-1-\sin\theta+\cos 2\theta, 1-\cos\theta-\sin 2\theta)$ since $\triangle b_0^B p_6 t_0^T$ is a right triangle with an oblique side of length 1.

(The coordinates of b_1^B) Let p_7 be the intersection point of the perpendicular line from point b_0^B to the x-axis and the perpendicular line from point b_1^B to the y-axis, and p_8 be the intersection point of the auxiliary line drawn perpendicular to the line segment $t_0^T b_0^B$ at point b_0^B and the y-axis. The angle $\angle b_1^B b_0^B p_8$ is θ since it is the exterior angle of F_T, $\angle p_6 b_0^B t_0^T$ is $\pi/2 - 2\theta$ since $\triangle b_0^B p_6 t_0^T$ is a right triangle, $\angle p_8 b_0^B p_7 (= \angle p_8 b_0^B p_6)$ is 2θ since $\angle p_8 b_0^B t_0^T$ is a right angle, and $\angle b_1^B b_0^B p_7$ is 3θ by adding $\angle b_1^B b_0^B p_8$ and $\angle p_8 b_0^B p_7$. As a result, the coordinate of point b_1^B is $(-1-\sin\theta+\cos 2\theta+\sin 3\theta, 1-\cos\theta-\sin 2\theta+\cos 3\theta)$ since $\triangle b_1^B p_7 b_0^B$ is a right triangle with an oblique side of length 1. □

C.2 Proof of Lemma 3.6

Proof. **(i)** For a point p, the x and y coordinates are denoted as $x(p)$ and $y(p)$, respectively. We here show that b_0^B is in the third quadrant, that is, $x(b_0^B) < 0$ and $y(b_0^B) < 0$. From Claim 3.7, $x(b_0^B) = -1-\sin\theta+\cos 2\theta$. Since $-\sin\theta < -\sin 0$ (=

0), $\cos 2\theta < \cos 0$ $(= 1)$ in $0 < \theta \leq 2\pi/29$, we obtain

$$x(b_0^B) = -1 - \sin\theta + \cos 2\theta < -1 - \sin 0 + \cos 0 = 0.$$

Next we show $y(b_0^B) < 0$. Let a function $f(\theta) = 1 - \cos\theta - \sin 2\theta$. We show that $f(\theta)$ is a monotonically decreasing function in $0 < \theta \leq 2\pi/29$, and $f(0)$ is equal to 0. The differentiation of $f(\theta)$ yields

$$\begin{aligned} f'(\theta) &= \sin\theta - 2\cos 2\theta \\ &= \sin\theta - 2(1 - 2\sin^2\theta) \\ &= 4\sin^2\theta + \sin\theta - 2 \\ &= 4\left(\sin^2\theta + \sin\theta + \frac{1}{64}\right) - \frac{1}{16} - 2 \\ &= 4\left(\sin\theta + \frac{1}{8}\right)^2 - \frac{33}{16}. \end{aligned}$$

To show $f'(\theta)$ is a monotonically increasing function in the range of θ, and $f'(2\pi/29)$ is less than 0, we consider the second derivative of $f(\theta)$. The differentiation of $f'(\theta)$ yields

$$f''(\theta) = 8\left(\sin\theta + \frac{1}{8}\right)\cos\theta.$$

Since $\sin\theta > \sin 0$ $(= 0)$, $\cos\theta > \cos(2\pi/29)$ $(\approx 0.97) > 0$, $f'(\theta)$ is greater than 0, and $f'(\theta)$ is a monotonically increasing function in the range of θ. Since $f'(2\pi/29)$ $(\approx -1.60) < 0$, $f'(\theta)$ is less than 0, and $f(\theta)$ is a monotonically decreasing function. Since $f(0) = 1 - \cos 0 - \sin 0 = 0$, the following equation holds.

$$y(b_0^B) = 1 - \cos\theta - \sin 2\theta < 0$$

Thus, b_0^B is in the third quadrant.

(ii) We here show that b_1^B is in the first quadrant, that is, $x(b_1^B) > 0$ and $y(b_1^B) > 0$. From Claim 3.7, $x(b_1^B) = -1 - \sin\theta + \cos 2\theta + \sin 3\theta$. To show $x(b_1^B) > 0$, let a function $f(\theta) = -1 - \sin\theta + \cos 2\theta + \sin 3\theta$, we show that $f(\theta)$ is a monotonically increasing function for $0 < \theta \leq 2\pi/29$, and $f(0)$ in equal to 0. The differentiation of $f(\theta)$ yields

$$\begin{aligned} f'(\theta) &= \frac{d}{d\theta}\left(-(\sin^2\theta + \cos^2\theta) - \sin\theta + (\cos^2\theta - \sin^2\theta) + (3\sin\theta - 4\sin^3\theta)\right) \\ &= \frac{d}{d\theta}(2\sin\theta - 4\sin^3\theta - 2\sin^2\theta) \\ &= 2\cos\theta - 12\sin^2\theta\cos\theta - 4\sin\theta\cos\theta \\ &= 2\cos\theta(1 - 6\sin^2\theta - 2\sin\theta). \end{aligned}$$

Since $2\cos\theta \geq 2\cos(2\pi/29)$ $(\approx 0.97) > 0$, $-6\sin^2\theta \geq -6\sin^2(2\pi/29)$ (≈ -0.27), and $-2\sin\theta \geq -2\sin(2\pi/29)$ (≈ -0.43), we obtain

$$\begin{aligned} f'(\theta) &= 2\cos\theta(1 - 6\sin^2\theta - 2\sin\theta) \\ &> 2\cos\frac{2\pi}{29}\left(1 - 6\sin^2\frac{2\pi}{29} - 2\sin\frac{2\pi}{29}\right) \approx 0.57 > 0. \end{aligned}$$

Hence, $f(\theta)$ is a monotonically increasing function in the range of θ. Since $f(0) = -1 - \sin 0 + \cos 0 + \sin 0 = 0$, the following equation holds.

$$x(b_1^B) = -1 - \sin\theta + \cos 2\theta + \sin 3\theta > 0$$

Next we show $y(b_1^B) = 1 - \cos\theta - \sin 2\theta + \cos 3\theta > 0$. Since $-\cos\theta > -\cos 0$ $(= -1)$, $-\sin 2\theta \geq -\sin(4\pi/29)$ (≈ -0.41), and $\cos 3\theta \geq \cos(6\pi/29)$ (≈ 0.79) in the range of θ, we obtain

$$\begin{aligned} y(b_1^B) &= 1 - \cos\theta - \sin 2\theta + \cos 3\theta \\ &> 1 - \cos 0 - \sin\frac{4\pi}{29} + \cos\frac{6\pi}{29} \approx 0.37 > 0. \end{aligned}$$

Thus, b_1^B is in the first quadrant.

(iii) Let p_2 be an intersection point of the perpendicular line from point b_0^B to the y-axis and y-axis; that is, the coordinates of p_2 are $(0, 1 - \cos\theta - \sin 2\theta)$. We can show Lemma 3.6 (iii) by the following claim.

Claim C.1. *The length of the line segment p_2p_1 is longer than that of $p_2b_0^{f_1}$.*

The length of the line segment $b_0^Bp_2$ is not zero because of the condition **(i)**. To show Claim C.1, we show $p_2b_0^{f_1}/b_0^Bp_2$ is greater than $p_2p_1/b_0^Bp_2$. $p_2b_0^{f_1}/b_0^Bp_2$ and $p_2p_1/b_0^Bp_2$ can denote

$$\frac{p_2b_0^{f_1}}{b_0^Bp_2} = \frac{0 - (1 - \cos\theta - \sin 2\theta)}{0 - (-1 - \sin\theta + \cos 2\theta)} = \frac{-1 + \cos\theta + \sin 2\theta}{1 + \sin\theta - \cos 2\theta}, \quad \frac{p_2p_1}{b_0^Bp_2} = \frac{\cos 3\theta}{\sin 3\theta}.$$

Therefore, we here show that the following equation holds.

$$\frac{-1 + \cos\theta + \sin 2\theta}{1 + \sin\theta - \cos 2\theta} < \frac{\cos 3\theta}{\sin 3\theta} \tag{C.1}$$

Since $1 + \sin\theta - \cos 2\theta > 1 + \sin 0 - \cos 0 = 0$ and $\sin 3\theta > \sin 0 = 0$ in the range of θ, we can multiply both sides of equation (C.1) by $(1 + \sin\theta - \cos 2\theta)\sin 3\theta$, and obtain

$$(-1 + \cos\theta + \sin 2\theta)\sin 3\theta < \cos 3\theta(1 + \sin\theta - \cos 2\theta). \tag{C.2}$$

To show the equation (C.2), we subtract the right side from the left side, and we define a function $f(\theta) = (-1 + \cos\theta + \sin 2\theta)\sin 3\theta - \cos 3\theta(1 + \sin\theta - \cos 2\theta)$. We show that $f(\theta)$ is less than 0. Here, we partition the cases based on the value of θ: one where θ is in the range $2\pi/61 < \theta \leq 2\pi/29$, and the other where θ is in the range $0 < \theta \leq 2\pi/62$. When $2\pi/61 < \theta \leq 2\pi/29$, we can demonstrate through a numerical calculation for each corresponding value of n that $f(\theta)$ is less than zero[1]. In the range of $0 < \theta \leq 2\pi/62$, we differentiate the function $f(\theta)$ and use the result to provide an analytical proof as follows.

[1]We use WolframScript 1.11.0 for the numerical calculations.

The differentiation of $f(\theta)$ yields

$$\begin{aligned}
f'(\theta) &= \frac{d}{d\theta}\left(-\sin 3\theta + \sin 3\theta\cos\theta + \sin 3\theta \sin 2\theta - \cos 3\theta - \cos 3\theta \sin\theta + \cos 3\theta \cos 2\theta\right) \\
&= \frac{d}{d\theta}\left(-\sin 3\theta - \cos 3\theta + \sin 3\theta\cos\theta - \cos 3\theta \sin\theta + \sin 3\theta \sin 2\theta + \cos 3\theta \cos 2\theta\right) \\
&= \frac{d}{d\theta}\left(-\sin 3\theta - \cos 3\theta + \sin\left(3\theta - \theta\right) + \cos\left(3\theta - 2\theta\right)\right) \\
&= \frac{d}{d\theta}\left(-\sin 3\theta - \cos 3\theta + \sin 2\theta + \cos\theta\right) \\
&= -3\cos 3\theta + 3\sin 3\theta + 2\cos 2\theta - \sin\theta \\
&= -3(4\cos^3\theta - 3\cos\theta) + 3(3\sin\theta - 4\sin^3\theta) + 2(\cos^2\theta - \sin^2\theta) - \sin\theta \\
&= -12(\cos^3\theta - \sin^3\theta) + 9(\cos\theta + \sin\theta) + 2(\cos^2\theta - \sin^2\theta) - \sin\theta \\
&= -12(\cos\theta + \sin\theta)(\cos^2\theta - \cos\theta\sin\theta + \sin^2\theta) + 9(\cos\theta + \sin\theta) \\
&\qquad + 2(\cos\theta + \sin\theta)(\cos\theta - \sin\theta) - \sin\theta \\
&= -12(\cos\theta + \sin\theta)\left(1 - \frac{1}{2}\sin 2\theta\right) + 9(\cos\theta + \sin\theta) \\
&\qquad + 2(\cos\theta + \sin\theta)(\cos\theta - \sin\theta) - \sin\theta \\
&= (\cos\theta + \sin\theta)(-12 + 6\sin 2\theta + 9 + 2\cos\theta - 2\sin\theta) - \sin\theta \\
&= \sin\left(\theta + \frac{\pi}{4}\right)(6\sin 2\theta + 2\cos\theta - 2\sin\theta - 3) - \sin\theta.
\end{aligned}$$

Let a function $g(\theta) = 6\sin 2\theta + 2\cos\theta - 2\sin\theta - 3$. Since $\sin\left(\theta + \pi/4\right) > \sin\pi/4$ (≈ 0.71) > 0, and $\sin\theta < \sin 0$ ($= 0$), if $g(\theta)$ is less than 0, we can say $f'(\theta) < 0$. We show that $g(\theta)$ is a monotonically increasing function in $0 < \theta \leq 2\pi/62$, $g(2\pi/62)$ is less than 0. The differentiation of $g(\theta)$ yields

$$\begin{aligned}
g'(\theta) &= 12\cos 2\theta - 2\sin\theta - 2\cos\theta \\
&= 12\cos 2\theta - 2(\sin\theta + \cos\theta) \\
&= 12\cos 2\theta - 2\sqrt{2}\sin\left(\theta + \frac{\pi}{4}\right).
\end{aligned}$$

To show $g'(\theta)$ is a monotonically decreasing function in the range of θ, and $g'(2\pi/62)$ is greater than 0, we consider the second derivative of $g(\theta)$. The differentiation of $g'(\theta)$ yields

$$g''(\theta) = -24\sin 2\theta - 2\sqrt{2}\cos\left(\theta + \frac{\pi}{4}\right).$$

Since $\sin 2\theta > \sin 0$ ($= 0$), $\cos\left(\theta + \pi/4\right) > \cos\left(2\pi/62 + \pi/4\right)$ (≈ 0.88), $g''(\theta)$ is less than 0, and $g'(\theta)$ is a monotonically decreasing function in the range of θ. Since $g'(2\pi/62) \approx 9.56$, $g'(\theta)$ is greater than 0, and $g(\theta)$ is a monotonically increasing function. Since $g(2\pi/62) \approx -0.004$, the following equation holds.

$$g(\theta) = 6\sin 2\theta + 2\cos\theta - 2\sin\theta - 3 < 0$$

Therefore, $f'(\theta)$ is less than 0, and $f(\theta)$ is a monotonically decreasing function in $0 < \theta \leq 2\pi/62$. Since $f(0) = (-1 + \cos 0 + \sin 0)\sin 0 - \cos 0(1 + \sin 0 - cos0) = 0$,

the following equation is hold.

$$f(\theta) = (-1 + \cos\theta + \sin 2\theta)\sin 3\theta - \cos 3\theta(1 + \sin\theta - \cos 2\theta) < 0$$

Thus, the length of the line segment p_2p_1 is longer than that of $p_2b_0^{f_1}$. □

C.3 Proof of Claim 3.11

Proof. **(The coordinates of b_1^B)** Let p_2 be the intersection point of the perpendicular line from point b_1^B to the x-axis, and p_3 be the intersection point of the auxiliary line extending the line segment $t_2^Tt_1^T$ in the t_1^T direction and the line segment $t_0^Tb_1^B$. The angle $\angle p_3t_1^Tb_1^B$ is $\pi/3-\theta$ since $\angle t_0^Tt_1^Tb_1^B$ is $\pi/3$, and the $\angle b_1^Bt_1^Tp_2$ is θ since $\angle p_3t_1^Tp_2$ is $\pi/3$. As a result, the coordinate of point b_1^B is $(-1+\cos\theta, -\sin\theta)$ since $\triangle b_1^Bp_2t_1^T$ is a right triangle with an oblique side of length 1.

(The coordinates of b_2^B) Let p_4 be the intersection point of the perpendicular line from point b_2^B to the y-axis and the perpendicular line from point b_1^B to the x-axis, p_5 be the intersection point of the auxiliary line extending the line segment $b_2^Bb_1^B$ in the b_1^B direction and the line segment $t_0^Tb_0^B$, and p_6 be the intersection point of the auxiliary line extending the line segment $b_0^Bb_1^B$ in the b_1^B direction and the x-axis. The angle $\angle b_2^Bb_1^Bp_4$ is divided into two cases concerning the value of n.

[For $19 \le n \le 24$] The angle $\angle t_0^Tb_1^Bp_5$ is $\pi/3-\theta$ since $\angle p_5b_1^Bb_0^B$ is the exterior angle of F_B, $\angle p_2b_1^Bt_1^T$ is $\pi/2-\theta$ since $\triangle b_1^Bp_2t_1^T$ is a right triangle, and $\angle b_2^Bb_1^Bp_4$ is $2\theta-\pi/6$ since $\angle p_5b_1^Bb_2^B - \angle t_0^Tb_1^Bp_5 + \angle t_1^Tb_1^Bt_0^T + \angle p_2b_1^Bt_1^T = \pi-(\pi/3-\theta)+\pi/3+(\pi/2-\theta) = 2\theta-\pi/6$. As a result, the coordinate of point b_2^B is $(-1+\cos\theta+\sin(2\theta-\pi/6), -\sin\theta+\cos(2\theta-\pi/6))$ since $\triangle b_2^Bp_4b_1^B$ is a right triangle with an oblique side of length 1.

[For $n \ge 25$] The angle $\angle b_2^Bb_1^Bt_1^T$ is $\pi/3+\theta$ since $\angle p_6b_1^Bt_1^T + \angle p_1b_1^Bp_6 = \pi/3+\theta$, and $\angle p_4b_1^Bb_2^B$ is $\pi/6-2\theta$ since $\angle p_2b_1^Bt_1^T - \angle t_1^Tb_1^Bb_2^B = \pi/2-\theta-(\pi/3+\theta) = \pi/6-2\theta$. As a result, the coordinate of point b_2^B is $(-1+\cos\theta-\sin(\pi/6-2\theta), -\sin\theta+\cos(\pi/6-2\theta))$ since $\triangle b_1^Bp_4b_2^B$ is a right triangle with an oblique side of length 1. Since $-\sin(\pi/6-2\theta) = \sin(2\theta-\pi/6)$, and $\cos(\pi/6-2\theta) = \cos(2\theta-\pi/6)$, the coordinate of point b_2^B can be transformed into $(-1+\cos\theta+\sin(2\theta-\pi/6), -\sin\theta+\cos(2\theta-\pi/6))$.

(The coordinates of p_1) The equation of the line with points b_1^B and b_2^B is

$$y = \frac{y(b_2^B)-y(b_1^B)}{x(b_2^B)-x(b_1^B)}(x-x(b_1^B))+y(b_1^B) = \frac{\cos\left(2\theta-\frac{\pi}{6}\right)}{\sin\left(2\theta-\frac{\pi}{6}\right)}(x-(-1+\cos\theta))-\sin\theta. \quad \text{(C.3)}$$

Here, by substituting $y = y(p_1) = 0$ into the equation (C.3), we get

$$\begin{aligned}
x(p_1) &= (y(p_1) + \sin\theta)\ \frac{\sin\left(2\theta - \frac{\pi}{6}\right)}{\cos\left(2\theta - \frac{\pi}{6}\right)} - 1 + \cos\theta \\
&= \frac{\sin\theta \sin\left(2\theta - \frac{\pi}{6}\right)}{\cos\left(2\theta - \frac{\pi}{6}\right)} + \cos\theta - 1 \\
&= \frac{\sin\theta \sin\left(2\theta - \frac{\pi}{6}\right) + \cos\theta\cos\left(2\theta - \frac{\pi}{6}\right)}{\cos\left(2\theta - \frac{\pi}{6}\right)} - 1 \\
&= \frac{\cos\left(\theta - \left(2\theta - \frac{\pi}{6}\right)\right)}{\cos\left(2\theta - \frac{\pi}{6}\right)} - 1 \\
&= \frac{\cos\left(\frac{\pi}{6} - \theta\right)}{\cos\left(2\theta - \frac{\pi}{6}\right)} - 1.
\end{aligned}$$

□

C.4 Proof of Lemma 3.10

Proof. **(i)** We here show that b_1^B is in the third quadrant, that is, $x(b_1^B) < 0$ and $y(b_1^B) < 0$. From Claim 3.11 $x(b_1^B) = -1 + \cos\theta$. Since $\cos\theta < \cos 0\ (= 1)$ from the range of θ, we obtain

$$x(b_1^B) < -1 + \cos 0 = 0.$$

From Claim 3.11 $y(b_1^B) = -\sin\theta$. Since $-\sin\theta < -\sin 0\ (= 0)$, $y(b_1^B) < 0$. Thus, b_1^B is in the third quadrant.

(ii) We here show that the y-coordinate of point b_2^B is positive, that is, $y(b_2^B) > 0$. From Claim 3.11 $y(b_2^B) = -\sin\theta + \cos(2\theta - \pi/6)$. Since $-\sin\theta \geq -\sin 2\pi/19 (\approx -0.32)$, $\cos 2\theta \geq \cos 4\pi/19 (\approx 0.78)$, and $\sin 2\theta \geq \sin 0 (= 0)$ from the range of θ, we obtain

$$\begin{aligned}
y(b_2^B) &= -\sin\theta + \cos\left(2\theta - \frac{\pi}{6}\right) \\
&= -\sin\theta + \cos 2\theta \cos\frac{\pi}{6} + \sin 2\theta \sin\frac{\pi}{6} \\
&> -\sin\frac{2\pi}{19} + \frac{\sqrt{3}}{2}\cos\frac{4\pi}{19} + \frac{1}{2}\sin 0 \approx 0.35 > 0.
\end{aligned}$$

Thus, $y(b_2^B)$ is positive.

(iii) We here show that the x-coordinate of point p_1 is greater than -1 and less than 0, that is, $x(p_1) > -1$ and $x(p_1) < 0$. From Claim 3.11 $x(p_1) = \cos(\pi/6 - \theta)/\cos(2\theta - \pi/6) - 1$. First, we show $x(p_1) > -1$, that is, $\cos(\pi/6 - \theta)/\cos(2\theta - \pi/6) > 0$. Since the

following inequalities hold:

$$0 < \frac{\pi}{6} - \frac{2\pi}{19} \left(= \frac{7\pi}{114}\right) \leq \frac{\pi}{6} - \theta < \frac{\pi}{6} - 0 \left(= \frac{\pi}{6}\right) < \frac{\pi}{2}$$
$$-\frac{\pi}{2} < 0 - \frac{\pi}{6} \left(= -\frac{\pi}{6}\right) < 2\theta - \frac{\pi}{6} \leq 2 \cdot \frac{2\pi}{19} - \frac{\pi}{6} \left(= \frac{5\pi}{114}\right) < \frac{\pi}{2},$$

we obtain

$$\cos\left(\frac{\pi}{6} - \theta\right) > 0 \qquad \cos\left(2\theta - \frac{\pi}{6}\right) > 0. \tag{C.4}$$

Thus, $x(p_1) > -1$.

Next, we show $x(p_1) < 0$, that is,

$$\frac{\cos\left(\frac{\pi}{6} - \theta\right)}{\cos\left(2\theta - \frac{\pi}{6}\right)} - 1 < 0. \tag{C.5}$$

Since $\cos\left(2\theta - \frac{\pi}{6}\right) > 0$ according to equation (C.4), by multiplying both sides of equation (C.5) by $\cos\left(2\theta - \frac{\pi}{6}\right)$, we obtain

$$\cos\left(\frac{\pi}{6} - \theta\right) - \cos\left(2\theta - \frac{\pi}{6}\right) < 0.$$

We define a function $f(\theta) = \cos(\pi/6 - \theta) - \cos(2\theta - \pi/6)$. We show that $f(\theta)$ is a concave down function from $0 < \theta \leq 2\pi/19$, and both $f(0)$ and $f(2\pi/19)$ are less than 0. The differentiation of $f(\theta)$ yields

$$f'(\theta) = \sin\left(\frac{\pi}{6} - \theta\right) + 2\sin\left(2\theta - \frac{\pi}{6}\right).$$

To show $f'(\theta)$ is a monotonically increasing function, $f'(0)$ is less than 0, and $f'(2\pi/19)$ is larger than 0, we consider the second derivative of $f(\theta)$. The differentiation of $f'(\theta)$ yields

$$\begin{aligned}
f''(\theta) &= -\cos\left(\frac{\pi}{6} - \theta\right) + 4\cos\left(2\theta - \frac{\pi}{6}\right) \\
&= -\cos\frac{\pi}{6}\cos\theta - \sin\frac{\pi}{6}\sin\theta + 4\cos 2\theta\cos\frac{\pi}{6} + 4\sin 2\theta\sin\frac{\pi}{6} \\
&= -\frac{\sqrt{3}}{2}\cos\theta - \frac{1}{2}\sin\theta + 2\sqrt{3}\cos 2\theta + 2\sin 2\theta \\
&= -\frac{\sqrt{3}}{2}\cos\theta - \frac{1}{2}\sin\theta + 2\sqrt{3}\cos^2\theta - 2\sqrt{3}\sin^2\theta + 4\sin\theta\cos\theta \\
&= \sin\theta\left(4\cos\theta - 2\sqrt{3}\sin\theta - \frac{1}{2}\right) + \cos\theta\left(2\sqrt{3}\cos\theta - \frac{\sqrt{3}}{2}\right).
\end{aligned}$$

Since $4\cos\theta < 4\cos(2\pi/19)$ (≈ 3.78), $-2\sqrt{3}\sin\theta < -2\sqrt{3}\sin(2\pi/19)$ (≈ -1.12), and $2\sqrt{3}\cos\theta > 2\sqrt{3}\cos(2\pi/19)$ (≈ 3.27), we obtain

$$4\cos\theta - 2\sqrt{3}\sin\theta - 1/2 \approx 2.15 > 0$$
$$2\sqrt{3}\cos\theta - \frac{\sqrt{3}}{2} \approx 2.40 > 0.$$

Hence, $f''(\theta) > 0$ and $f'(\theta)$ is a monotonically increasing function. Since $f'(0) = \sin(\pi/6)+2\sin(-\pi/6) = -0.5 < 0$ and $f'(2\pi/19) = \sin(2\pi/19 - \pi/6)+2\sin(4\pi/19 - \pi/6) \approx 0.46 > 0$, $f(\theta)$ is a concave down function. Herein, $f(0) = \cos(\pi/6) - \cos(-\pi/6) = 0$, and $f(2\pi/19) = \cos(\pi/6 - 2\pi/19) - \cos(4\pi/19 - \pi/6) \approx -0.009$, $f(\theta) < 0$. Thus, $x(p_1) < 0$. □

References

[AO92] Boris Aronov and Joseph O'Rourke. Nonoverlap of the Star Unfolding. *Discrete Comput. Geom.*, 8:219–250, 1992.

[BDD+98] Therese C. Biedl, Erik D. Demaine, Martin L. Demaine, Anna Lubiw, Mark H. Overmars, Joseph O'Rourke, Steve Robbins, and Sue Whitesides. Unfolding Some Classes of Orthogonal Polyhedra. In *10th Canadian Conference on Computational Geometry*, 1998.

[BG20] Nicholas Barvinok and Mohammad Ghomi. Pseudo-Edge Unfoldings of Convex Polyhedra. *Discrete & Computational Geometry*, 64(3):671–689, 2020.

[Bry86] Randal E. Bryant. Graph-Based Algorithms for Boolean Function Manipulation. *IEEE Trans. Computers*, 35(8):677–691, 1986.

[CFG91] Hallard T. Croft, Kenneth J. Falconer, and Richard K. Guy. *Unsolved Problems in Geometry*. Springer-Verlag, reissue edition, 1991.

[DDRW20] Kristin DeSplinter, Satyan L. Devadoss, Jordan Readyhough, and Bryce Wimberly. Nets of higher-dimensional cubes. In *32nd Canadian Conference on Computational Geometry*, 2020.

[DO07] Erik D. Demaine and Joseph O'Rourke. *Geometric Folding Algorithms: Linkages, Origami, Polyhedra*. Cambridge University Press, 2007.

[Dür25] Albrecht Dürer. Underweysung der Messung, mit dem Zirckel und Richtscheyt, in Linien Ebenen unnd gantzen corporen, 1525.

[Grü03] Branko Grünbaum. Are Your Polyhedra the Same as My Polyhedra? *Discrete and Computational Geometry*, 25:461–488, 2003.

[Hea18] Robert Hearn. personal communication, 2018.

[Hir15] Kenta Hirose. Hanseitamentai no tenkaizu no kasanari ni tsuite (On the overlap of Archimedean solids), in Japanese, 2015. Saitama Univ. graduation thesis. Supervisor: Takashi Horiyama.

[HMS18] Takashi Horiyama, Masahiro Miyasaki, and Riku Sasaki. Isomorphism Elimination by Zero-Suppressed Binary Decision Diagrams. In *30th Canadian Conference on Computational Geometry*, 2018.

[HS11] Takashi Horiyama and Wataru Shoji. Edge Unfoldings of Platonic Solids Never Overlap. In *23rd Canadian Conference on Computational Geometry*, 2011.

[HS13] Takashi Horiyama and Wataru Shoji. The Number of Different Unfoldings of Polyhedra. In *24th International Symposium on Algorithms and Computation*, volume 8283 of *LNCS*, pages 623–633. Springer, 2013.

[IM13] Hiroaki Iwashita and Shin-ichi Minato. Efficient Top-Down ZDD Construction Techniques Using Recursive Specifications. Technical Report TCS-TRA-1369, Graduate School of Information Science and Technology, Hokkaido University, 2013.

[Joh66] Norman Johnson. Convex Polyhedra with Regular Faces. *Canadian Journal of Mathematics*, 18:169–200, 01 1966.

[KIIM17] Jun Kawahara, Takeru Inoue, Hiroaki Iwashita, and Shin-ichi Minato. Frontier-Based Search for Enumerating All Constrained Subgraphs with Compressed Representation. *IEICE Transactions on Fundamentals of Electronics, Communications and Computer Sciences*, E100-A(9):1773–1784, 2017.

[KSU24] Tonan Kamata, Takumi Shiota, and Ryuhei Ueharaa. A Characterization of the Overlap-free Polyhedra. In *The 8th International Meeting on Origami in Science, Mathematics and Education*, 2024.

[Lew82] Mordechai Lewin. A Generalization of the Matrix-Tree Theorem. *Mathematische Zeitschrift*, 181(1), 1982.

[Min93] Shin-ichi Minato. Zero-Suppressed BDDs for Set Manipulation in Combinatorial Problems. In *Proceedings of the 30th Design Automation Conference*, pages 272–277. ACM Press, 1993.

[MU08] Jun Mitani and Ryuhei Uehara. Polygons Folding to Plural Incongruent Orthogonal Boxes. In *20th Canadian Conference on Computational Geometry*, 2008.

[NF93] Makoto Namiki and Komei Fukuda. Unfolding 3-dimensional convex polytopes, 1993. A package for Mathematica 1.2 or 2.0, Mathematica Notebook.

[Sch89] Catherine Anne Schevon. Algorithms for geodesics on convex polytopes, 1989. The Johns Hopkins University, Master's thesis.

[Sch97] Wolfram Schlickenrieder. Nets of Polyhedra. Master's thesis, Technische Universität Berlin, 1997.

[She75] G. C. Shephard. Convex polytopes with convex nets. *Mathematical Proceedings of the Cambridge Philosophical Society*, 78(3):389–403, 1975.

[SS86] Micha Sharir and Amir Schorr. On Shortest Paths in Polyhedral Spaces. *SIAM J. Comput.*, 15(1):193–215, 1986.

[Ste22] Ernst Steinitz. Polyeder und raumeinteilungen. In *Encyclopädie der mathematischen Wissenschaften*, volume 3-1-2 (Geometrie), chapter 12, pages 1–139. 1922.

[Sug18] Hiroshi Sugiura. personal communication, 2018.

[Uno08] Takeaki Uno. personal communication, 2008.

Research achievements

Refereed International Journal Papers

1. Takumi Shiota, Tonan Kamata and Ryuhei Uehara: "Overlapping of Lattice Unfolding for Cuboids", IEICE Transactions on Foundations of Computer Science, Mathematical Foundations of Computer Science and Its Application, advance online publication, August, 2024.

2. Takumi Shiota and Toshiki Saitoh: "Overlapping edge unfoldings for convex regular-faced polyhedra", Theoretical Computer Science, vol.1002:114593, June, 2024.

Refereed Conference Proceedings

1. Yuta Nomi, Takumi Shiota, Tonan Kamata, Ryuhei Uehara: "Dissections of a Net of a Regular Octahedron into Nets of Regular Octahedra", The 26th Japan Conference on Discrete and Computational Geometry, Graphs, and Games (JCDCGGG 2024), accepted, September 16-18, 2024, Tokyo (Japan).

2. Keita Maeda, Yuta Fujioka, Takumi Iwasaki, Takumi Shiota, Toshiki Saitoh: "Divide-and-conquer Algorithms for Counting Paths using Zero-suppressed Binary Decision Diagrams", The 24th Korea–Japan Joint Workshop on Algorithms and Computation (WAAC2024), accepted, August 2–3, 2024, Seoul (Koria).

3. Tonan Kamata, Takumi Shiota, Ryuhei Uehara: "A Characterization of the Overlap-free Polyhedra", The 8th International Meeting on Origami in Science, Mathematics and Education (8OSME), July 16-18, 2024, Melbourne (Australia).

4. Takumi Shiota, Yudai Enomoto, Takashi Horiyama, Toshiki Saitoh: "The Number of Non-overlapping Edge Unfoldings in Convex Regular-faced Polyhedra", 40th European Workshop on Computational Geometry (EuroCG 2024), March 13-15, 2024, Ioannina (Greece).

5. Takashi Horiyama, Tonan Kamata, Hironori Kiya, Hirotaka Ono, Takumi Shiota, Ryuhei Uehara, Yushi Uno: "Critical Sets of n-omino Sudoku", The 25th

Indonesia-Japan Conference on Discrete and Computational Geometry, Graphs, and Games (IJCDCGGG3 2023), September 22-24, 2023, Bali (Indonesia).

6. Takumi Shiota, Tonan Kamata, Ryuhei Uehara: "Overlapping of Lattice Unfolding for Cuboids", Canadian Conference on Computational Geometry (CCCG 2023), pp. 27–33, August 3-5, 2023, Montréal (Canada).

7. Takumi Shiota and Toshiki Saitoh: "Overlapping Edge Unfoldings for Archimedean Solids and (Anti)prisms", The 17th International Conference and Workshop on Algorithms and Computation (WALCOM 2023), Lecture Notes in Computer Science, vol. 13973, pp. 36–48, March 22–24, 2023, Hsinchu (Taiwan) and online.

Domestic Workshops (No peer review)

1. 鎌田 斗南, 能美 雄太, 塩田 拓海, 上原 隆平: "Dissections of a Net of a Regular Octahedron into Nets of Regular Octahedra", 第 37 回折り紙の科学・数学・教育研究集会, 2024 年 11 月 30 日-12 月 1 日, 九州大学 大橋キャンパス デザインコモン 2 階 (福岡).

2. 塩田 拓海, 榎本 優大, 五郎部 誠士, 堀山 貴史, 鎌田 斗南, 斎藤 寿樹, 上原 隆平: "凸多面体の重なりを持たない展開図の数え上げ", 第 200 回アルゴリズム研究発表会, IPSJ SIG Technical Report, vol. 2024-AL-200, no. 11, pp. 1–8, 2024 年 11 月 26 日-27 日, 室ガス文化センター (北海道).

3. 高雄 奏摩, 新竹 優駿, 江藤 宏, 宮野 英次, 斎藤 寿樹, 塩田 拓海: "変更制約付き最長共通部分列問題に対する多項式時間アルゴリズム", 2024 年度 32 回電子情報通信学会 九州支部 学生会講演会, pp. A-17:1-2, 2024 年 9 月 25 日, 鹿児島大学 郡元キャンパス (鹿児島).

4. 塩田 拓海, 榎本 優大, 堀山 貴史, 斎藤 寿樹: "整面凸多面体の重なりを持たない辺展開図の数え上げ", 2023 年度 冬の LA シンポジウム, pp.33S:1-11, 2024 年 2 月 19 日-2 月 21 日, 京都大学 北部総合教育研究棟 益川ホール (京都).

5. 前田 惠太, 岩崎 巧実, 藤岡 祐太, 塩田 拓海, 斎藤 寿樹: "ZDD を用いた分割統治法によるパス数え上げアルゴリズム", アルゴリズム研究会, IPSJ SIG Technical Report, vol. 2024-AL-196, no. 2, pp. 1–8, 2024 年 1 月 20 日-21 日, 東京大学 本郷キャンパス 工学部六号館 2 階 63 講義室（東京）

6. 鎌田 斗南, 塩田 拓海, 上原 隆平: "Overlap-free な多面体の完全な分類", 第 35 回折り紙の科学・数学・教育研究集会, 2023 年 11 月 18 日-19 日, 東京大学 駒場キャンパス 15 号館 104 室 (東京).

7. 鎌田 斗南, 塩田 拓海, 上原 隆平: "Overlap-free な多面体の完全な分類", アルゴリズム研究会, IPSJ SIG Technical Report, vol. 2023-AL-195, no. 4, pp. 1–6, 2023 年 11 月 16 日-17 日, 那覇市 IT 創造館（沖縄）.

8. 塩田 拓海，榎本 優大，堀山 貴史，斎藤 寿樹: “整面凸多面体の重なりを持たない辺展開図の列挙”，九州地区における若手 OR 研究交流会 2023，2023 年 10 月 28 日-29 日，FIT セミナーハウス (大分).

9. 吉渡 叶，塩田 拓海，鎌田 斗南: “オストルの PSPACE 困難性”，2023 年度 夏の LA シンポジウム，pp.39:1-7，2023 年 7 月 3 日-5 日，サン・リフレ函館 (北海道).

10. 塩田 拓海，鎌田 斗南，上原 隆平: “直方体の格子展開図における重なり”，アルゴリズム研究会，IPSJ SIG Technical Report，vol. 2023-AL-193，no. 4，pp. 1–6，2023 年 5 月 10 日-11 日，北海道大学 工学部 B2 棟 2F アカデミックラウンジ 1（北海道）.

11. 塩田 拓海，鎌田 斗南，上原 隆平: “直方体の格子展開図における重なり”，2022 年度 冬の LA シンポジウム，pp.9:1-12，2023 年 1 月 30 日-2 月 1 日，京都大学 数理解析研究所 (京都).

12. 有吉 優聖，塩田 拓海，斎藤 寿樹: “タンパク質連接ネットワークの中心性とランダムコイル指標の関係”，日本オペレーションズ・リサーチ学会九州支部 若手 OR 交流会 2022，2022 年 10 月 29 日，福岡大学 文系センター棟 15 階 第 6 会議室 (福岡).

13. 塩田 拓海，鎌田 斗南，上原 隆平: “立方体の格子展開図における重なり”，日本オペレーションズ・リサーチ学会九州支部 若手 OR 交流会 2022，2022 年 10 月 29 日，福岡大学 文系センター棟 15 階 第 6 会議室 (福岡).

14. 塩田 拓海，斎藤 寿樹: “アルキメデスの（反）角柱の重なりを持つ辺展開図”，2021 年度 冬の LA シンポジウム，pp.5:1-11，2022 年 2 月 1 日-3 日，オンライン.

15. 塩田 拓海，斎藤 寿樹: “アルキメデスの角柱の重なりを持つ辺展開図”，日本オペレーションズ・リサーチ学会九州支部 若手 OR 交流会 2021，2021 年 11 月 20 日，オンライン.

16. 塩田 拓海，斎藤 寿樹: “回転展開法を用いた自己重複を持つ部分的な辺展開図の数え上げ”，2021 年度（第 74 回）電気・情報関係学会九州支部連合大会，2021 年 9 月 24 日，オンライン.

17. 塩田 拓海，斎藤 寿樹: “回転展開法を用いた自己重複を持つ部分的な辺展開図の数え上げ”，2021 年度 夏の LA シンポジウム，pp.3:1-8，2021 年 7 月 20 日-21 日，オンライン.

18. 塩田 拓海，斎藤 寿樹: “フロンティア法によるアルキメデスの立体の辺展開図の列挙”，日本オペレーションズ・リサーチ学会九州支部 若手 OR 交流会 2020，2020 年 11 月 28 日，博多バスターミナル 9F 第 10・11 ホール (福岡).

Articles for Journal of Societies

1. 塩田 拓海: “展開図に魅せられて”，LA シンポジウム会誌 (発表論文賞記念記事)，第 83 号，pp. 8-12，2024 年 7 月 16 日.

Awards

1. Takumi Shiota: 第 13 回 LA/EATCS-Japan Student Presentation Award，2024 年 2 月.

2. Yusei Ariyoshi, Tomoya Doi, Yuta Fujioka, Takumi Iwasaki, Keita Maeda, Toshiki Saitoh, Takumi Shiota, Naoya Taguchi: International Competition on Graph Counting Algorithms(ICGCA) Ranking by the number of solved benchmarks 3rd place，2023 年 9 月.

3. 塩田 拓海: 電子情報通信学会 九州支部 2022 年度学術奨励賞，2023 年 3 月.

4. 塩田 拓海: 日本オペレーションズ・リサーチ学会九州支部 若手 OR 交流会 2022 優秀発表賞，2022 年 10 月.

5. 塩田 拓海: 日本オペレーションズ・リサーチ学会九州支部 若手 OR 交流会 2021 優秀発表賞，2021 年 11 月.

6. 塩田 拓海: 2021 年度 (第 74 回) 電気・情報関係学会九州支部連合大会 連合大会講演奨励賞，2021 年 9 月.

7. 塩田 拓海: 日本オペレーションズ・リサーチ学会九州支部 若手 OR 交流会 2020 最優秀発表賞 (学部生の部)，2020 年 11 月.

8. 塩田 拓海: 九州工業大学学長表彰 鳳龍奨学賞【優秀賞】，2018 年 3 月.